

AD-770 213

OPTICAL EMISSION PROPERTIES OF AIRCRAFT  
COMBUSTIBLE FLUIDS

R. M. F. Linford, et al

McDonnell Douglas Corporation

Prepared for:

Air Force Aero Propulsion Laboratory

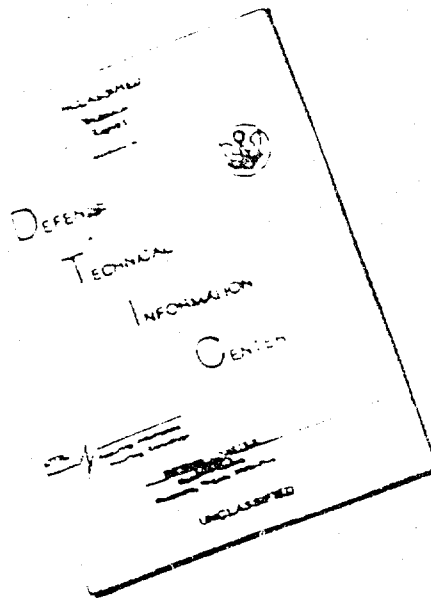
6 August 1973

DISTRIBUTED BY:

**NTIS**

National Technical Information Service  
U. S. DEPARTMENT OF COMMERCE  
5285 Port Royal Road, Springfield Va. 22151

# DISCLAIMER NOTICE



THIS DOCUMENT IS BEST  
QUALITY AVAILABLE. THE COPY  
FURNISHED TO DTIC CONTAINED  
A SIGNIFICANT NUMBER OF  
PAGES WHICH DO NOT  
REPRODUCE LEGIBLY.

REPRODUCED FROM  
BEST AVAILABLE COPY

Unclassified

AD 770 213

SECURITY CLASSIFICATION OF THIS PAGE (When Data Entered)

REPORT DOCUMENTATION PAGE		READ INSTRUCTIONS BEFORE COMPLETING FORM
1. REPORT NUMBER AFAPL-TR-73-83	2. GOVT ACCESSION NO.	3. RECIPIENT'S CATALOG NUMBER
4. TITLE (and Subtitle) Optical Emission Properties of Aircraft Combustible Fluids	5. TYPE OF REPORT & PERIOD COVERED Final Technical Report May 1972 through August 1973	
	6. PERFORMING ORG. REPORT NUMBER MDC A2454	
7. AUTHOR(s) R. M. F. Linford and C. F. Dillow	6. CONTRACT OR GRANT NUMBER(s) F33615-72-C-1857	
	10. PROGRAM ELEMENT, PROJECT, TASK AREA & WORK UNIT NUMBERS 304807	
9. PERFORMING ORGANIZATION NAME AND ADDRESS McDonnell Douglas Corporation Post Office Box 516 St. Louis, Missouri 63166	12. REPORT DATE 6 August 1973	
	13. NUMBER OF PAGES 98	
11. CONTROLLING OFFICE NAME AND ADDRESS Air Force Aero Propulsion Laboratory (AFSC) AFAPL/SFH Wright-Patterson Air Force Base, Ohio 45433	15. SECURITY CLASS. (of this report) Unclassified	
	15a. DECLASSIFICATION/DOWNGRADING SCHEDULE	
14. MONITORING AGENCY NAME & ADDRESS (if different from Controlling Office) AFPRO, McDonnell Douglas Corporation Post Office Box 516 St. Louis, Missouri 63166		
16. DISTRIBUTION STATEMENT (of this Report)  APPROVED FOR PUBLIC RELEASE, DISTRIBUTION UNLIMITED		
17. DISTRIBUTION STATEMENT (of the abstract entered in Block 20, if different from Report)		
18. SUPPLEMENTARY NOTES  Reproduced by NATIONAL TECHNICAL INFORMATION SERVICE U S Department of Commerce Springfield VA 22151		
19. KEY WORDS (Continue on reverse side if necessary and identify by block number) Aircraft Fluids Emission Spectra Ultraviolet Emission Spectra Visible Emission Spectra Infrared Emission Spectra High Altitude Combustion Spectra		
20. ABSTRACT (Continue on reverse side if necessary and identify by block number) Optical measurements have been made to determine the radiant energy emitted by diffusion flames from the following aircraft combustable fluids; JP-4, JP-5, JP-8, AVGAS, MIL-H5606B and MLO-68-5. Data was taken under sea level conditions and simulated altitude conditions up to 35,000 ft. The spectral range of data taken is from 200nm to 15um. Results indicate the majority of emitted energy is in the visible and near infrared. The major		

107

Unclassified

SECURITY CLASSIFICATION OF THIS PAGE(When Data Entered)

20. Abstract (cont'd)

differences in the spectra taken at 35,000 ft. versus the spectra taken at sea level is the decrease in IR and visible energy, with an anticipated increase in UV radiation.

fa

Unclassified

SECURITY CLASSIFICATION OF THIS PAGE(When Data Entered)

## SUMMARY

The object of this program was to determine the radiant energy emitted by small fires of the type that might occur in an aircraft engine nacelle. Spectral radiant intensity data were recorded on diffusion flames of JP-4, JP-5, JP-8, Aviation Gasoline, and MIL-H-5606B and MLO-68-5 hydraulic fluids. These fluids were burned in a high altitude combustion chamber at pressures corresponding to altitudes from sea level to 35,000 ft. The wavelength range of the intensity measurements was from the middle ultraviolet (200  $\mu\text{m}$ ) to the far infrared (15  $\mu\text{m}$ ). The results indicate that the bulk of the emitted radiation was in the visible and near infrared regions and originated at hot carbon particles in the diffusion flames. This total energy was found to decrease significantly at high altitudes. In addition, strong emissions bands were detected in the middle ultraviolet corresponding to electronic transitions of excited radicals in the flame. The most intense feature in each spectra recorded was the dominant 4.4  $\mu\text{m}$  emission band corresponding to excited carbon dioxide molecules.

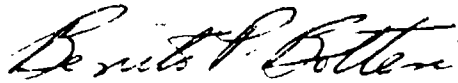
PREFACE

This report describes the results of Contract F33615-72-C-1857 conducted by McDonnell Douglas Corp., St. Louis, Mo. The work was conducted under Project 3048, "Fuels, Lubrication and Fire Protection", Task 304807, "Aerospace Vehicle Fire Protection" and was administered by the Fire Protection Branch, Air Force Aero Propulsion Laboratory, Wright-Patterson AFB, Ohio, with Mr. Terry M. Trumble as Project Engineer.

The principal investigator on this program was Dr. R. M. F. Linford. The following personnel contributed to the program: C. F. Dillow.

The report covers work accomplished by McDonnell Douglas from May 1972 to August 1973.

This technical report has been reviewed and is approved.

  
BENITO P. BOITERI  
Chief, Fire Protection Branch  
Fuels and Lubrication Division

## TABLE OF CONTENTS

SECTION	PAGE
I INTRODUCTION	1
II EXPERIMENTAL DETAILS	4
1. Selection of Fluids	4
2. Combustion and Fuel Handling System	6
3. Electro-Optical Systems	16
4. Data Acquisition and Reduction	29
5. Calibration of the Optical System	36
III EXPERIMENTAL RESULTS	42
1. Ultraviolet Emission Spectra (200 nm - 320 nm)	42
2. Visible and Near-Infrared Emission Spectra (300 nm - 2.6 $\mu\text{m}$ )	55
3. Far Infrared Emission Spectra (2.5 $\mu\text{m}$ - 15 $\mu\text{m}$ )	63
IV DISCUSSION	70
1. Altitude Effects	72
2. Emitting Species	78
3. Significance of Results	81
V CONCLUSIONS	83
LIST OF EQUIPMENT AND INSTRUMENTS	85
REFERENCES	86
APPENDIX A	87
APPENDIX B	93

## LIST OF ILLUSTRATIONS

FIGURE		PAGE
1.	The Combustion Nozzle Assembly	9
2.	High Altitude Combustion Chamber	11
3.	Variation of Atmospheric Pressure with Altitude Above Sea Level	13
4.	Fuel and Air Flow Systems for High Altitude Combustion of Aircraft Fluids	15
5.	Optical System for Spectral Radiant Intensity Measurements	19
6.	Spectral Response of Cesium Telluride Photocathode Behind Magnesium Fluoride Window	20
7.	Optical Transfer System	21
8.	Overall View of the Optical Emissions Equipment	24
9.	Spectral Response of the EMI 9558QC Photomultiplier	25
10.	Typical Spectral Response of a Lead Sulphide Detector	26
11.	Optical System for Spectral Radiant Intensity Measurements (2.0 - 15.0 $\mu\text{m}$ )	28
12.	Spectral Response of the Block Engineering 195T Interferometric Spectrometer	28
13.	Data Acquisition and Reduction System	30
14.	Typical Computer Plot of Uncalibrated Data from a Spectral Scan of the Radiant Intensity Standard	33
15.	Typical Computer Plot of Uncalibrated Data from a Spectral Scan of a JP-4 Flame	34
16.	Typical Computer Plot of the Spectral Radiant Intensity of a JP-4 Flame	35
17.	Calibration Curve for the First Radiant Intensity Standard	39



FIGURE		PAGE
18.	Calibration Curve for the Second Radiant Intensity Standard (300 nm - 2.5 $\mu$ m)	41
19.	Spectral Radiant Intensity of JP-4 Burning at Sea Level, Over the Three Wavelength Ranges Scanned in the Middle Ultraviolet	44
20.	The Ultraviolet Emissions from JP-4 Burning at Sea Level	46
21.	Spectral Radiant Intensity of JP-4 Burning at Sea Level (200 - 320 nm)	46
22.	Spectral Radiant Intensity of JP-5 Burning at Sea Level (200 - 320 nm)	47
23.	Spectral Radiant Intensity of JP-8 Burning at Sea Level (200 - 320 nm)	47
24.	Spectral Radiant Intensity of Aviation Gas Burning at Sea Level (200 - 320 nm)	49
25.	Spectral Radiant Intensity of MIL-H-5606B Burning at Sea Level	49
26.	Spectral Radiant Intensity of MLO-68-5 Burning at Sea Level	50
27.	Ultraviolet Emissions from JP-4 Burning at Various Altitudes	52
28.	Integral Radiant Intensity of JP-4 Flames Burning at Various Altitudes (Data Normalized for Unit Fuel Flowrate)	54
29.	Integral Radiant Intensity of JP-8 Flames Burning at Various Altitudes (Data Normalized for Unit Flowrate)	56
30.	Integral Radiant Intensity of Aviation Gasoline Burning at Various Altitudes (Data Normalized for Unit Fuel Flowrate)	57
31.	Spectral Radiant Intensity of JP-4 Burning at 35,000 Ft (190 Torr)	58
32.	Visible and Near Infrared Emissions from JP-4 Burning at Various Altitudes	62

FIGURE		PAGE
33.	Visible and Near Infrared Emissions from JP-5 Burning at Various Altitudes	64
34.	Visible and Near Infrared Emissions from JP-8 Burning at Various Altitudes	64
35.	Visible and Near Infrared Emissions from Aviation Gas Burning at Various Altitudes	65
36.	Far Infrared Emissions from JP-4 Burning at Sea Level	67
37.	Optical Emissions from JP-4 Burning at 35,000 Ft (190 Torr)	71
38.	Ultraviolet Power Emitted by Burning Aircraft Fuels at Various Altitudes	73
39.	Visible and Near Infrared Power Emitted by Burning Aircraft Fuels at Various Altitudes	74
40.	Spectral Radiant Intensity of the 4.4 $\mu\text{m}$ CO <sub>2</sub> Emission Peak for JP-4 Burning at Several Altitudes	76
41.	Emission Spectra of JP-4 Burning at 35,000 Ft (190 to 275 nm)	79
42.	Emission Spectra of JP-4 Burning at 35,000 Ft (185 to 220 nm)	80

SECTION I  
INTRODUCTION

Optical sensing systems are used for fire detection in a wide variety of industrial and military applications. The wavelengths of operation of the sensors range from the middle ultraviolet to the far infrared and a particular detection system may utilize two or more sensors which are sensitive to different wavelengths.

In an aircraft engine nacelle the majority of the potentially combustible materials are hydrocarbon fluids. Fuels, hydraulic fluids and lubricants are all highly flammable and are present in copious quantities near aircraft engines. In the event of a fire these fluids burn with a bright open flame and thus optical sensors are strong candidates for engine nacelle fire detection systems. The object of this program was to determine the radiant intensity emitted by fires of this type.

All optical fire detectors operate on the principle of responding to the optical radiation emitted by the fire materials while discriminating against background radiation. The background may include solar radiation, artificial lighting, gunfire, sparks, or any hot body in the field of view of the detector. The device must also withstand the physical stresses imposed by vibration, shock and the high temperatures.

To evaluate the performance of an optical sensor as a fire detector in this type of application certain analyses are necessary. Data required for such analyses include the spectral calibration of the sensor, the spectral radiant intensity of the fire and information on the sources of background radiation. The program described in this report was designed to provide information on the second of these parameters: the radiation emitted by aircraft engine fires.

Flame spectroscopy had its origin in the work of men like Newton, Bunsen, Kirchoff and Herschel, and in the last 40 years the literature has been filled with publications on the optical emissions from flames. In particular, recent issues of the Combustion Institute's biennial publication (1) have included many articles on the spectroscopy of hydrocarbon flames. However, the emphasis of most of this work has been on analyses of combustion phenomena by identification of chemical species in the flame, with an occasional measurement of the relative intensities of prominent spectral peaks. The designer of a fire detection system should not be concerned with the reaction chemistry of the flame, but he has a requirement for calibrated spectral radiant intensity data for potential fires. Despite the long history of work in this area, as cited above, such data have never been determined for burning aircraft fluids.

The program described in this report was designed to produce calibrated spectral emission data which are truly representative of

actual fires in an aircraft engine nacelle. The experiments involved spectroscopy, at wavelengths between 200 nm and 15  $\mu\text{m}$ , on hydrocarbon flames burning in air at altitudes between sea-level and 35,000 feet. Six commonly used aircraft combustible fluids were burned as diffusion flames and were studied in ten consecutive spectral ranges spanning the middle ultraviolet to the far infrared. More than two hundred spectral scans were recorded during the program and the data was normalized with respect to NBS-traceable radiant intensity standards. Computerized data reduction techniques were used to compile the large volume of spectral radiant intensity information and present it in a form adaptable to the needs of the designers of advanced optical fire detection systems.

Full details of the experiments are described in this report, the data are presented, and their significance is discussed.

SECTION II  
EXPERIMENTAL DETAILS

Combustible fluids were selected from those which are in common use in modern aircraft, or are under consideration for future use. A burning system was devised to produce reproducible flames in atmospheres ranging from sea-level to 35,000 feet. Three different optical systems were assembled to record the spectral emissions over the wavelength range from 200 nm to 15  $\mu$ m, and standard sources were calibrated to provide reference to the National Bureau of Standards. In the paragraphs that follow each facet of the experiment is described in detail.

1. SELECTION OF FLUIDS

The working fluids in an aircraft engine nacelle include fuels, hydraulic fluids and lubricants. These organic liquids represent the greatest fire hazard in the vehicle since most of these fluids are extremely flammable and several of the fuels have very low flash points. In selecting the materials for the program, fluids were included which are either in common use or have potential application in the foreseeable future. The original selection is summarized in Table 1.

Each of the first six fluids was extensively studied throughout the various phases of the program; but, despite several attempts, it proved impossible to burn MIL-L-7808 lubricant in a controlled or repeatable

TABLE 1 COMBUSTIBLE FLUIDS SELECTED FOR THE BURNING EXPERIMENTS

Material Identification	Usage	Description	Flash Point	Reference
JP4	Fuel	Wide Cut, Gasoline Type	-20	2
JP5	Fuel	High Flash Point, Kerosene Type	140	3
JP8	Fuel	-	110	--
Aviation Gasoline	Fuel	-	-40	2
MIL-H-5606B	Hydraulic Fluid	Mineral Oil	209	5
MLO-68-5	Hydraulic Fluid	Hydrocarbon with Fluoride Additives	410	5
Oronite M2	Hydraulic Fluid	-	430	6
MIL-L-7808	Lubricant	Synthetic Diester	437	4

flame. Oronite M2 hydraulic fluid was eliminated from the program when it was removed from the list of potential new hydraulic fluids for military or civilian applications.

## 2. COMBUSTION AND FUEL HANDLING SYSTEM

### a. Burner Development

The design of the combustion system was crucial to the whole program as the resultant flame had to be "truly representative of actual fires." The most likely cause of small fires in an engine nacelle is the ignition of a fine jet of flammable liquid leaking through a small hole in a pipe or fitting. Large leaks of fluids into the nacelle and the subsequent fire would be impossible to simulate in a controlled manner, and such fires would probably be readily detected. Flames burning at a fine leak would present the most severe problem to a detection system. Such flames were therefore selected as the basis of the simulation of an engine nacelle fire.

Fuel/air mixtures burning at a leak in a pressurized line produce diffusion flames, as all mixing occurs downstream from the "nozzle". Therefore, standard burners with premixing could not be used to simulate such flames and a special combustion system had to be developed to produce diffusion flames for the spectroscopic measurements.

A further constraint on the burner design was the need to restrict the size of the flame to the field of view of the optical



systems used. Fire detectors respond to radiation emitted by all parts of the flame and spectroscopy on a selected portion of the flame would be unrepresentative. As described in a later section, the optical system was designed to collect radiation from a flame approximately 175 mm tall.

Lastly, the burner system had to generate stable diffusion flames for a variety of combustible liquids at several altitudes. The flames had also to be reproducible over a period of weeks and the nozzle had to be demountable for cleaning.

A burner nozzle meeting all the above requirements was developed through a series of preliminary experiments in an explosion-proof cell. Several nozzle assemblies were tried without success before stable flames were achieved with a domestic oil-burner nozzle. The smallest commercially available nozzle was 0.2 mm diameter, and, with as little as  $6.9 \times 10^3 \text{ Nm}^{-2}$  (1.0 psi) hydraulic pressure, flames several meters high were generated. Special inserts with 0.075 mm apertures were then machined to fit standard Delavan\* nozzles. A nichrome wire heater was wound on the base of the nozzle assembly and was potted in ceramic paste. With the fine insert, the preheater and a pressure differential of approximately  $10^4 \text{ Nm}^{-2}$  (1.5 psi), stable, repeatable flames were achieved with a flow rate of approximately  $0.2 \text{ cm}^3 \text{ min}^{-1}$ .

\*Delavan Manufacturing Company, Des Moines, Iowa

Remote ignition of the flame was provided by two wire electrodes set approximately 20 mm apart and 30 mm above the nozzle and connected to a 15 kV neon-sign transformer. The final version of the burner is illustrated in Figure 1.

During the early experiments a thermocouple was attached to the nozzle, and it was determined that the optimum nozzle temperature for burning JP-4 and the other fuels with a stable flame was approximately 95°C (200°F). The thermocouple attachment would not withstand the repeated handling of the nozzle required for cleaning; therefore, temperature measurements were abandoned at an early stage. However, the same heater control settings were used for each burning experiment, and it is estimated that the nozzle temperature was 100°C ±15°C throughout the program.

b. Combustion Atmosphere

The requirements of the program dictated that the various fluids should be burned in environments simulating the atmospheres from sea level to high altitudes. While maintaining the appropriate air pressure it was also important to ensure that an adequate supply of fresh oxygen was available to maintain the flame, as would be the case in an aircraft-engine fire. This air flow had also to be provided without perturbing the flame as flame flicker would have introduced severe noise into the electro-optical measurements.

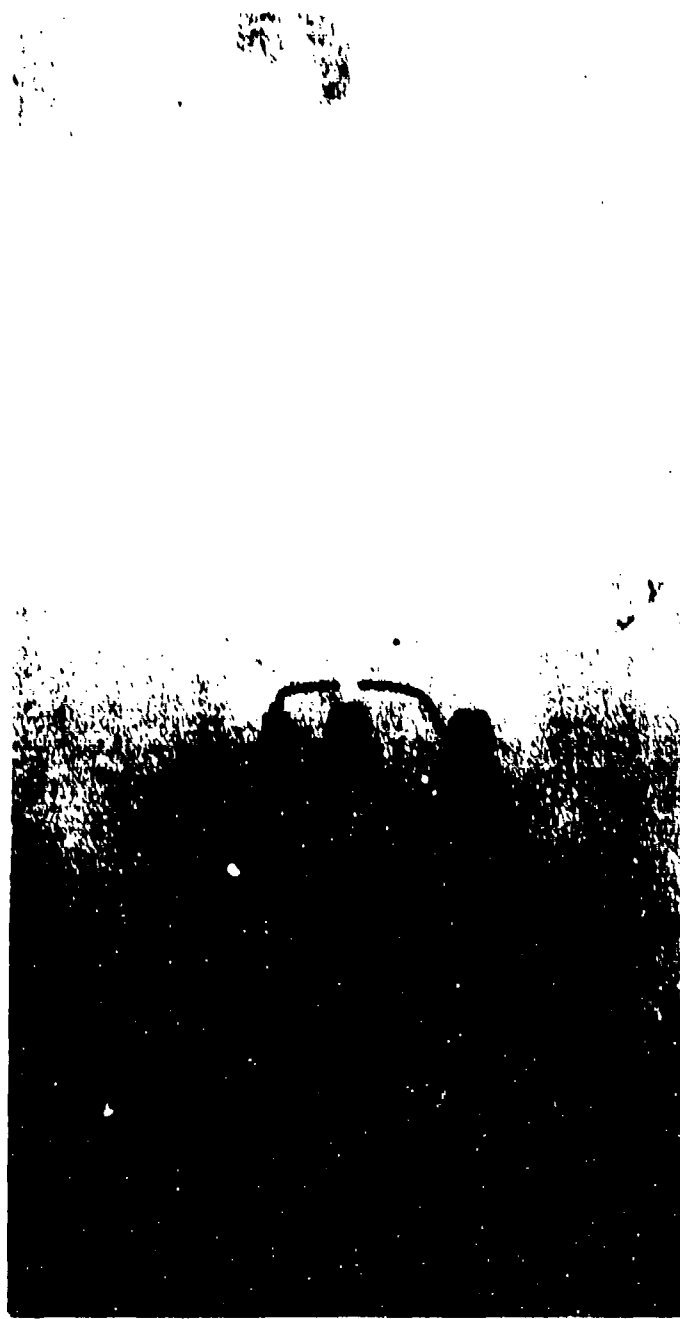


FIGURE 1 THE COMBUSTION NOZZLE ASSEMBLY

(1) Sea Level

Initial sea level experiments were run with the burner installed in a laboratory fume hood. (The exhaust fan was turned off during optical measurements to reduce drafts.) Later experiments were performed in the high altitude combustion chamber with the vacuum flanges removed.

(2) High Altitudes

All the optical emission measurements on fluids burning in high-altitude atmospheres were performed in the combustion chamber illustrated in Figure 2. The main chamber was a converted vacuum chamber with a 380 mm (15 inch) internal diameter, and a 685 mm (27 inch) height; the extension snout was added to accommodate the field of view of the optical system without installing a large diameter optical window. Air was supplied to the flame through an automotive air filter mounted on the base plate of the chamber. This filter ensured that air was introduced into the combustion chamber without excessive turbulence to disturb the flame.

The chamber was evacuated with a  $24 \text{ l s}^{-1}$  (50 cfm) mechanical pump through a port in the top plate. A second air filter was installed in the pumping line to prevent dense black smoke from entering the pump. The chamber pressure was adjusted by throttling the air-inlet valve to balance the evacuation rate of the mechanical pumping system. A dial gauge was used to monitor the pressure in the

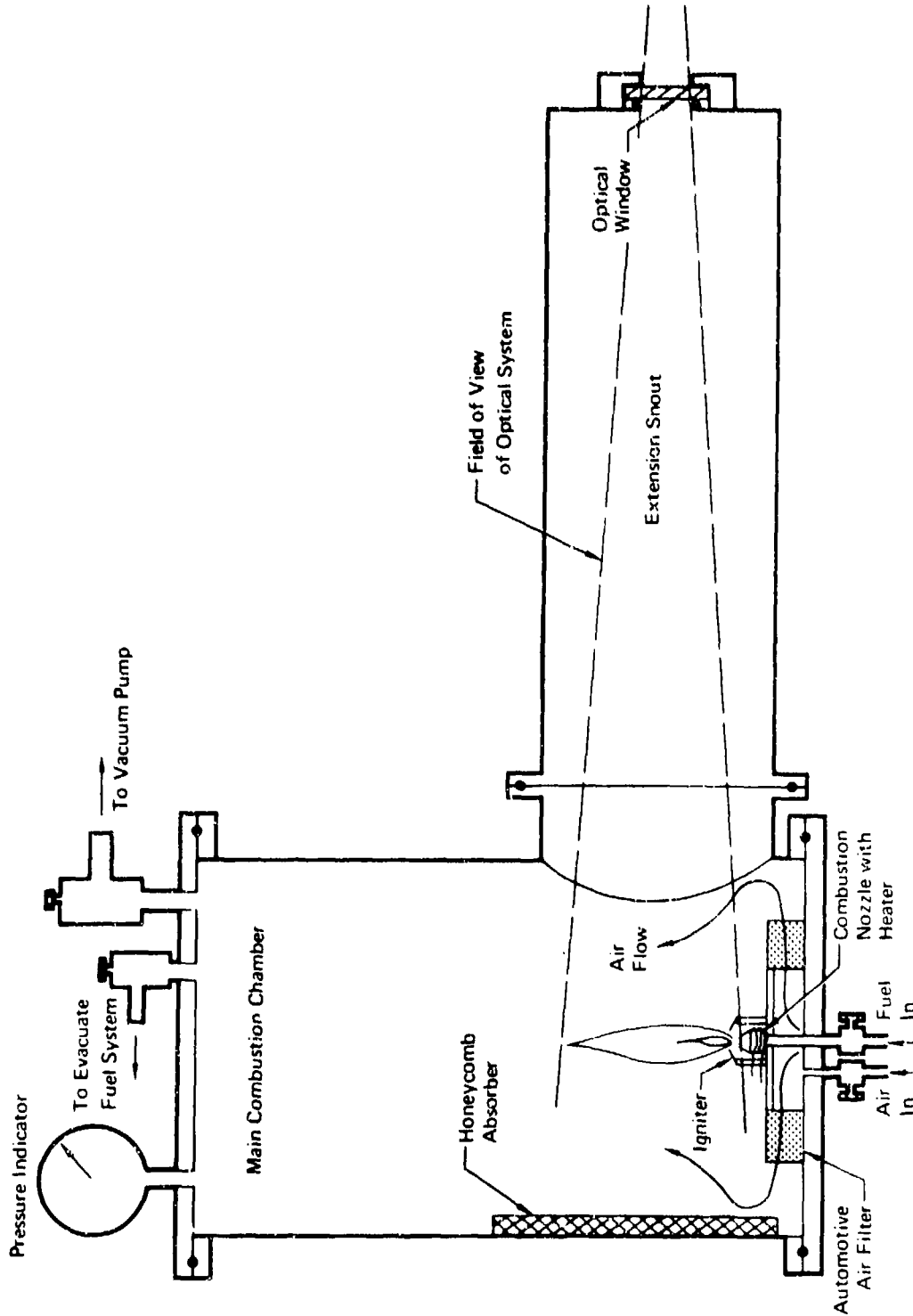


FIGURE 2 HIGH ALTITUDE COMBUSTION CHAMBER

chamber, and the corresponding altitude was determined from the curve in Figure 3.

A calculation of the effective speed of the pumping system indicated that approximately  $10 \text{ l min}^{-1}$  of air was drawn through the chamber. Using a simplified molecular structure for JP-4,  $\text{C}_8\text{H}_{18}$ , it was calculated that  $0.2 \text{ cm}^3 \text{ min}^{-1}$  of the fuel would require approximately  $2.5 \text{ l min}^{-1}$  of fresh air for complete combustion. To confirm that adequate air was drawn through the chamber the optical output from a JP-4 flame burning at 35,000 feet (190 torr) was monitored for a period of time following ignition. No systematic variations in the level of optical energy emitted by the flame were detected for a period of more than an hour, indicating that the flame was not starved of oxygen. This test also confirmed that negligible contamination of the optical window occurred.

To prevent the reflection of radiation from the chamber walls into the optical system a black honeycomb absorber was installed behind the flame.

c. Fuel System

The fuel flowrate through a nozzle is a function of the pressure drop across the nozzle; therefore, during the high altitude experiments, the pressure in the fuel system had to be adjusted to maintain a constant pressure differential. This was achieved with the

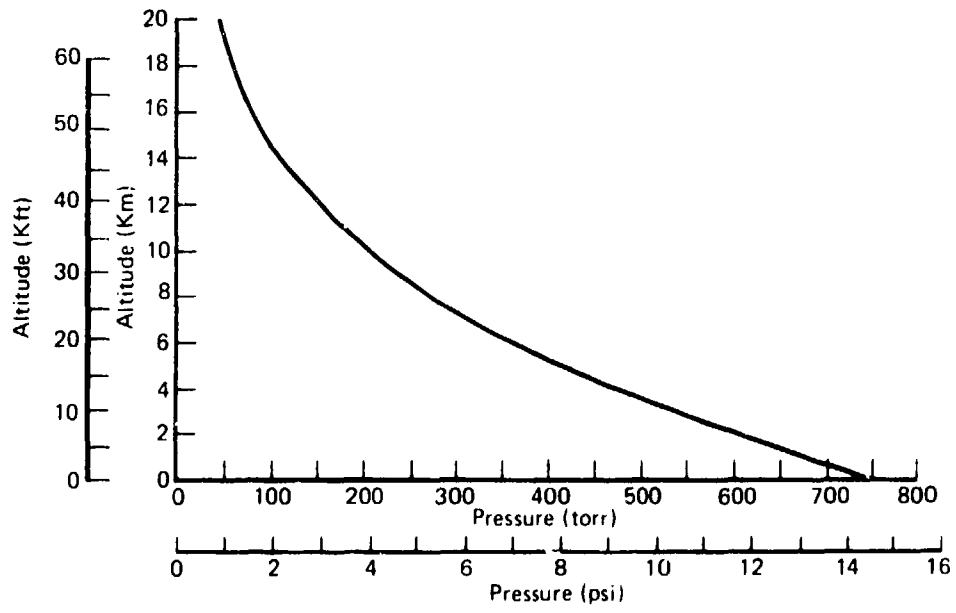


**FIGURE 3 VARIATION OF ATMOSPHERIC PRESSURE WITH ALTITUDE ABOVE SEA LEVEL**  
(Am. Inst. of Phys. Handbook)

fuel system illustrated in Figure 4.

Pressure in the 7.5-liter fuel reservoir was adjusted by evacuating it to the same pressure as the combustion chamber and then repressurizing the reservoir slightly with dry nitrogen. The fuel flowrate to the burner nozzle was then controlled by adjusting the pressure, and was measured on the calibrated flow meter. This meter was of the rotometer type and had to be calibrated for each fluid used in the system (see Appendix A).

Despite this careful calibration, errors were introduced into the flowrate measurement by pockets of air in the fuel lines. Each time the fuel system was opened to change fluids, air was introduced which would collect in pockets when the system was re-evacuated. Before attempting to take optical data following a fluid change, a flame was burned for several hours in an attempt to eliminate all the air bubbles from the fuel lines. This approach was never entirely successful, and, although steady repeatable flames were achieved, good flowrate measurements could not be guaranteed. Therefore, it was elected to adjust the height of the flame to a constant level, rather than maintain a constant flow rate. The flowrates required for a 175 mm flame varied between  $0.2 \text{ cm}^3 \text{ min}^{-1}$  and  $0.3 \text{ cm}^3 \text{ min}^{-1}$  for the different fuels at the various altitudes.



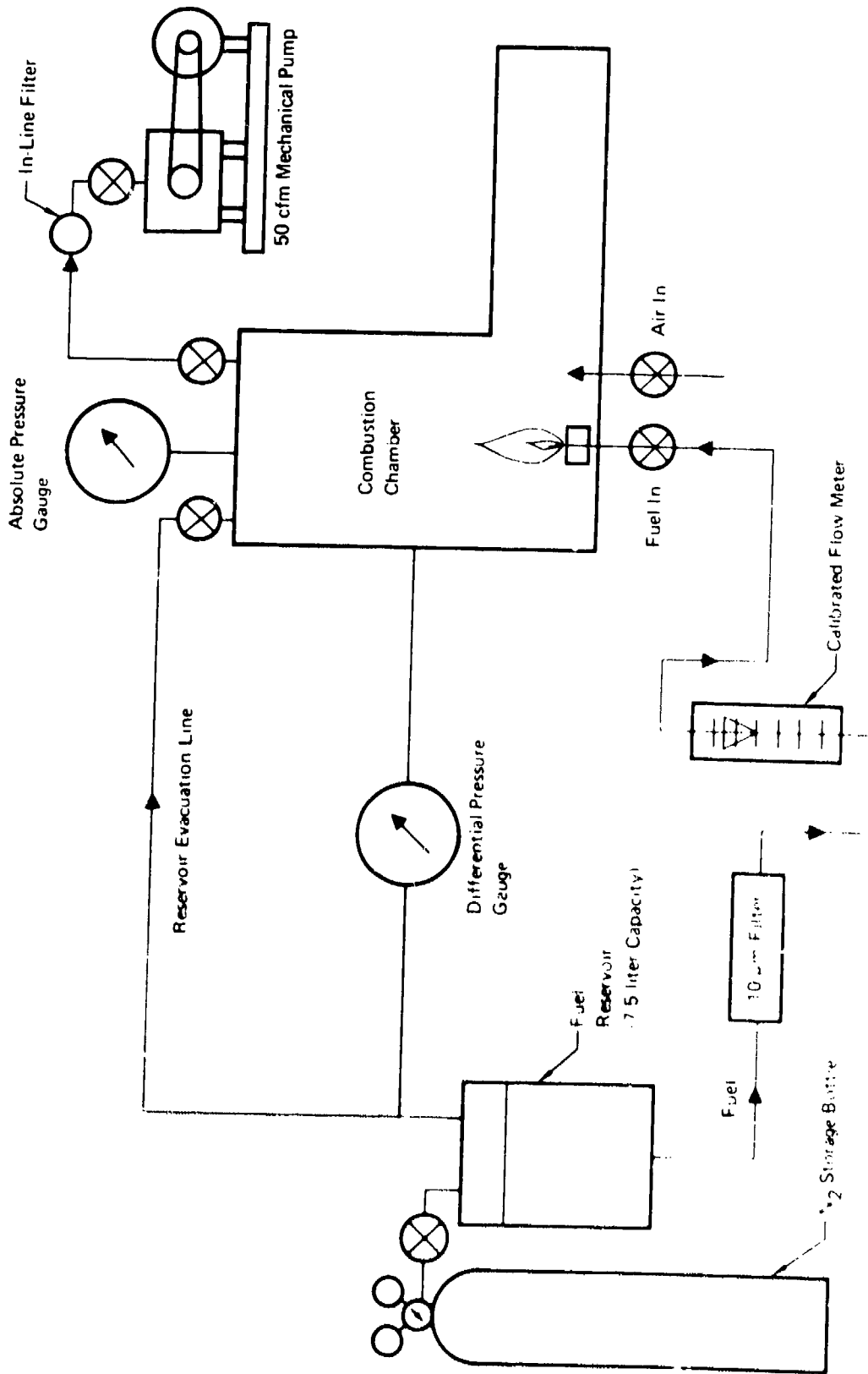


FIGURE 4 FUEL AND AIR FLOW SYSTEMS FOR HIGH ALTITUDE COMBUSTION OF AIRCRAFT FLUIDS

### 3. ELECTRO-OPTICAL SYSTEMS

As discussed in paragraph 2 it was important that the optical measurements should be made on the entire flame rather than on portions of the flame front selected by focussing collection optics. This constraint, and the need to determine absolute radiant intensity values by frequent calibrations with a standard source, influenced the design of the optical systems.

To cover the entire spectral range from 200 nm to 15  $\mu\text{m}$  the optical measurements were performed in three series:

- 200 nm to 320 nm - the ultraviolet series
- 300 nm to 2.65  $\mu\text{m}$  - the visible/near infrared series
- 2.0  $\mu\text{m}$  to 15.0  $\mu\text{m}$  - the far infrared series

Each of these series was conducted as a separate experiment with each fluid/altitude combination being studied before continuing to the next series. This division of the program arose out of the equipment requirements for each spectral range and the order of magnitude variations in the intensity of the radiation emitted by the flames at different wavelengths. For similar reasons each of the first two series was further subdivided into short spectral ranges. Each range in a series was studied one after another with only a short break to change filters, diffraction gratings or detectors. The breakdown of the ten different spectral ranges and the optical equipment changes is summarized in Table 2.

**TABLE 2 SUMMARY OF THE OPTICAL COMPONENTS USED IN THE SPECTRAL RADIANT INTENSITY MEASUREMENTS**

Spectral Range	Spectrometer	Order Filters*	Grating		Bandwidth	Detector		
			Ruling	Blaze				
200-243 nm 240-283 nm 280-323 nm	Jarrell Ash 1/2 m Grating Spectrometer	None None None	1180 $\ell$ /mm	300 nm 300 nm 300 nm	1.6nm	Photomultiplier - Varian G 26H215		
300-471 nm 470-641 nm 640-811 nm	Jarrell Ash 1/2 m Grating Spectrometer	Soda Glass 440 nm <sup>(1)</sup> 440 nm <sup>(1)</sup>		300 nm 750 nm 750 nm			1.6nm	Photomultiplier - EMI 9558 OC
0.80-1.49 $\mu$ m 1.48-2.16 $\mu$ m 2.00-2.65 $\mu$ m	Jarrell Ash 1/2 m Grating Spectrometer	0.76 $\mu$ m <sup>(2)</sup> 1.00 $\mu$ m <sup>(3)</sup> 1.80 $\mu$ m <sup>(4)</sup>		295 $\ell$ /mm 1.5 $\mu$ m 1.5 $\mu$ m				
2.0-15.0 $\mu$ m	Block Engineering Interferometric Spectrometer			40cm <sup>-1</sup>	Thermistor			

\*Wavelengths listed are cut on values of long wavelength pass (LWP) filters.

(1) - Corning Glass CS 3-72

(2) - OCLI LWP Interference Filter

(3) - Corning Glass CS 4-71

(4) - OCLI LWP Interference Filter

The equipment required for each of the experimental series is described in the following sections.

a. Equipment for the Ultraviolet Series

The optical system illustrated in Figure 5 was used both for the ultraviolet series and, in modified form, for the visible/near infrared experiments. A Jarrell-Ash half meter grating spectrometer, equipped with a 1180 lines/mm diffraction grating and a Varian G-26H215 photomultiplier detector, was used for spectral measurements in the 200 - 320 nm region. With the entrance slit width set at 1 mm the bandwidth was 1.6 nm. The photomultiplier was selected for its high sensitivity in the middle ultraviolet and its "blindness" to wavelengths longer than 350 nm. (Figure 6 illustrates the spectral response of the cesium telluride photocathode/magnesium fluoride window combination.) This spectral response resulted in good rejection of background light in the spectrometer and resultant high sensitivity to the weak ultraviolet emissions from flames.

A photograph of the optical transfer system is included as Figure 7. Radiation from flames within the field of view of the system, as defined by the acceptance angle of the f/8.6 spectrometer optics, was incident on the entrance slit of the spectrometer through the window in the combustion chamber. This window was a 75 mm diameter, 6 mm thick synthetic fused silica disc (Suprasil 2, supplied

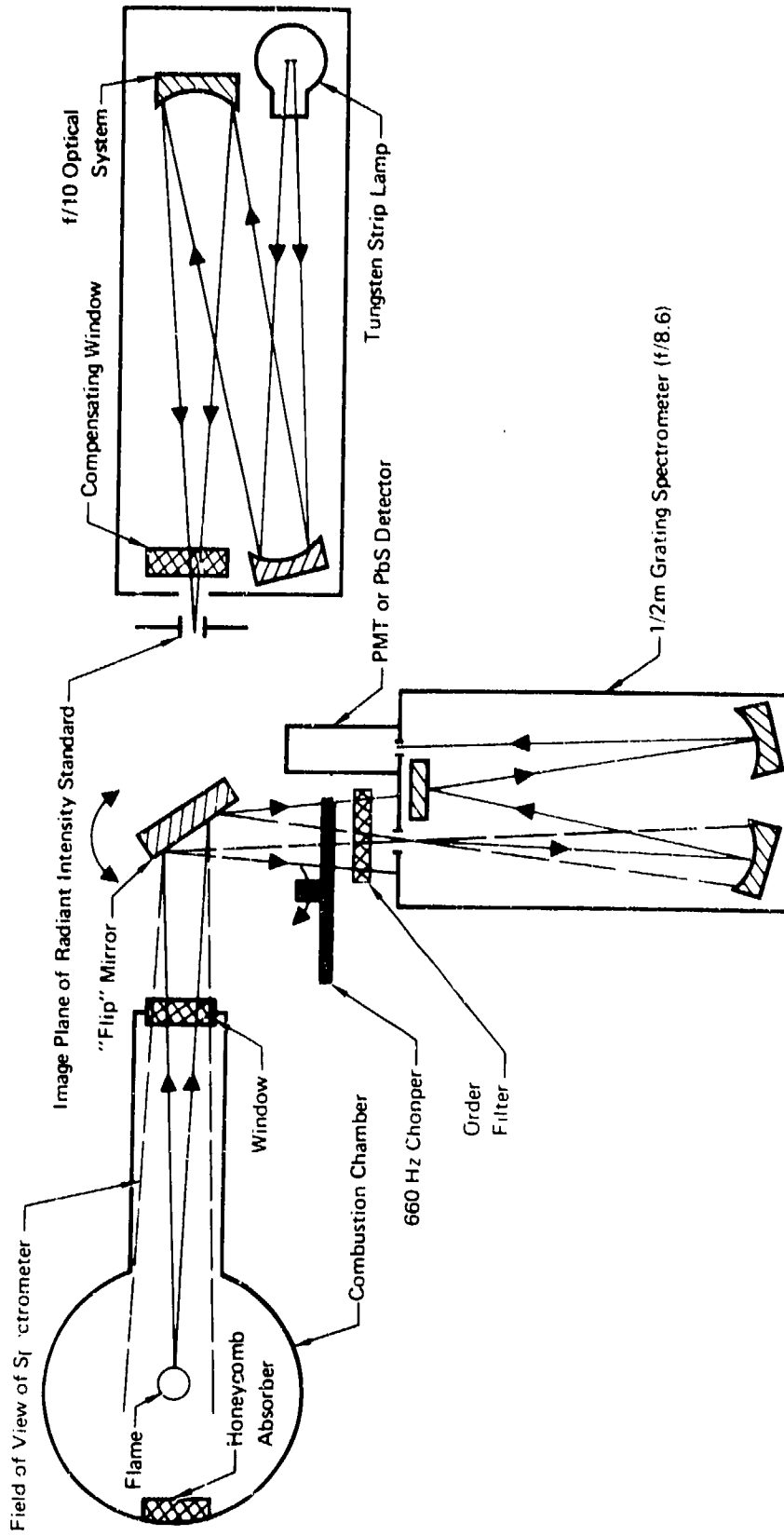
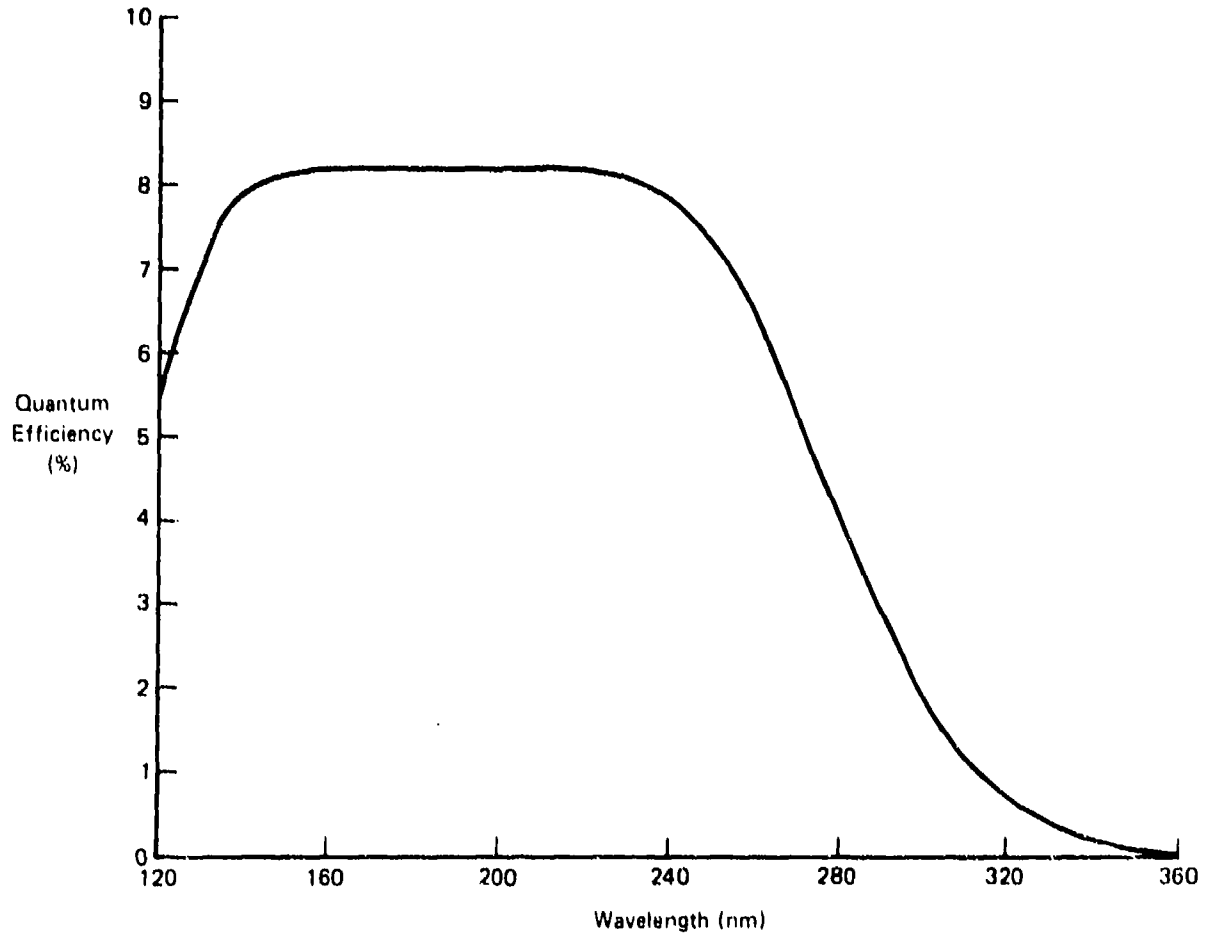


FIGURE 5 OPTICAL SYSTEM FOR SPECTRAL RADIANT INTENSITY MEASUREMENTS (0.2 - 2.6  $\mu\text{m}$ )



**FIGURE 6 SPECTRAL RESPONSE OF CESIUM TELLURIDE PHOTOCATHODE  
BEHIND MAGNESIUM FLUORIDE WINDOW  
(VARIAN/EMI DATA FOR THEIR MODEL #G-26H215 PHOTOMULTIPLIER)**

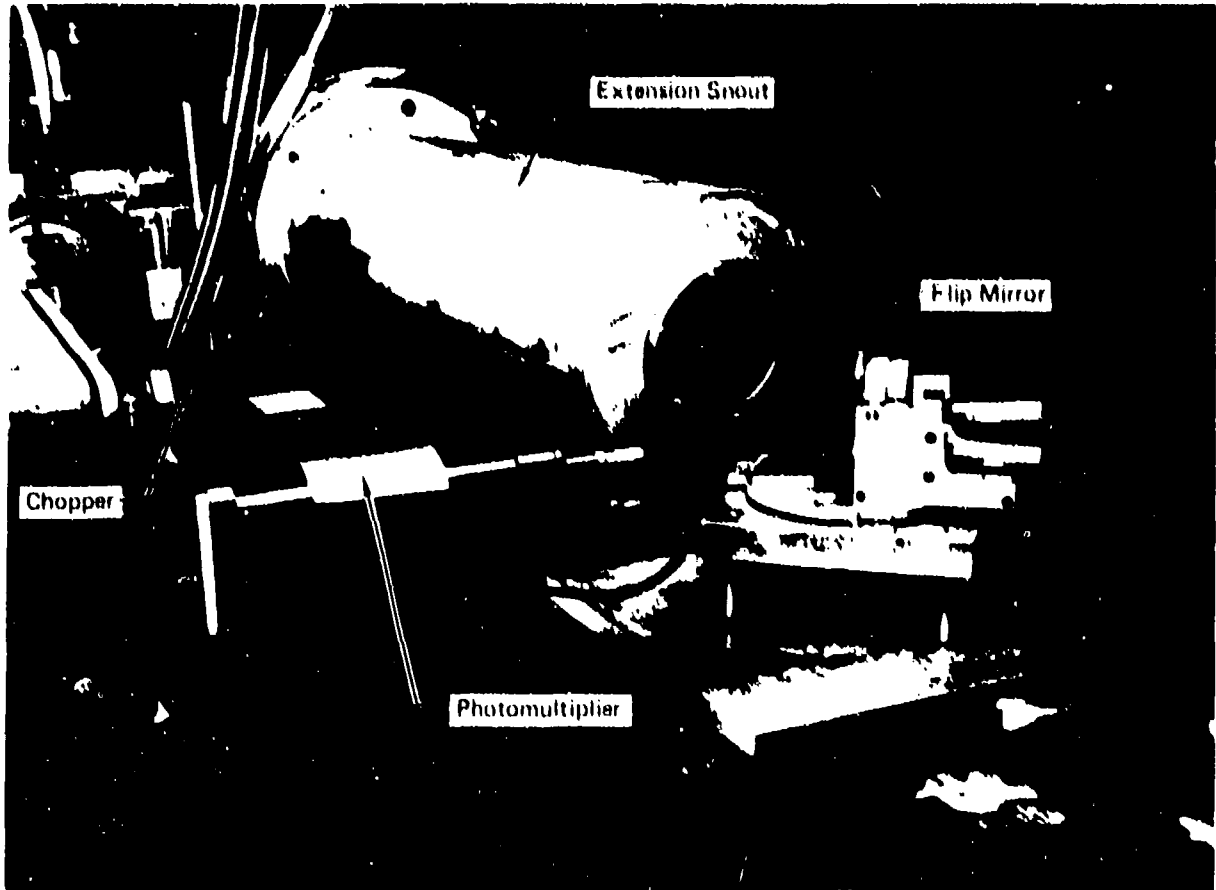


FIGURE 7 OPTICAL TRANSFER SYSTEM

AFAPL-TR-73-83

by Amersil Inc., New Jersey). The radiation from the flame was reflected onto the spectrometer slit by a rotatable "flip" mirror through a 660 Hz rotating-blade chopper and an absorbing order filter.

A secondary spectral radiant intensity standard was provided by the optical system shown in the upper right hand corner of Figure 5. A full-size image of the tungsten strip filament of a G.E. 30A/T24 lamp was formed by the f/10 optical system in the plane of the exit aperture. As described in paragraph 5 the radiance of this image was calibrated against a spectral radiance standard certified by the National Bureau of Standards. When a portion of this image was selected by a precision aperture a secondary radiant intensity standard was created. A fused-silica disc, identical to the combustion chamber window, was included in the radiance standard to compensate for absorption of optical radiation by that window.

The procedure adopted for the ultraviolet emission measurements was to scan the radiant intensity standard in all three spectral ranges at the beginning of each experimental day. For each range the aperture of the standard was changed to ensure that the standard spectra and the emission spectra from the flame being studied could both be recorded without adjustment of the gain settings of the amplifiers in the data acquisition system. The signal levels were determined in the course of preliminary experiments to establish the operational parameters.



The signal from the photomultiplier detector was a 660 Hz voltage proportional to the intensity of the radiation incident on the spectrometer. This voltage was demodulated with a Princeton Applied Research HR-8 Lock-In Amplifier which was referenced to a 660 Hz voltage from the chopper. A 0-10 V D.C. voltage from the amplifier provided the input to the data recording system. For the ultraviolet spectra the grating spectrometer was scanned at  $12.5 \text{ nm min}^{-1}$  with the spectrometer slit width set at 1 mm (1.6 nm bandwidth) and with the circuit time constant at 1 s.

An overall view of the equipment is shown in Figure 8.

b. Visible and Near Infrared Equipment

The equipment used to measure the visible and near-infrared emission spectra was almost identical to the ultraviolet equipment illustrated in Figure 5. Several components were changed: a new lamp was installed in the radiant intensity standard because the original lamp showed signs of aging; different diffraction gratings and order filters were used, as summarized in Table 2; and the detector was changed. For the wavelength range between 300 and 811 nm an EMI 9558QC photomultiplier with an S-20 photocathode was used, and this was replaced by a Kodak 20 mm x 4 mm lead sulphide cell, for the 800 nm ( $0.8 \mu\text{m}$ ) to  $2.65 \mu\text{m}$  range. The spectral responses of these detectors are shown in Figures 9 and 10. Between 300 and 811 nm



FIGURE 8 OVERALL VIEW OF THE OPTICAL EMISSIONS EQUIPMENT

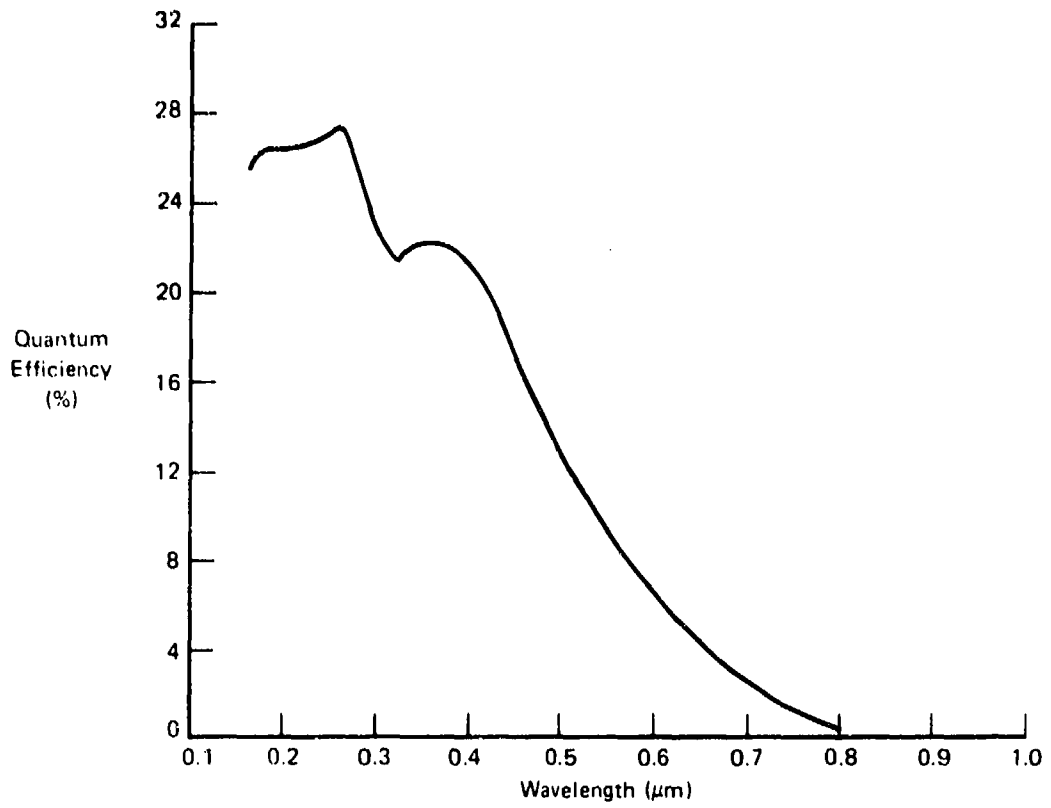


FIGURE 9 SPECTRAL RESPONSE OF THE EMI 9558QC PHOTOMULTIPLIER

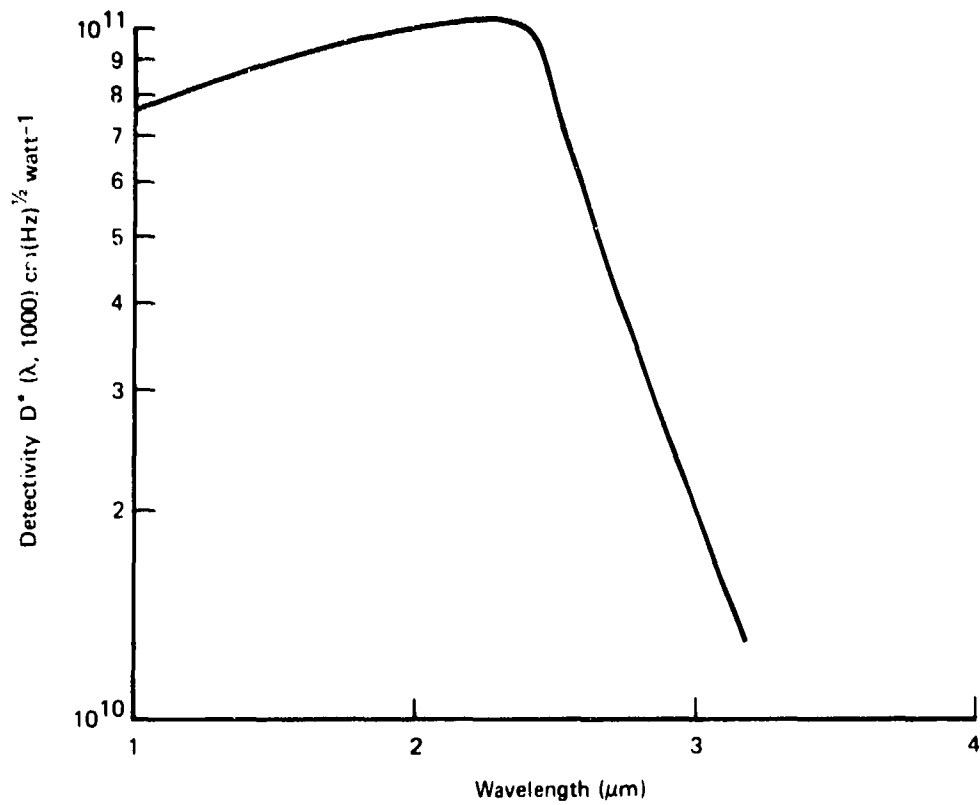


FIGURE 10 TYPICAL SPECTRAL RESPONSE OF A LEAD SULPHIDE DETECTOR

the spectrometer was scanned at  $25 \text{ nm min}^{-1}$ , the slits were set at 1 mm and the time constant was 1 s. From  $0.8 \text{ }\mu\text{m}$  to  $2.65 \text{ }\mu\text{m}$  the corresponding parameters were  $100 \text{ nm min}^{-1}$ ; 3 mm; and 1 s.

c. Far-Infrared Equipment

Entirely different equipment was utilized for spectral emission measurements at wavelengths in the  $2 \text{ }\mu\text{m}$  to  $15 \text{ }\mu\text{m}$  range (Figure 11). The grating spectrometer was replaced by a Block Engineering Model 165T Infrared Emission Spectrometer. This instrument is basically an oscillating interferometer cube with a built-in thermistor detector. The output of the detector is in the form of a complex interferogram and must be analyzed by a fast Fourier transform computer program. As described in Section 4, data was recorded on magnetic tape for subsequent computer reduction. The spectral response of the interferometer is shown in Figure 12.

The field of view of the interferometric spectrometer was such that the extension snout was not required on the combustion chamber. A 75 mm diameter, 6 mm thick potassium bromide window was mounted in the wall of the main chamber. For spectral calibration of the spectrometer an Electro Optical Industries  $1000^\circ\text{C}$  blackbody was installed in one arm of the optical system and a 10 mm, water-cooled aperture served as the radiant intensity standard.

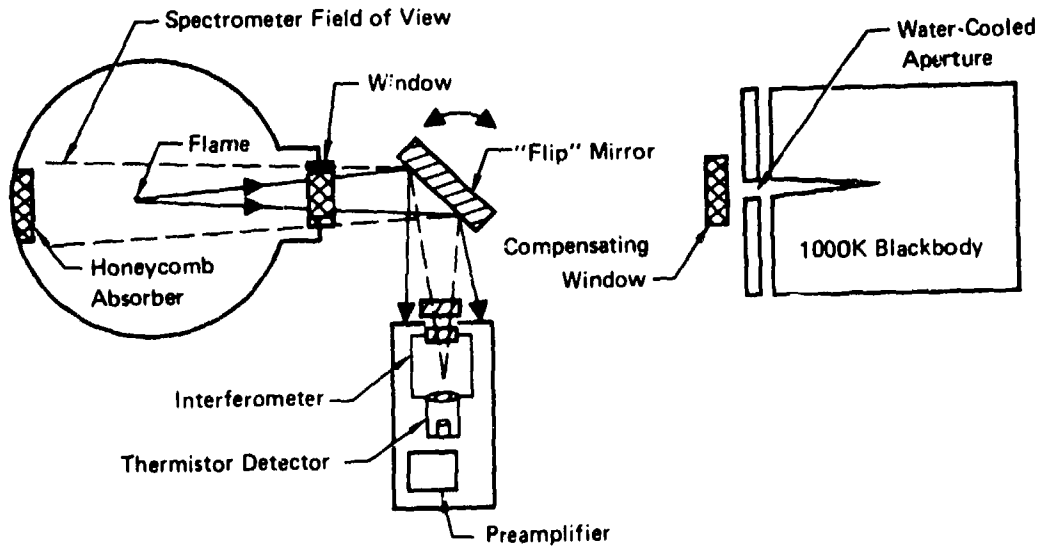


FIGURE 11 OPTICAL SYSTEM FOR SPECTRAL RADIANT INTENSITY MEASUREMENTS (2.0 - 15.0  $\mu\text{m}$ )

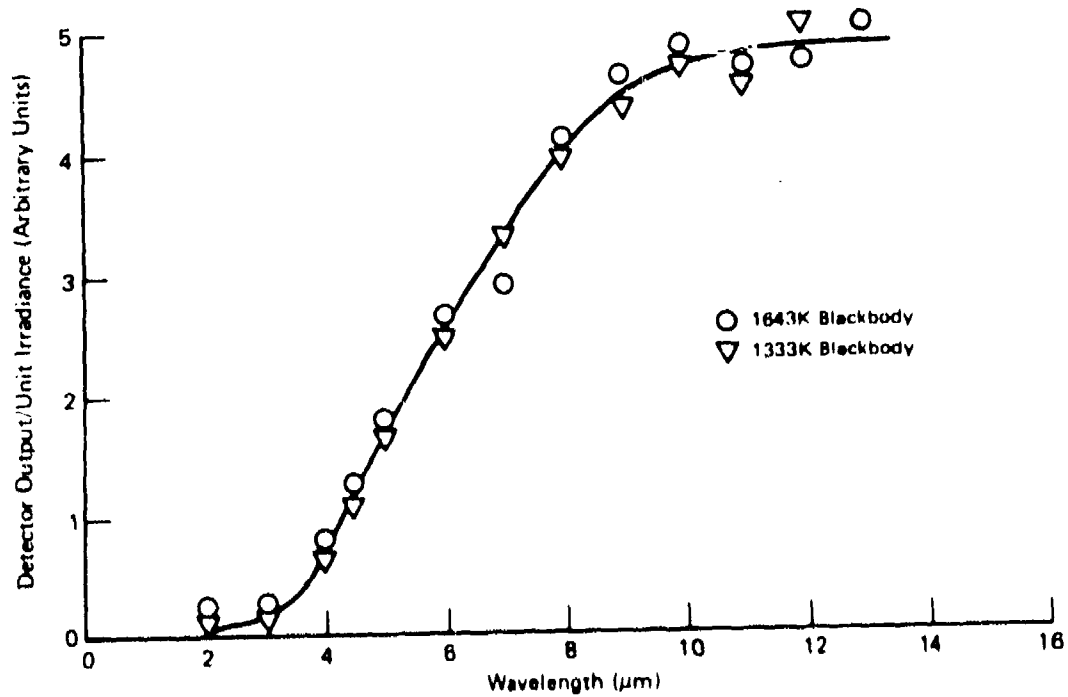


FIGURE 12 SPECTRAL RESPONSE OF THE BLOCK ENGINEERING 195T INTERFEROMETRIC SPECTROMETER

#### 4. DATA ACQUISITION AND REDUCTION

The components of the data acquisition system are identified in the diagram in Figure 13.

The experimental data was recorded in the memory of a Fabritek\* Model 1072 Instrument Computer. This instrument was used to convert the time variant analog data into 1024 12-bit digital words so that computer techniques could be utilized to reduce the data to calibrated spectra.

During experiments with the slow-scanning grating spectrometer the instrument computer address scan was synchronized with the wavelength scan of the spectrometer, and only a single scan was recorded. For the far infrared measurements with the interferometric spectrometer, up to 256 one-second scans were signal-averaged in the computer memory to establish good signal-to-noise ratios. After each run the contents of the memory were dumped onto digital magnetic tape.

Each set of data from a burning flame was recorded on a magnetic tape on which calibration data for the appropriate wavelength range had been previously recorded. At the end of each day the tape was hand-

\*Now Nicolet Inc.

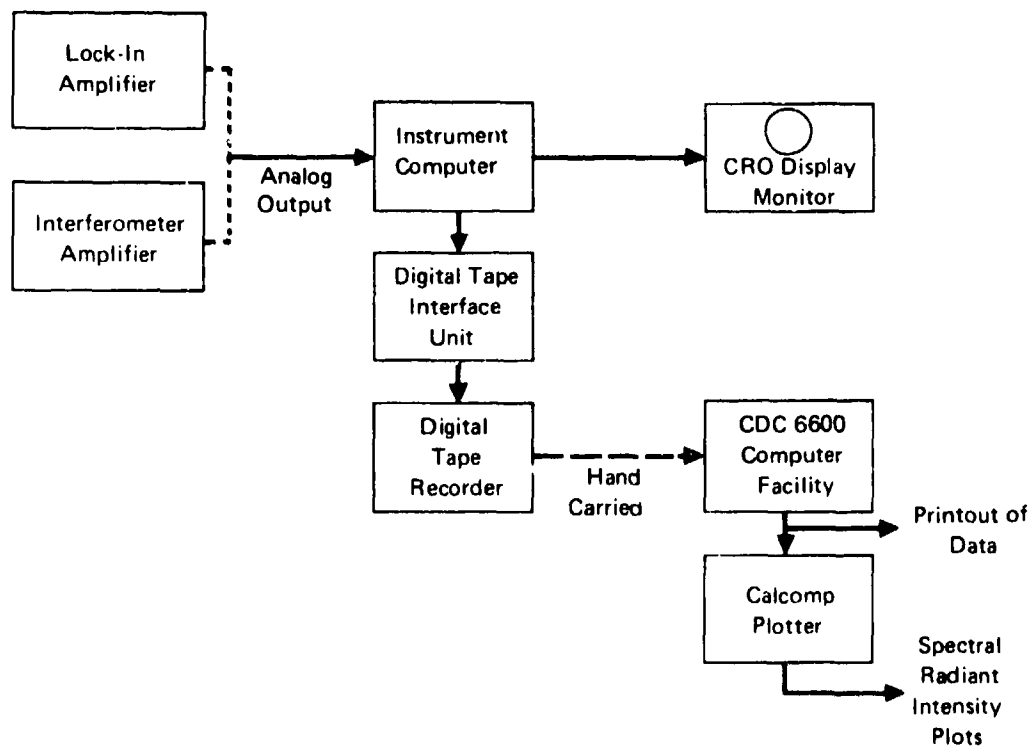


FIGURE 13 DATA ACQUISITION AND REDUCTION SYSTEM



carried to a large computer facility to be reduced. After inspection of the computer printouts the decision was made to prepare Calcomp<sup>(TM)</sup> graphical plots of the calibrated spectra.

The data reduction wrought by the computer programs was simple in concept, but it was extremely powerful in that a multiplicity of normalized data was generated with a minimum of manual effort. Each of the program listings is included as Appendix B to this report.

The spectral radiant intensity of the flame  $J_F(\lambda)$  was computed from the expression:

$$J_F(\lambda) = J_S(\lambda) \frac{V_F(\lambda)}{V_S(\lambda)} \cdot \left(\frac{d_F}{d_S}\right)^2 \quad (\text{W nm}^{-1} \text{ sr}^{-1}) \quad (2-1)$$

where:

$J_S(\lambda)$  is the spectral radiant intensity of the calibration source ( $\text{W nm}^{-1} \text{ sr}^{-1}$ ),

$V_F(\lambda), V_S(\lambda)$  are the voltages generated in the computer memory by the flame and the calibration source respectively (V),

$d_F(\lambda), d_S(\lambda)$  are the separations between the entrance aperture of the spectrometer and the flame or calibration source (m).

At each wavelength the value of  $J_S(\lambda)$  was computed from Planck's expression for the radiance of a blackbody,  $N_S(\lambda)$ :

$$J_S(\lambda) = A_S \cdot N_S(\lambda) = \frac{A_S}{\pi} \cdot \frac{C_1}{\lambda^5} \left[ \exp\left(\frac{C_2}{\lambda T(\lambda)}\right) - 1 \right]^{-1} \quad (2-2)$$

where:

$A_s$  is the area of the exit aperture on the calibration source ( $m^2$ ),

$T(\lambda)$  is the equivalent blackbody temperature of the calibration source at wavelength  $\lambda$  ( $^{\circ}K$ ),

$C_1, C_2$  are constants.

The values of  $T(\lambda)$  were determined from the calibration experiments, as described in paragraph 5.

The computer program illustrated in Appendix B reduced the data using Equations 2-1 and 2-2 and provided graphical plots of the values of  $V_F(\lambda)$ ,  $V_S(\lambda)$  and the calibrated value of  $J_F(\lambda)$ . Printouts of these quantities were also produced, together with values of  $N_S(\lambda)$  for comparison with the calibration of the source.

Reproductions of the raw computer plots are included in Figures 14 through 16. These data were taken during an experiment with JP-4 burning in a sea level atmosphere. Figure 14 illustrates the calibration run and is a plot of  $V_S(\lambda)$  vs  $\lambda$ ; Figure 15 is a plot of  $V_F(\lambda)$  vs  $\lambda$ , and Figure 16 is the end product of the data reduction; a plot of the spectral radiant intensity,  $J_F(\lambda)$ , against the wavelength,  $\lambda$ .

To cover the wavelength range 0.2  $\mu m$  to 15  $\mu m$  a total of ten scans were taken and the data was plotted on ten different computer

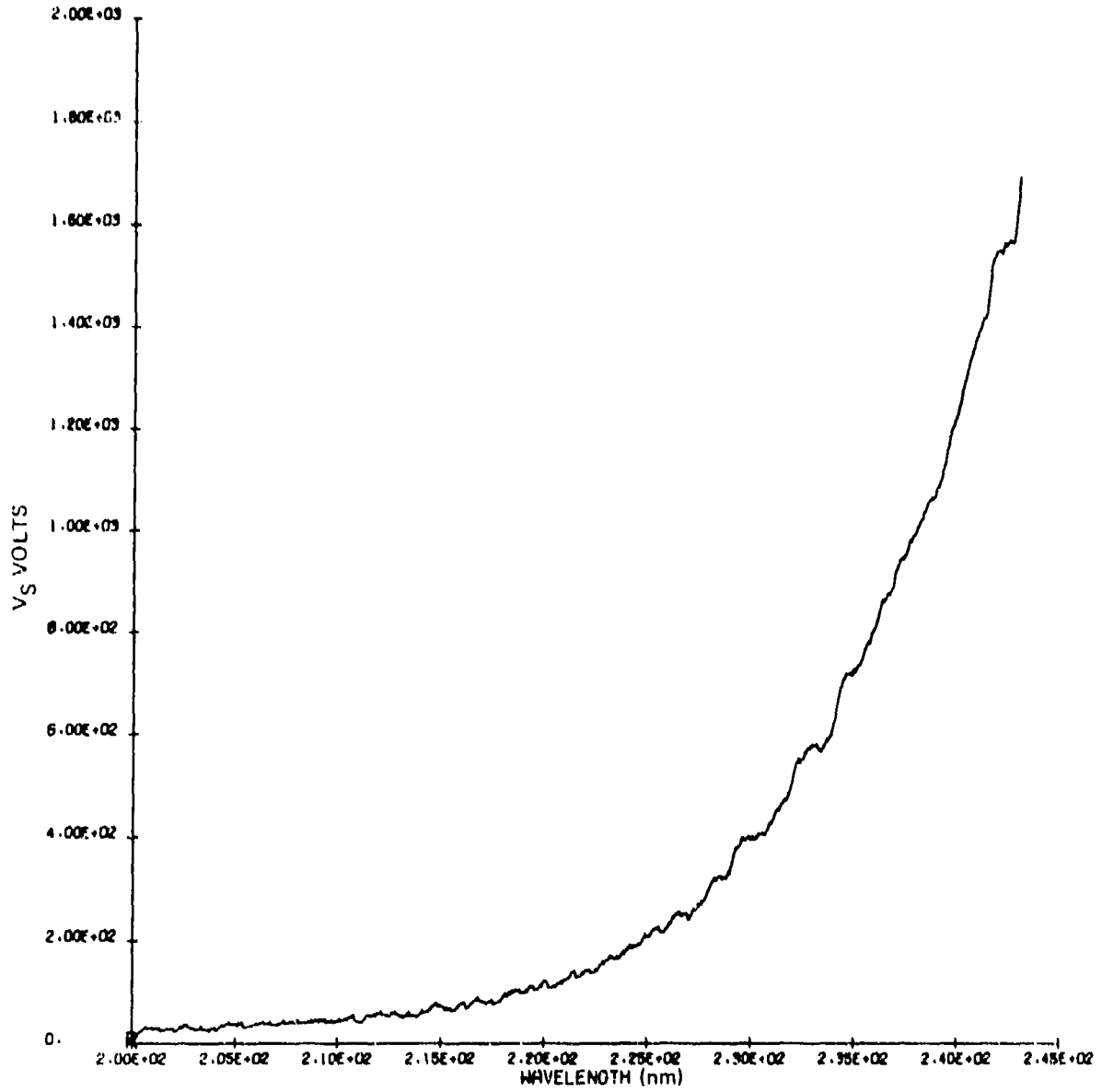


FIGURE 14 TYPICAL COMPUTER PLOT OF UNCALIBRATED DATA FROM A SPECTRAL SCAN OF THE RADIANT INTENSITY STANDARD

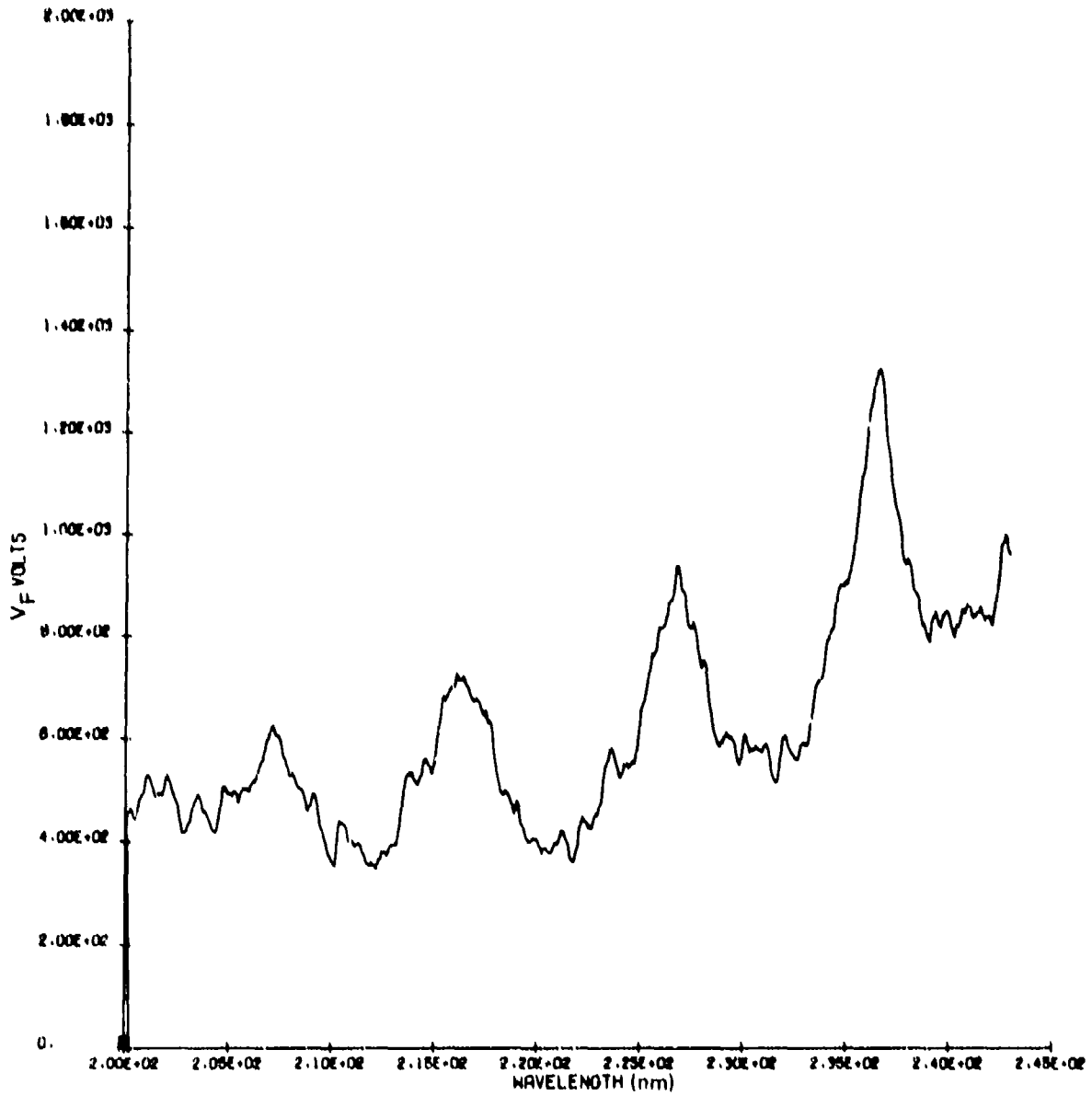


FIGURE 15 TYPICAL COMPUTER PLOT OF UNCALIBRATED DATA FROM A SPECTRAL SCAN OF A JP-4 FLAME

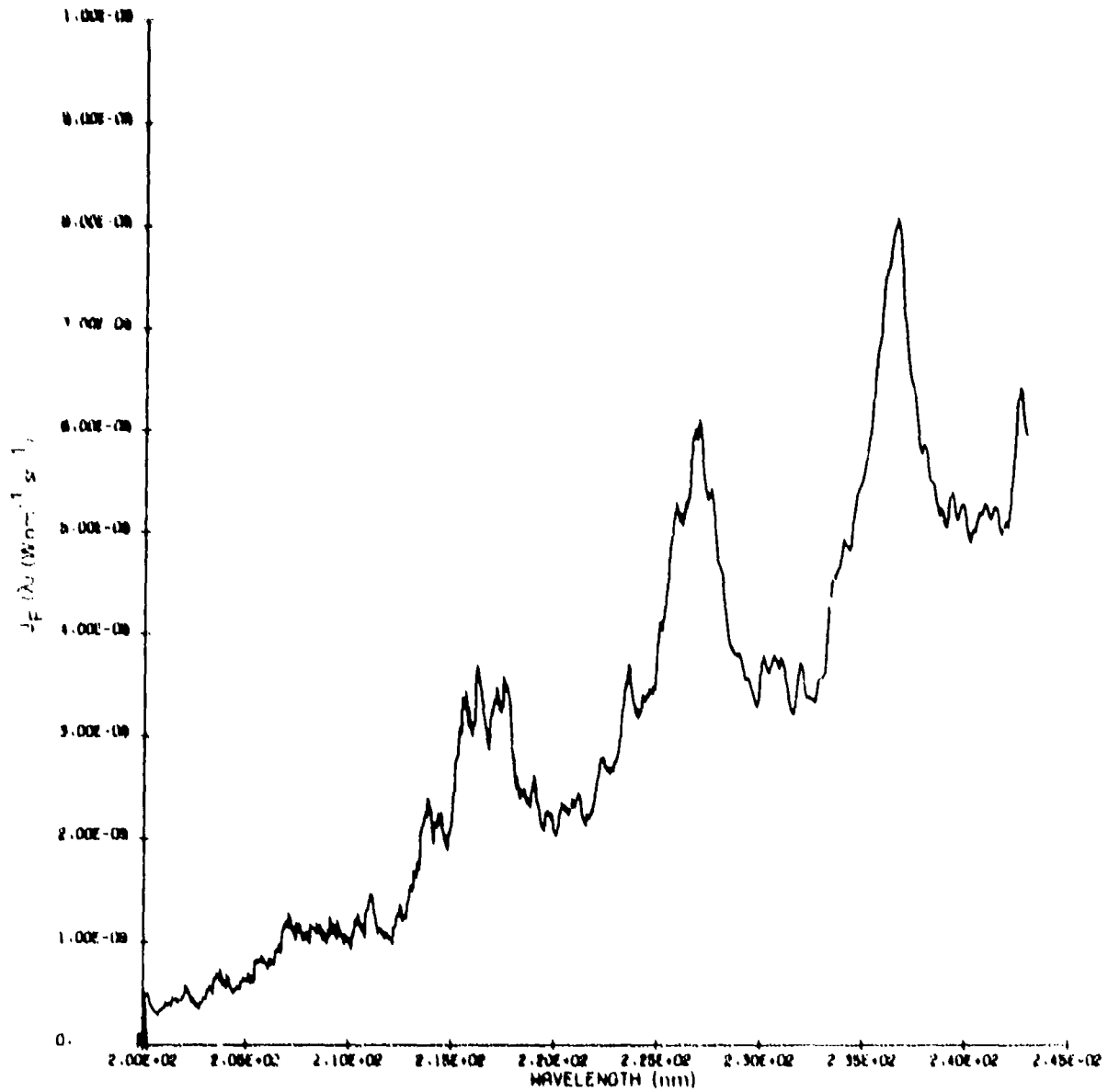


FIGURE 16 TYPICAL COMPUTER PLOT OF THE SPECTRAL RADIANT INTENSITY OF A JP-4 FLAME

plots. For presentation in this report composite curves were prepared on a Hewlett-Packard 9810A Programmable Calculator equipped with digitizer and plotter accessories.

## 5. CALIBRATION OF THE OPTICAL SYSTEM

To determine the absolute spectral radiant intensity of the burning aircraft fluids the optical system was calibrated against NBS-traceable standards, in the 200 nm to 2.65  $\mu\text{m}$  range and against a blackbody source in the 2.0  $\mu\text{m}$  to 15  $\mu\text{m}$  range (Figures 5 and 11). Daily calibration runs were made over the appropriate spectral range before each experimental series, and the data was stored on the magnetic tape.

### a. Calibration Standards (200 nm - 2.65 $\mu\text{m}$ )

The spectral emission data in the 200 nm to 2.65  $\mu\text{m}$  range was calibrated using the radiant intensity standard optical system illustrated in Figure 5. This secondary standard was calibrated by the McDonnell Bureau of Standards (MBS) against their NBS-calibrated standards. To cover the complete range over which the secondary standard was calibrated (225 nm to 2.5  $\mu\text{m}$ ) three separate experiments were necessary (see Table 3). This fragmentation of the range was caused by the limited calibration of the available primary standards, and also by the replacement of the original aged 6V lamp in the secondary standard by a new 3.5V lamp after the ultraviolet series of measurements. For the first two ranges, covering the 225 nm to 800 nm

TABLE 3 CALIBRATION OF THE SECONDARY STANDARD FOR SPECTRAL RADIANT INTENSITY MEASUREMENTS

Wavelength Range ( $\mu\text{m}$ )	Secondary Standard	Primary Standard	Optical Calibration System	
			Optical System	Detector
0.225-0.32	G.E. 30A/6V Spectral Radiance Lamp and Imaging System	NBS Calibrated G.E. 30A/6V Spectral Radiance Lamp	McDonnell Bureau of Standards Spectroradiometer Using a Cary Instruments Co. (P. Model 14 Monochromator	EMI 95580C Photomultiplier
0.30-0.80	G.E. 30A/3.5V Spectral Radiance Lamp and Imaging System	NBS Calibrated G.E. 30A/6V Spectral Radiance Lamp		EMI 95580C Photomultiplier
0.80-2.5	G.E. 30A/3.5V Spectral Radiance Lamp and Imaging System	Electro-Optical Ind. Model 146 Blackbody Radiation Source; NBS Calibrated Pyrometer Strip Lamp	Kodak P15 Cell	
2.5-15.0	Electro-Optical Ind. Model 143 Blackbody Radiation Source			

band, an NBS-calibrated tungsten strip radiance standard was used in conjunction with an Applied Physics Corporation Model 14 Monochromator equipped with an EMI 9558QC photomultiplier. Focussing optics were used to transfer images, first of the radiant intensity standard and then of the standard lamp, onto the entrance slit of the monochromator.

The calibration curve for the original or First Radiant Intensity Standard, resulting from such a comparison, is shown in Figure 17; the calibration certificate is included in Appendix A. The curve in Figure 17 is plotted in terms of the equivalent blackbody temperature for the secondary standard at each wavelength. This parameter was used as it varied by only a few percent over the wavelength range calibrated, while the intensity of the emitted radiation varied by several orders of magnitude. As the calibration curve had to be extrapolated to cover wavelengths below 225 nm, and interpolated between the calibration points, it was important that a realistic curve fit be made to the calibration data. The least-squares third order polynomial fitted to the data in Figure 17 was used in the data reduction computer programs.

For wavelengths in the 0.8  $\mu\text{m}$  to 2.65  $\mu\text{m}$  range the Second Radiant Intensity Standard was calibrated against a blackbody, the temperature of which was established with an NBS-calibrated pyrometer strip lamp. Despite the change in primary standards and the change of detector from a photomultiplier tube to a lead sulphide cell, excellent



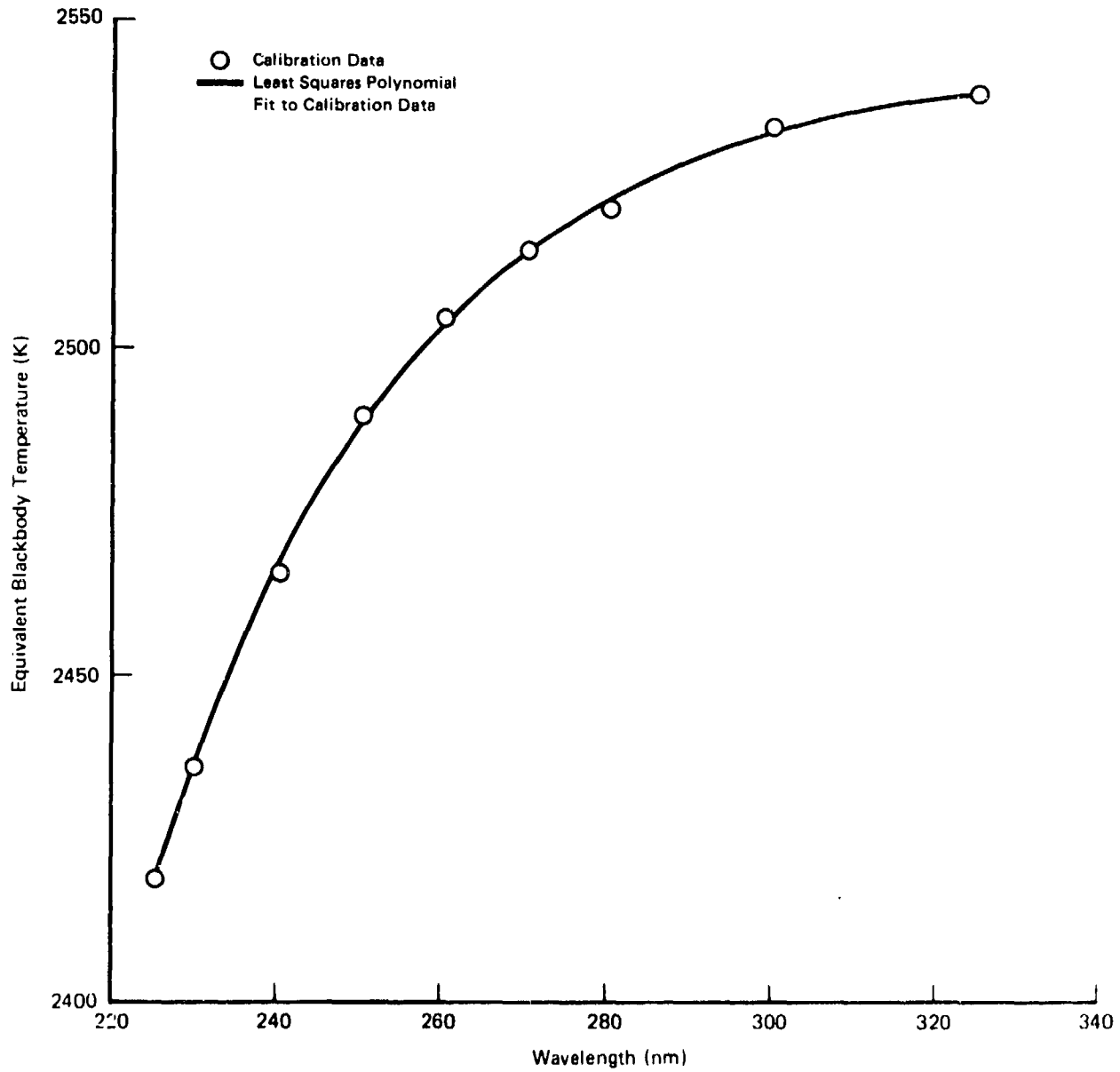


FIGURE 17 CALIBRATION CURVE FOR THE FIRST RADIANT INTENSITY STANDARD (200-320nm)

continuity was observed in the calibration at  $0.8 \mu\text{m}$  of the second radiant intensity standard. This continuity is evident in the data plotted in Figure 18.

b. Calibration Standard ( $2.0 \mu\text{m}$  to  $15.0 \mu\text{m}$ )

No NBS-traceable standards for far infrared wavelengths were available and so the interferometric spectrometer was calibrated with a  $1000^\circ\text{C}$  blackbody. It was established that the temperature of this source was stable within  $\pm 1^\circ\text{C}$  and the manufacturer certified that the emissivity of the cavity was  $0.99 \pm 0.01$ . A water-cooled aperture 10 mm in diameter was used to define the radiant intensity of this standard.

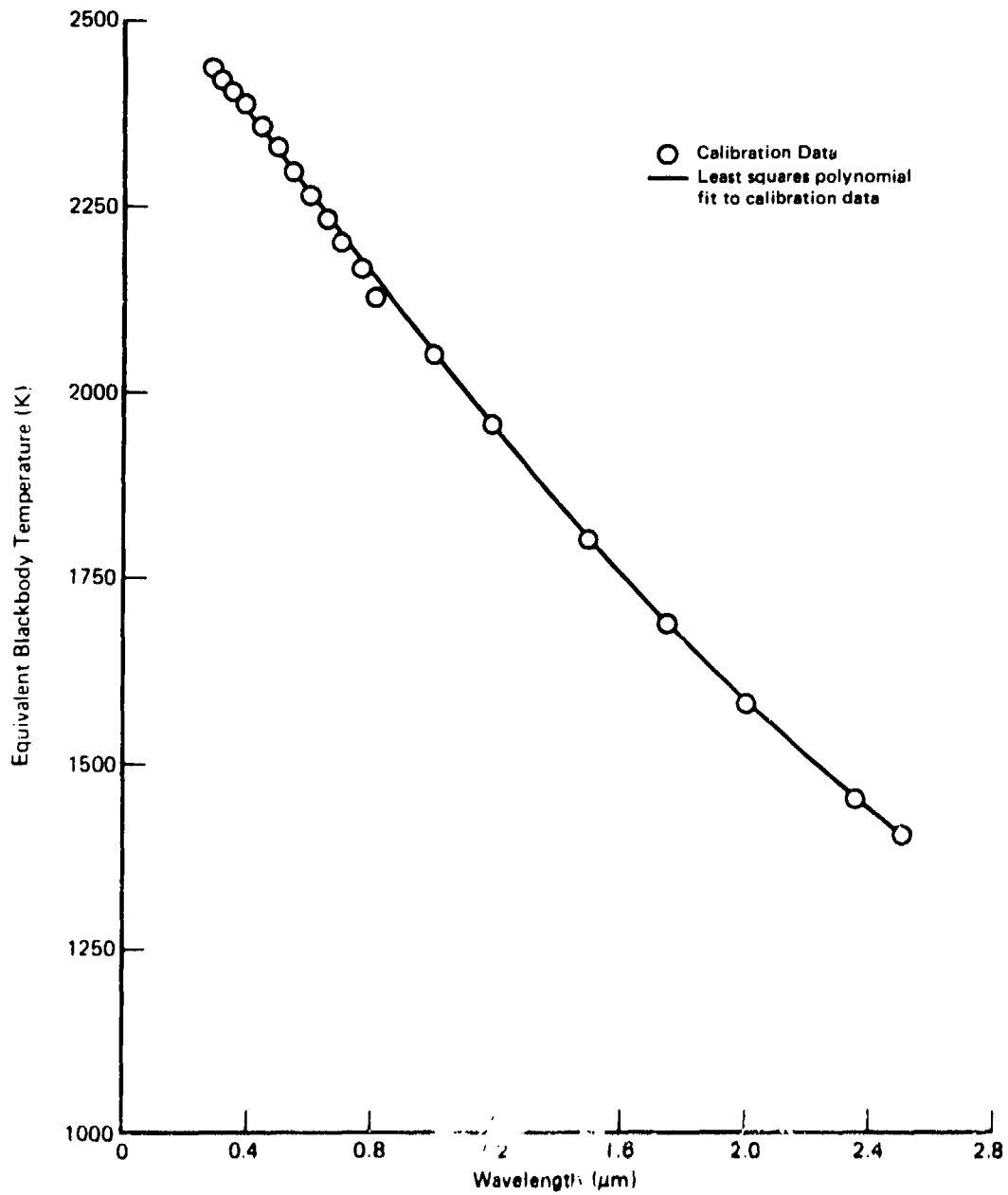


FIGURE 18 CALIBRATION CURVE FOR THE SECOND RADIANT INTENSITY STANDARD  
(300nm - 2.5μm)

### SECTION III

#### EXPERIMENTAL RESULTS

Spectral emission data was accumulated over ten spectral ranges on six fuels, burning at a minimum of four altitudes; over 250 radiant intensity curves were generated. In order to present and discuss this plethora of information without generating a volume of biblical proportions a good deal of summarization was necessary. Computer-generated spectral radiant intensity curves were reduced to composite curves using a Hewlett-Packard 9810A Programmable Computer equipped with digitizing and plotting accessories. To further ease the problem of data presentation the experimental results are discussed in three sections corresponding to the ultraviolet, the visible and near infrared, and the far infrared experimental series.

#### 1. ULTRAVIOLET EMISSION SPECTRA (200 nm - 320 nm)

This region is of considerable interest to designers, manufacturers and users of aircraft fire detectors because of the increasing use of solar-blind, ultraviolet sensors as the basic element in detection systems. The wavelengths of particular interest lie between a lower limit of approximately 200 nm, set by the absorption edge of many detector window materials and the absorption by atmospheric oxygen and an upper limit of 280 nm, above which solar radiation penetrates the ozone belts around the earth. In this study the ultraviolet measure-

ments were extended out to 320 nm to include the strong emission bands characteristic of the OH radical at 310 nm.

a. Sea Level Measurements

Each of the six fuels was burned in the laboratory atmosphere under the fume hood, as described in paragraph 1. Spectral radiant intensity data for JP-4 is shown in Figure 1 (a) through (c).

These curves were drawn from computer-generated curves of the type reproduced in Figure 16 (Figure 19 (a) is a replica of Figure 16), and they illustrate the strong band structure of the spectral emissions. Identification of the bands will be discussed in Section IV. Across the 200-320 nm range the spectral radiant intensity of the flame varied two orders of magnitude and the composite plot in Figure 20 emphasizes this distribution. To provide the reader with data in a more useable form the three ranges have been condensed onto one curve of the type shown in Figure 21. This format with split vertical scales results in easier comparisons of data.

Data recorded on JP-5 burning at sea level (Figure 22) is almost identical to that for JP-4. The spectral bands are common to both fuels, and the intensities of the peaks are very similar except at 310 nm. Similar results were obtained for JP-8 (Figure 23). The limited variance in the data for three dissimilar hydrocarbon fuels

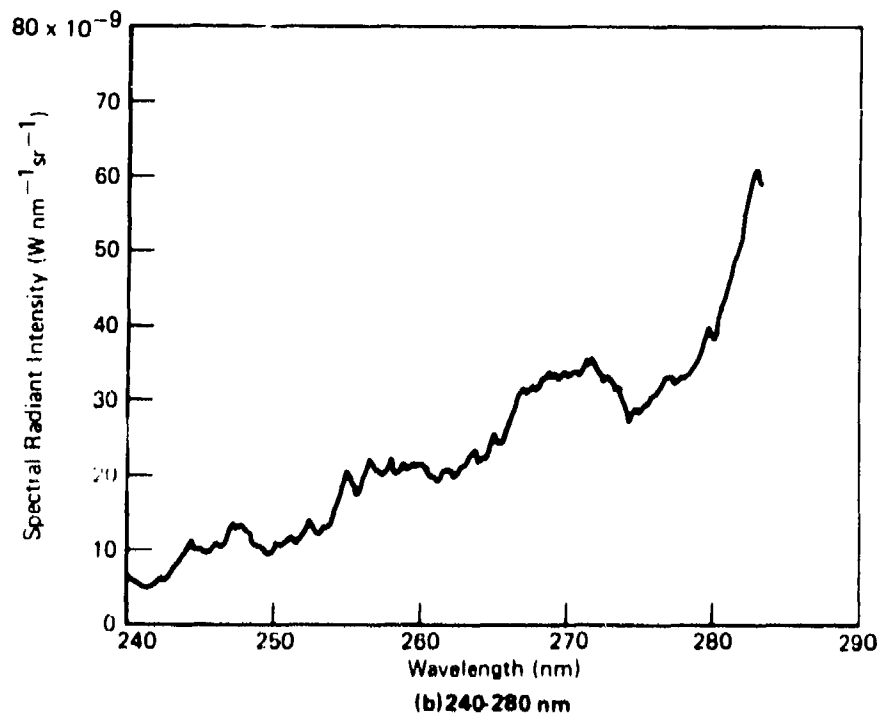
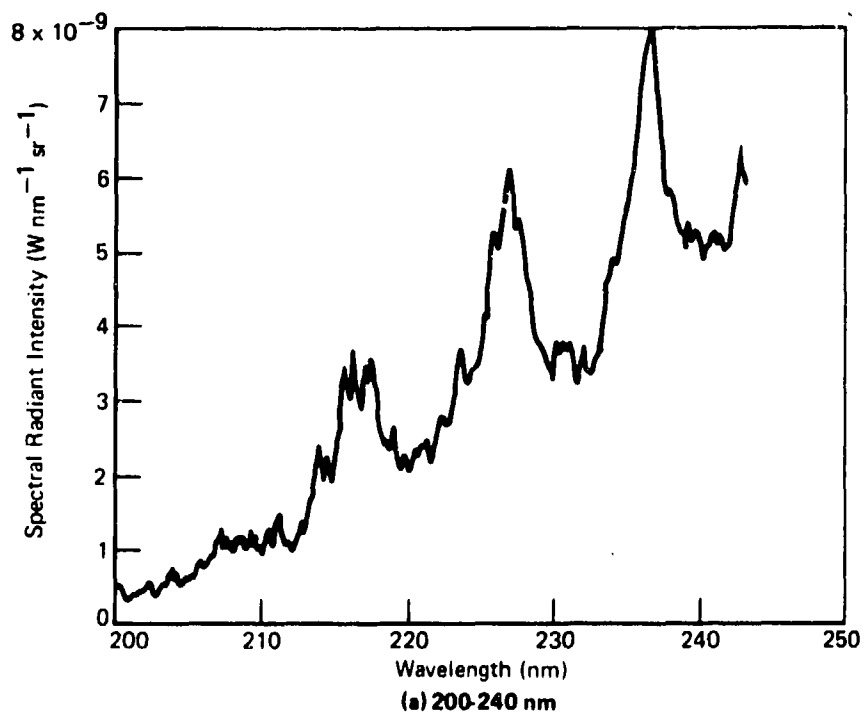


**FIGURE 19 SPECTRAL RADIANT INTENSITY OF JP-4 BURNING AT SEA LEVEL, OVER THE THREE WAVELENGTH RANGES SCANNED IN THE MIDDLE ULTRAVIOLET**

CONTINUED

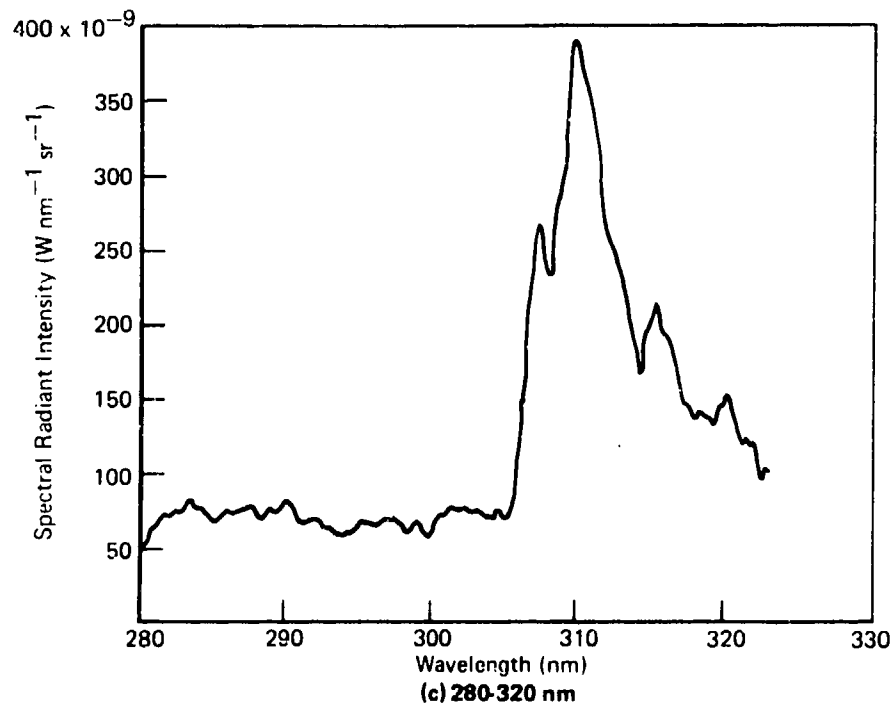


FIGURE 19 SPECTRAL RADIANT INTENSITY OF JP-4 BURNING AT SEA LEVEL,  
OVER THE THREE WAVELENGTH RANGES SCANNED  
IN THE MIDDLE ULTRAVIOLET

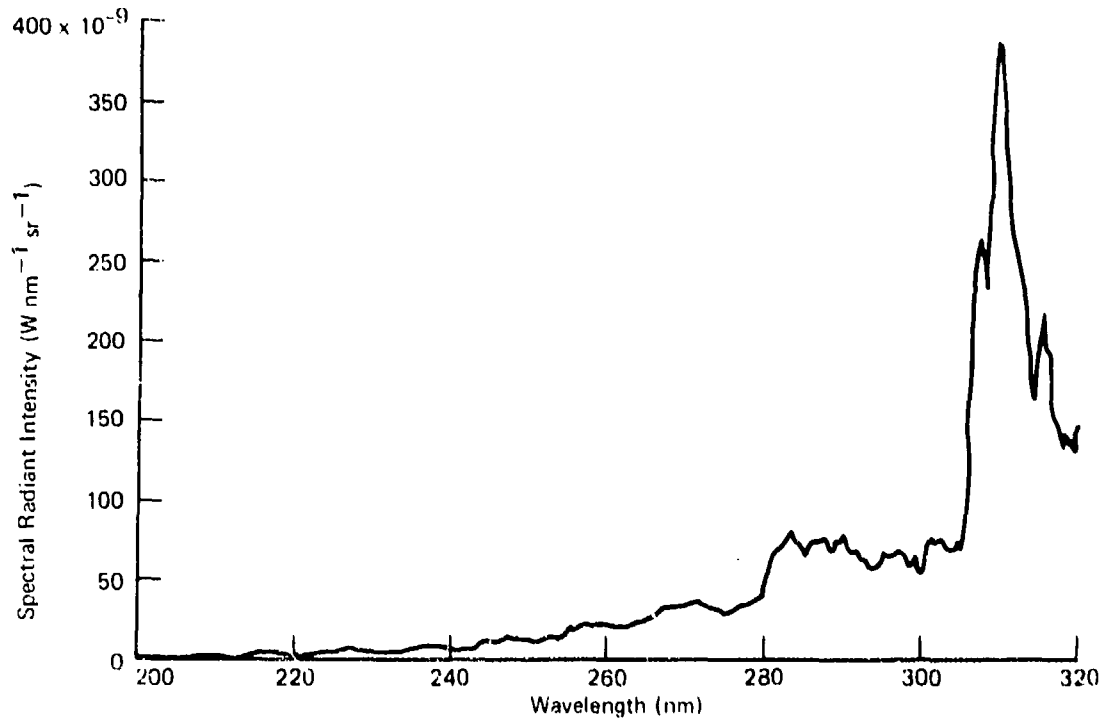


FIGURE 20 THE ULTRAVIOLET EMISSIONS FROM JP-4 BURNING AT SEA LEVEL

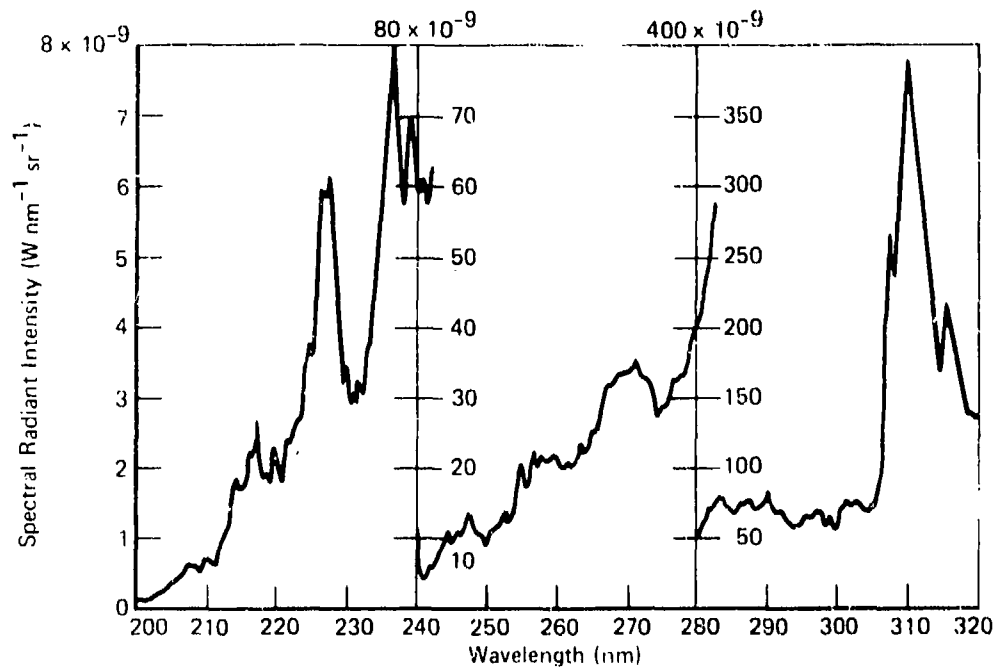


FIGURE 21 SPECTRAL RADIANT INTENSITY OF JP-4 BURNING AT SEA LEVEL (200-320 nm)



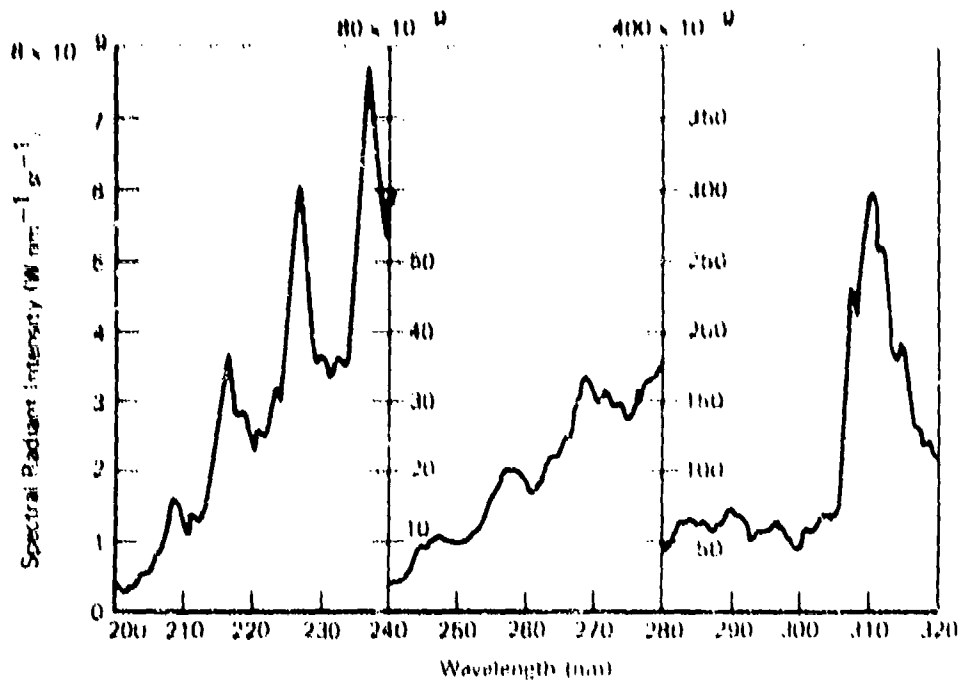


FIGURE 22 SPECTRAL RADIANT INTENSITY OF JP-5 BURNING AT SEA LEVEL (200-320 nm)

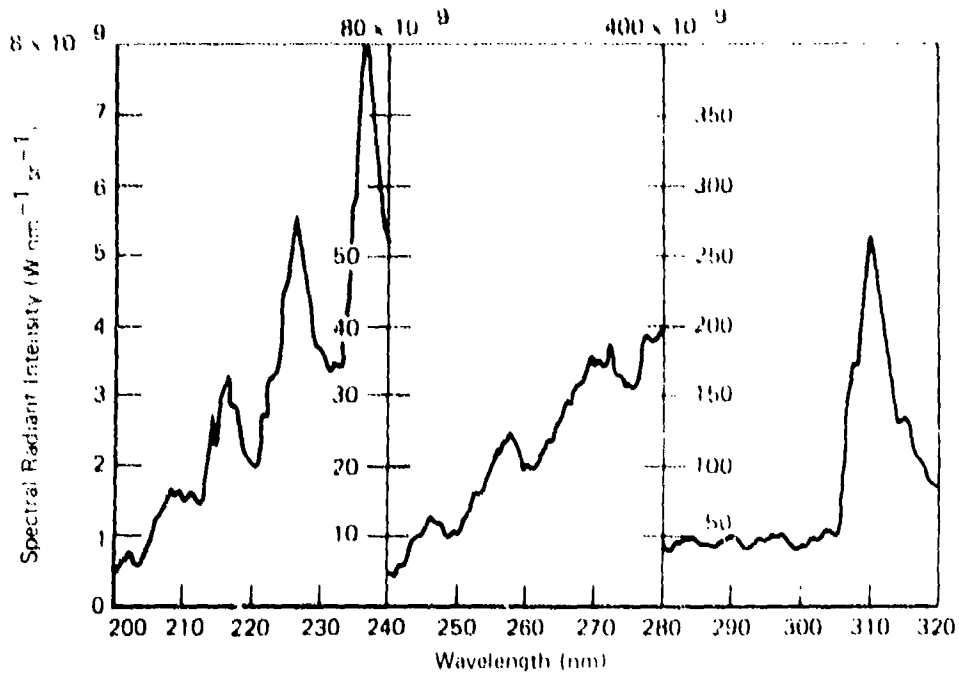


FIGURE 23 SPECTRAL RADIANT INTENSITY OF JP-8 BURNING AT SEA LEVEL (200-320 nm)

made it unnecessary to consider batch variations or subtle changes in such parameters as the aromatic content or distillation point.

Spectral curves for Aviation Gasoline, MIL-H-56060, and MIL-O-68-5, are drawn in figures 24, 25 and 26, respectively. The principal feature of these curves, compared to the JP-series data, is the appearance of different emission bands. There was little overall change in the total energy emitted by the six flames as demonstrated in a later section of this report.

b. High Altitude Experiments

The aircraft fuels burned readily at high altitudes in the combustion chamber illustrated in Figure 2. Each of the JP-series fuels burned with a steady flame, once the convection in the chamber was controlled by installation of the automotive air filter. Aviation gasoline flames were more difficult to control and tended to be unrepeatable; but, with persistence, spectral data were recorded. Both the hydraulic fluids defied all attempts to generate stable flames on the reduced pressure environment. An apparent cause of the problem was fractional distillation of the lighter fractions in the fluid leaving a viscous residue which obstructed the nozzle.

In preliminary combustion measurements it was established that stable flames could be maintained up to altitudes of 35,000 feet (190 torr). At higher altitudes (lower pressures) the flame would self extinguish.

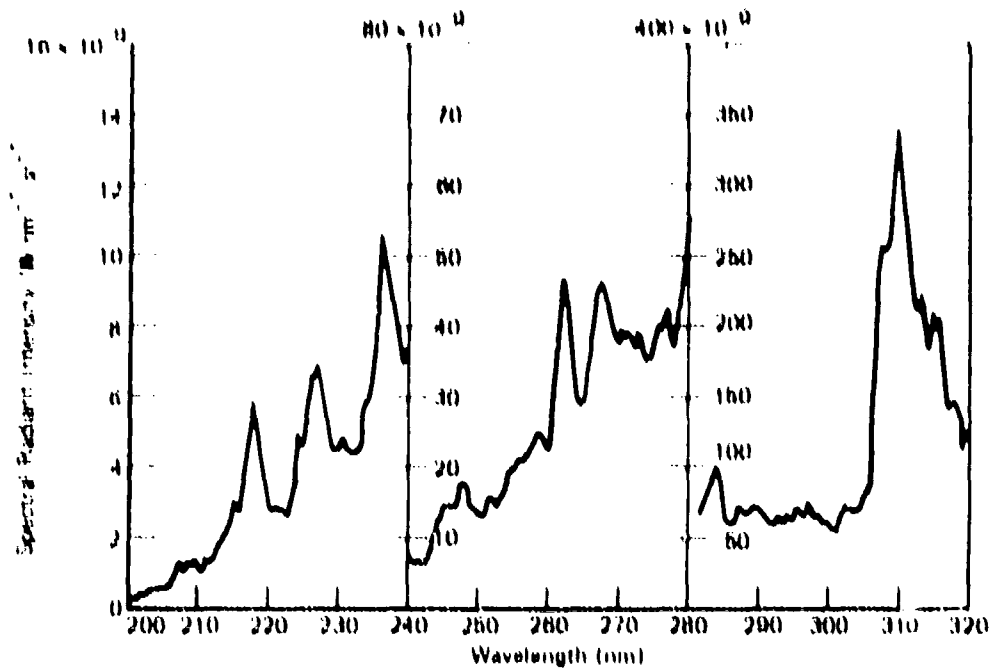


FIGURE 24 SPECTRAL RADIANT INTENSITY OF AVIATION GAS BURNING AT SEA LEVEL (200-320 nm)

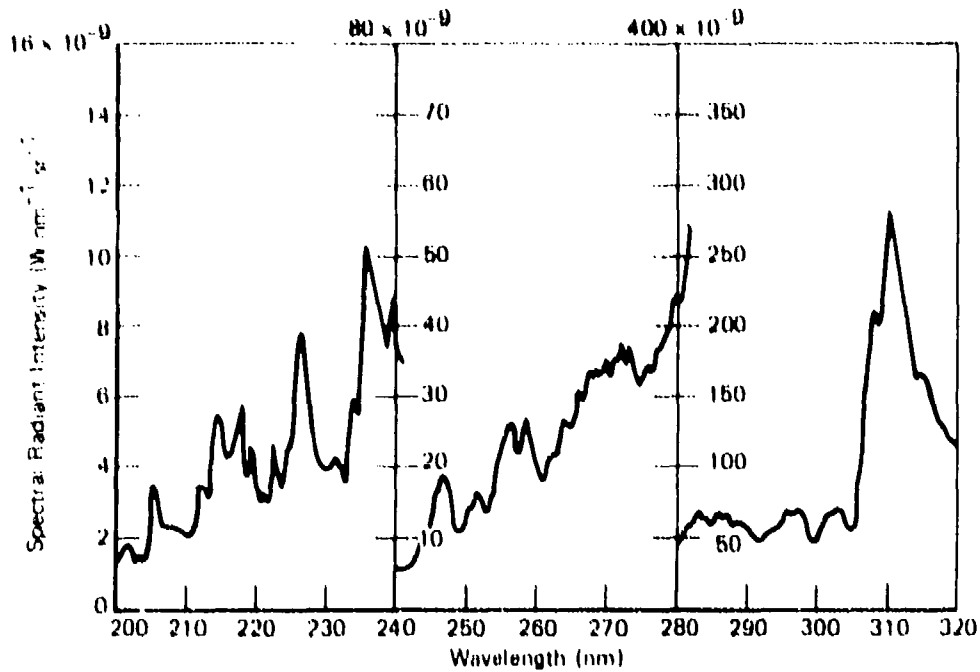


FIGURE 25 SPECTRAL RADIANT INTENSITY OF MIL-H-5606 BURNING AT SEA LEVEL (200-320 nm)

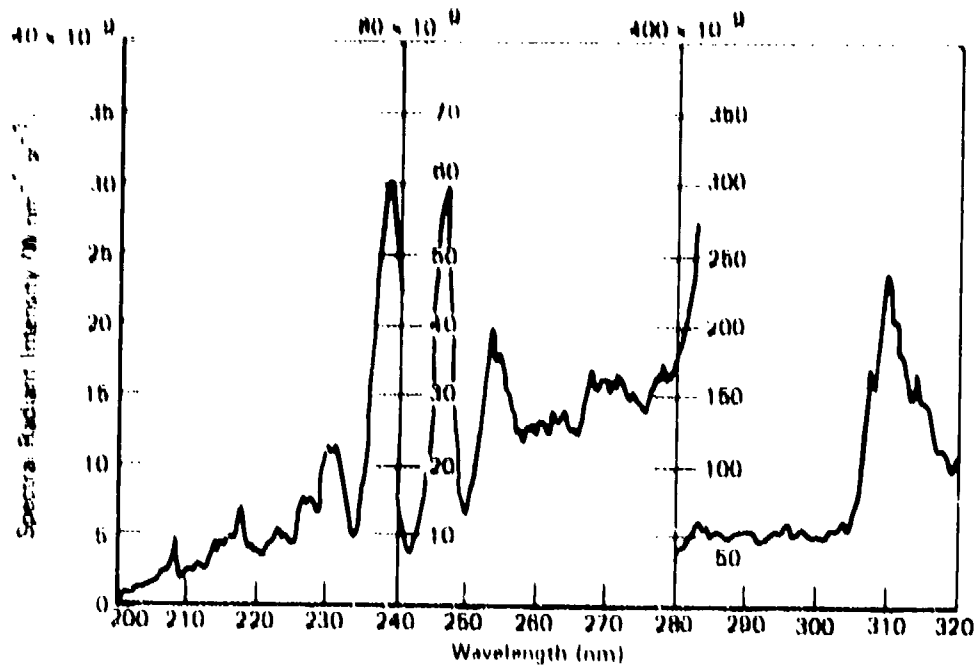


FIGURE 26 SPECTRAL RADIANT INTENSITY OF MLO-68-5 BURNING AT SEA LEVEL (200-320 nm)

Spectral emission data were recorded at 18,000 feet (380 torr), 24,000 feet (305 torr), and 35,000 feet (190 torr). Results of a series of experiments on JP-4 are shown in Figure 27; only three altitudes, including sea level, are represented for the sake of clarity. Similar results were obtained for the other fuels.

It is apparent that the radiation emitted in the ultraviolet region by JP-4 flames increases with increasing altitude. This increase is particularly marked at the peaks in the spectra; the peak at 215 nm is more than ten times stronger at 35,000 feet than at sea level.

c. Integral Radiant Intensity

Spectral radiant intensity curves such as those illustrated in Figure 19 through 27 provide important information on the distribution of the emitted radiation. However, the designer of a fire detection system must be concerned with the total energy emitted by the fire in the spectral range of the sensor. This range is established by the 200 nm lower limit of the transparency of the window materials and the atmosphere, and the upper wavelength limit of the sensor sensitivity; this latter parameter can be controlled by the selection and preparation of the photosensitive surfaces.

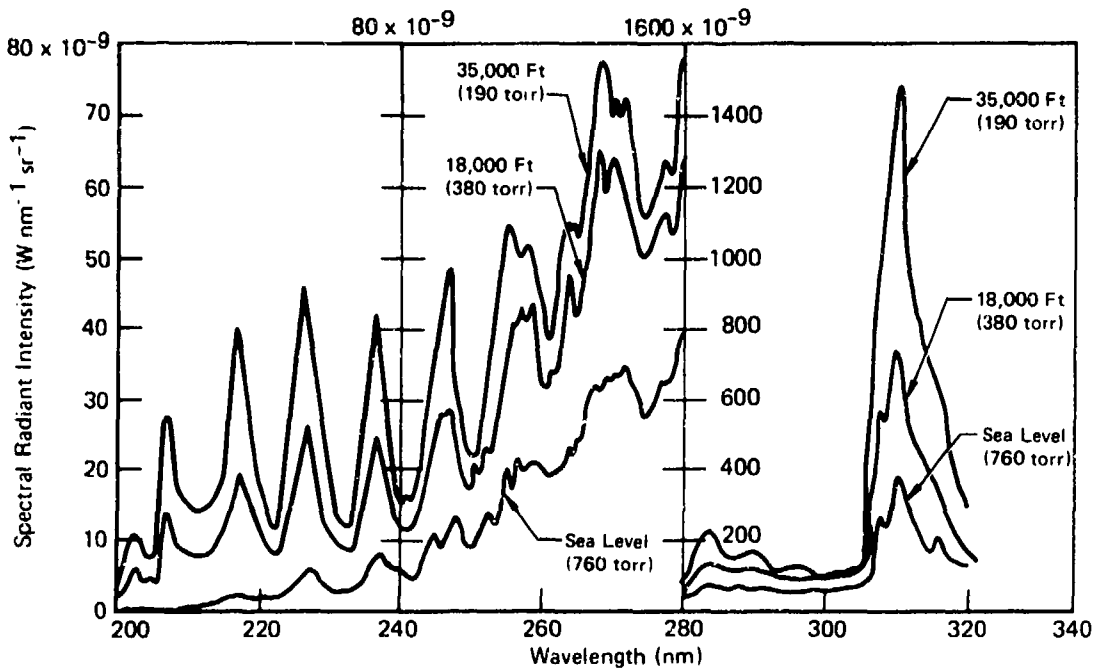


FIGURE 27 ULTRAVIOLET EMISSIONS FROM JP-4 BURNING AT VARIOUS ALTITUDES

To assist the designer the spectral data was converted to values for the integral radiant intensity,  $P_F(\lambda)$ . This parameter is defined by the expression:

$$P_F(\lambda) = \int_{200}^{\lambda} J_F(\lambda) d\lambda \quad \text{Wsr}^{-1}$$

where  $J_F(\lambda)$  ( $\text{Wnm}^{-1}\text{sr}^{-1}$ ) is the spectral radiant intensity of the flame. The value of  $P_F(\lambda)$  represents the total energy emitted by the flame in the wavelength range between 200 nm and  $\lambda$ , and, therefore, the energy available for detection by a sensor which has a long wavelength cutoff of  $\lambda$ . Values of  $P_F(\lambda)$  for JP-4 burning at various altitudes are illustrated in Figure 28. The lower, sea level curve was obtained by a series of integrations of the area under the sea level curves in Figure 19, using the Hewlett-Packard 9810A Programmable Calculator. Each of the high altitude curves in Figure 28 was derived from appropriate radiant intensity plots similar to those illustrated in Figure 19. The curves in Figure 28 emphasize the increase in the ultraviolet emissions from JP-4 flames at high altitudes; there is an order of magnitude difference between the energy emitted at 35,000 feet and at sea level. The energy available for detection is also a critical function of the upper wavelength limit of the sensor used; for example, a detector responding to wavelengths up to 280 nm will receive twice the detectable radiation to which a 260 nm-limited detector would respond.

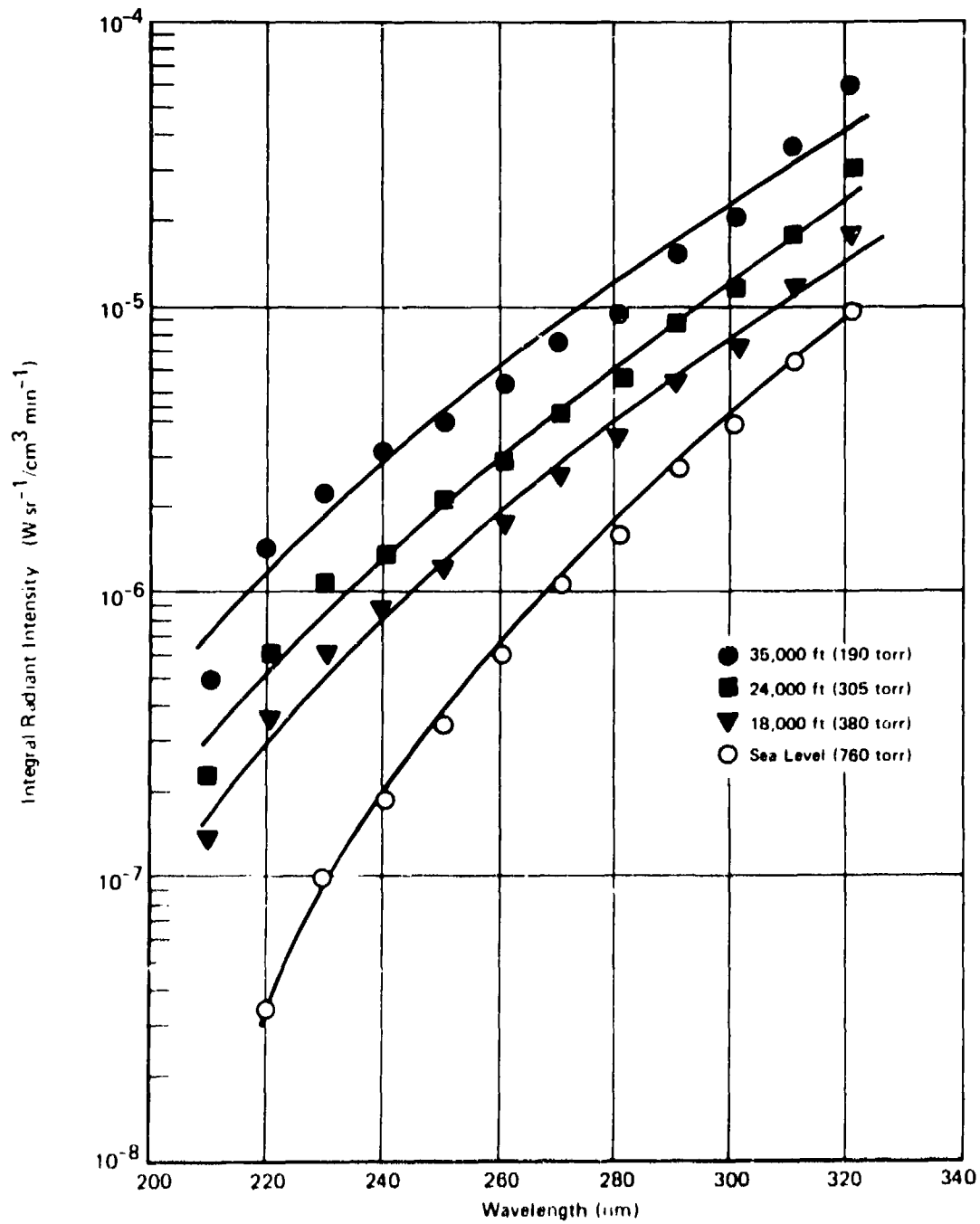


FIGURE 28 INTEGRAL RADIANT INTENSITY OF JP-4 FLAMES BURNING AT VARIOUS ALTITUDES (DATA NORMALIZED FOR UNIT FUEL FLOWRATE)



Similar curves of  $P(\lambda)$  vs  $\lambda$  for the JP-8 and Aviation Gasoline are shown in Figures 29 and 30, respectively; while they are not duplicates of the JP-4 data, the results for these two fluids show strong similarities.

## 2. VISIBLE AND NEAR-INFRARED EMISSION SPECTRA (300 nm - 2.6 $\mu$ m)

Despite the high background radiation in this wavelength range in many applications, several fire detection systems utilize devices sensitive to visible and near-infrared radiation.

Spectral radiant intensity measurements were made in the 300 nm to 2.6  $\mu$ m range on each of the four fuels, at several altitudes including sea level. The combustion chamber illustrated in Figure 2 was used throughout all the burning experiments; for the sea level measurements the extension snout and the top and bottom flanges were removed, and the shell of the chamber was used only as a screen against drafts. All details of the optical system were the same as those for the ultraviolet measurements except for the grating, filter, and detector changes identified in Table 2. The Second Radiant Intensity Standard was used to calibrate the optical system throughout this phase of the measurements.

The spectral data were recorded in six separate but consecutive scans and examples of the results are shown in Figures 31 (a) through

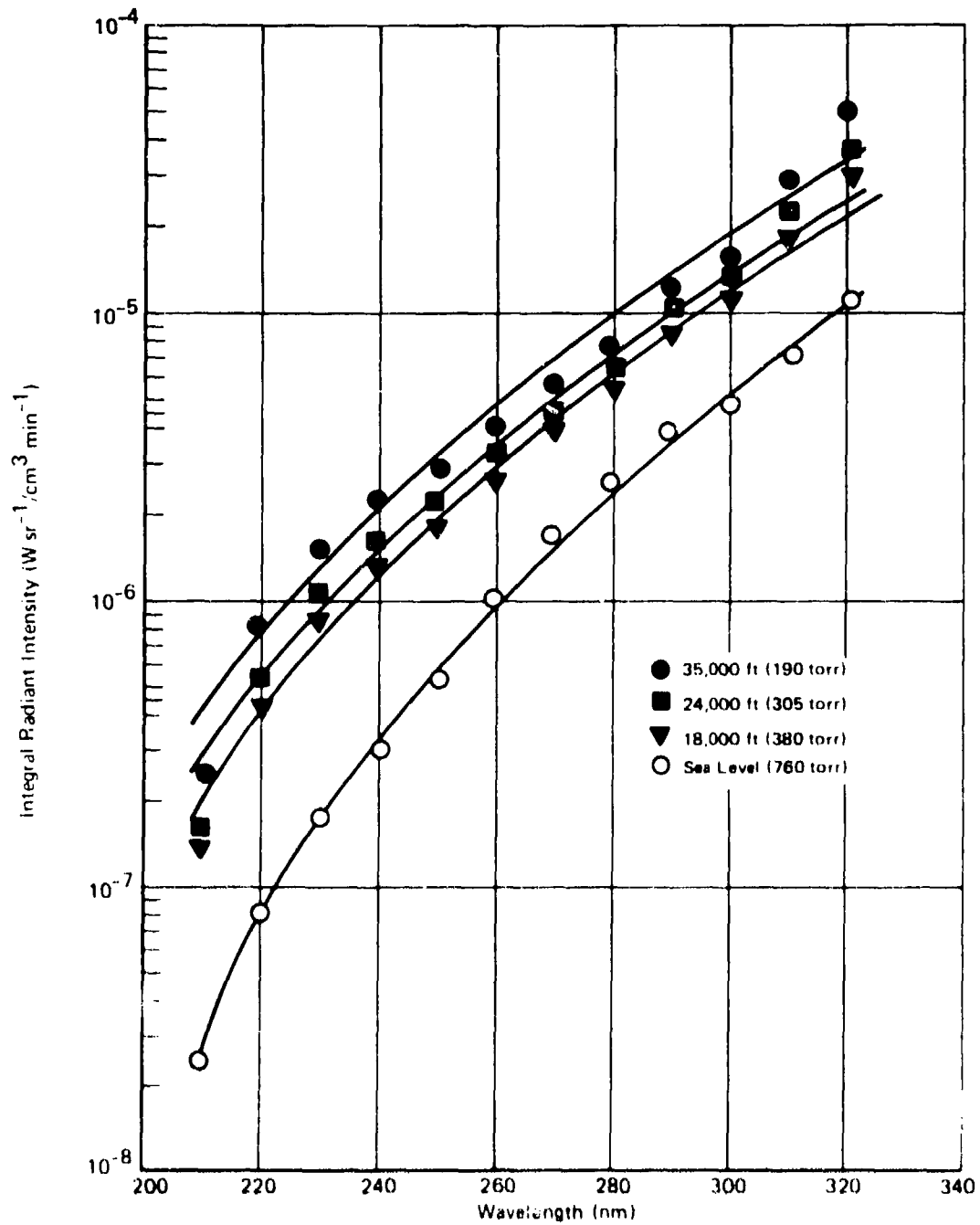


FIGURE 29 INTEGRAL RADIANT INTENSITY OF JP-8 FLAMES BURNING AT VARIOUS ALTITUDES (DATA NORMALIZED FOR UNIT FLOWRATE)

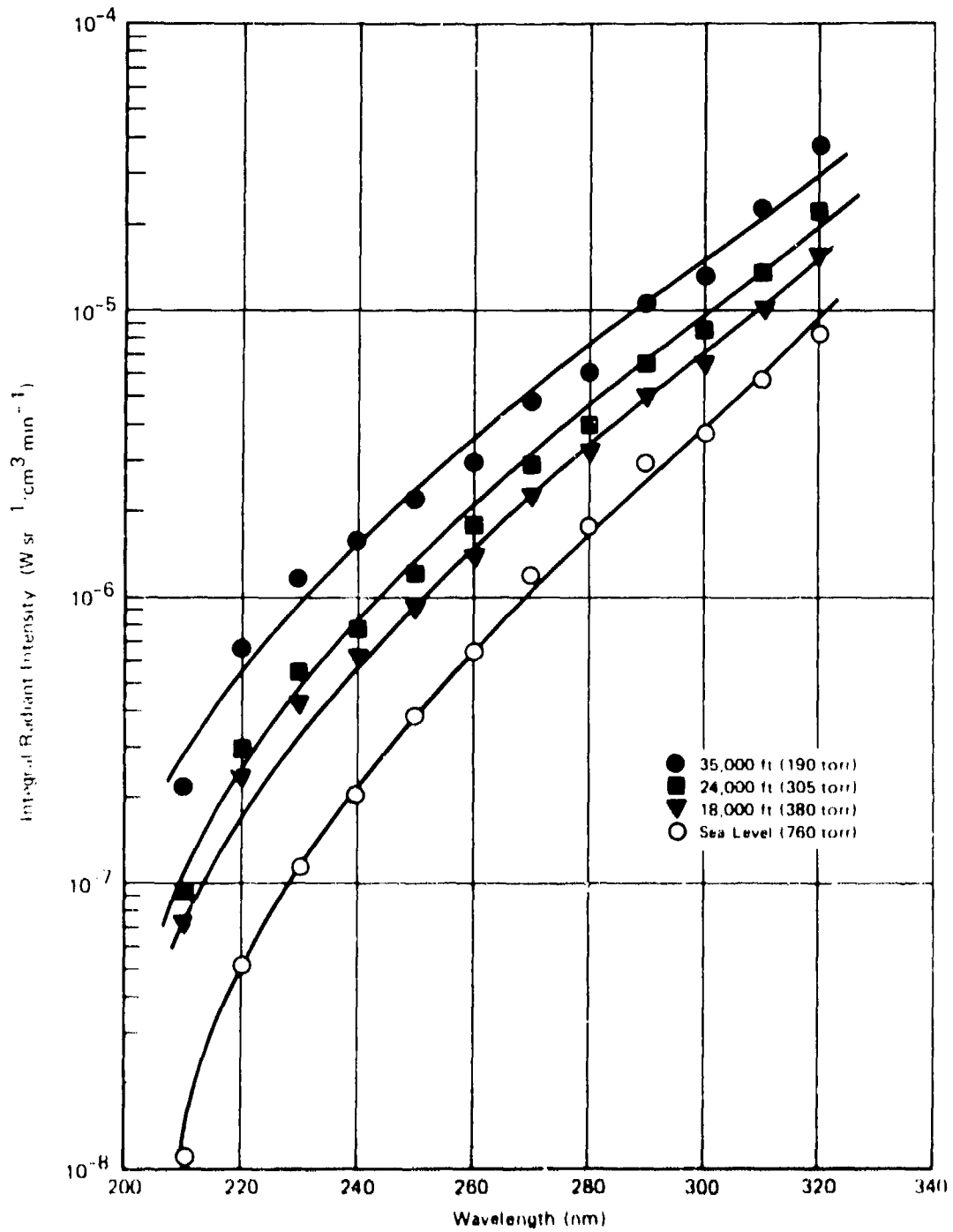
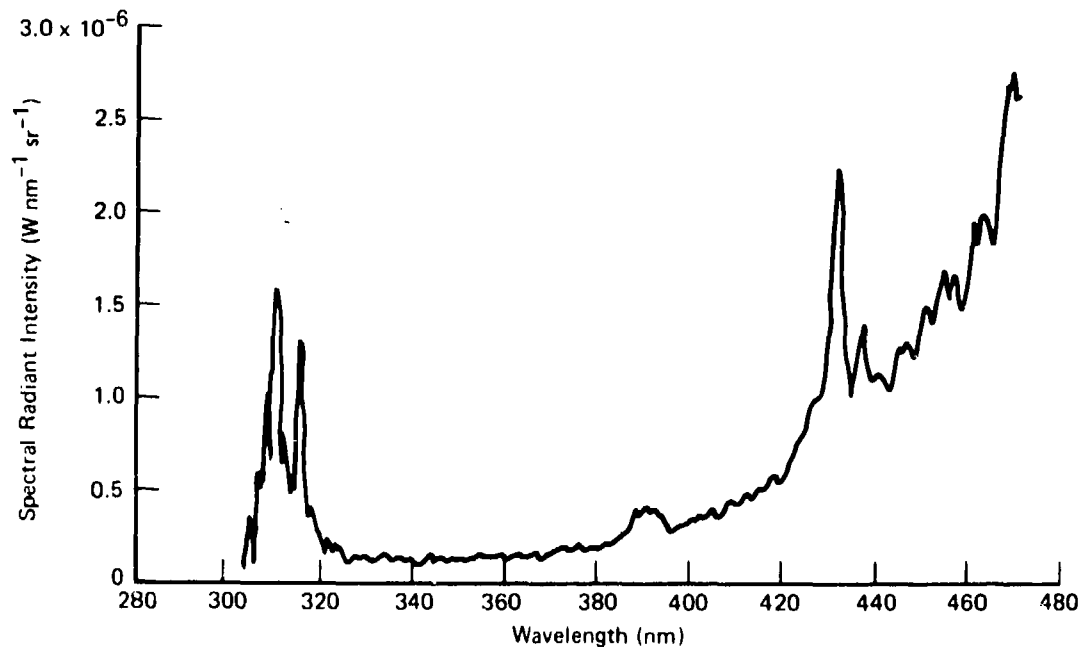
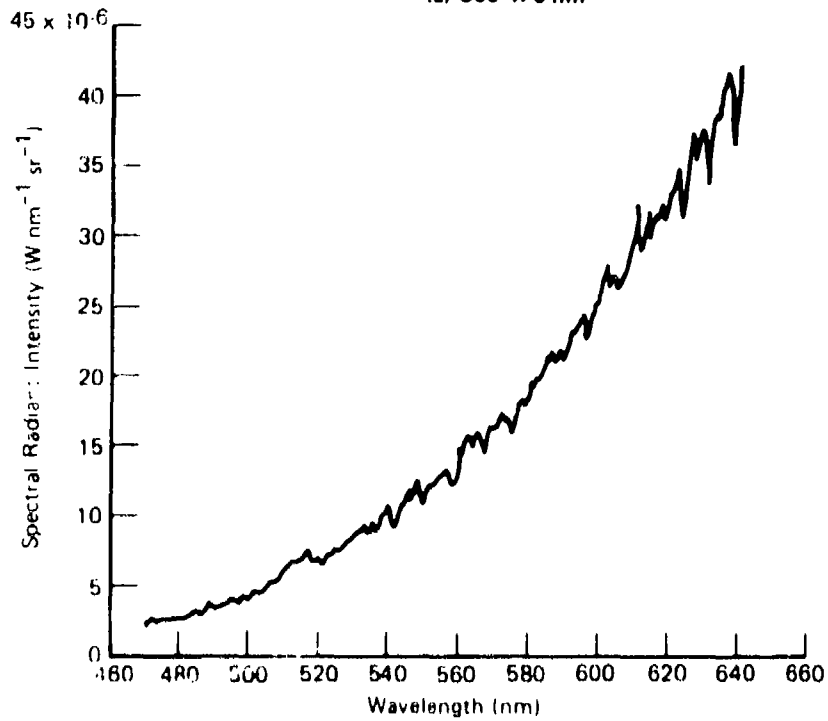


FIGURE 30 INTEGRAL RADIANT INTENSITY OF AVIATION GASOLINE BURNING AT VARIOUS ALTITUDES (DATA NORMALIZED FOR UNIT FUEL FLOWRATE)



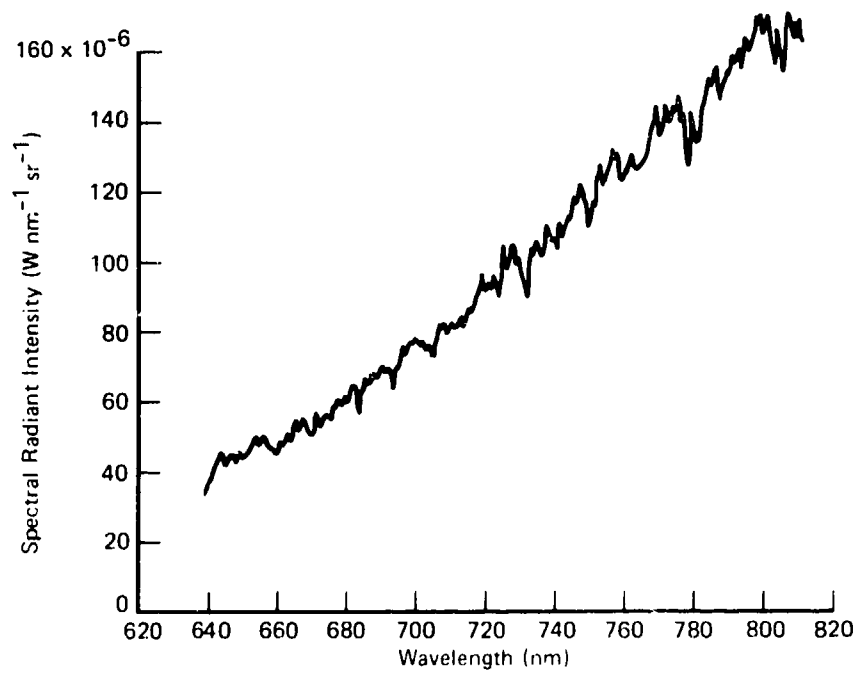
(a) 300-470 nm



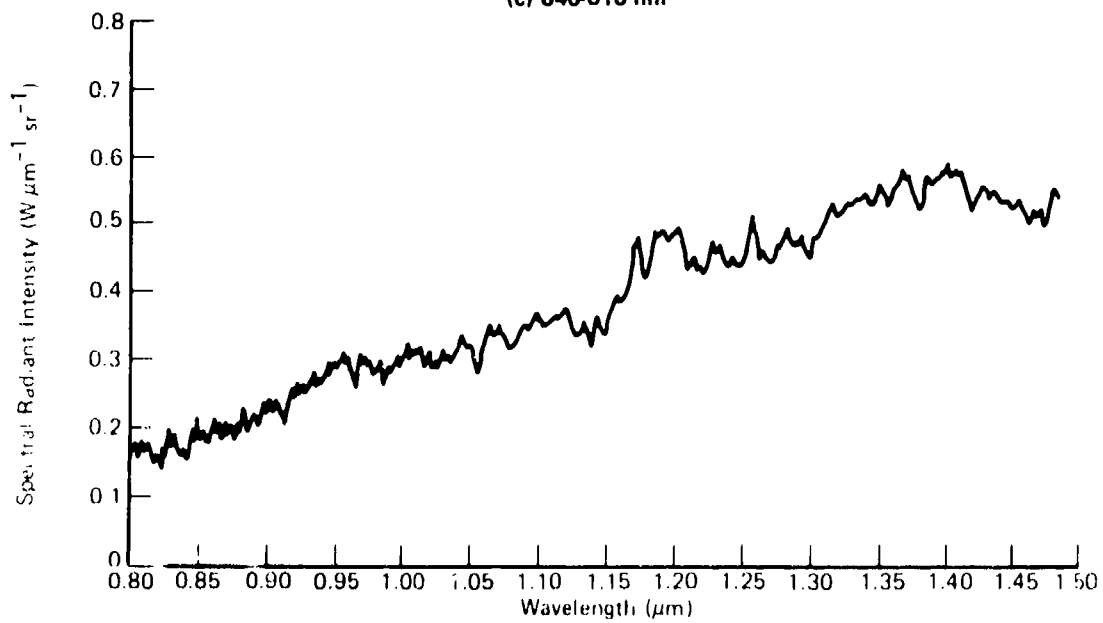
(b) 470-640 nm

FIGURE 31 SPECTRAL RADIANT INTENSITY OF JP-4 BURNING AT 35,000 FT (190 TORR)

CONTINUED



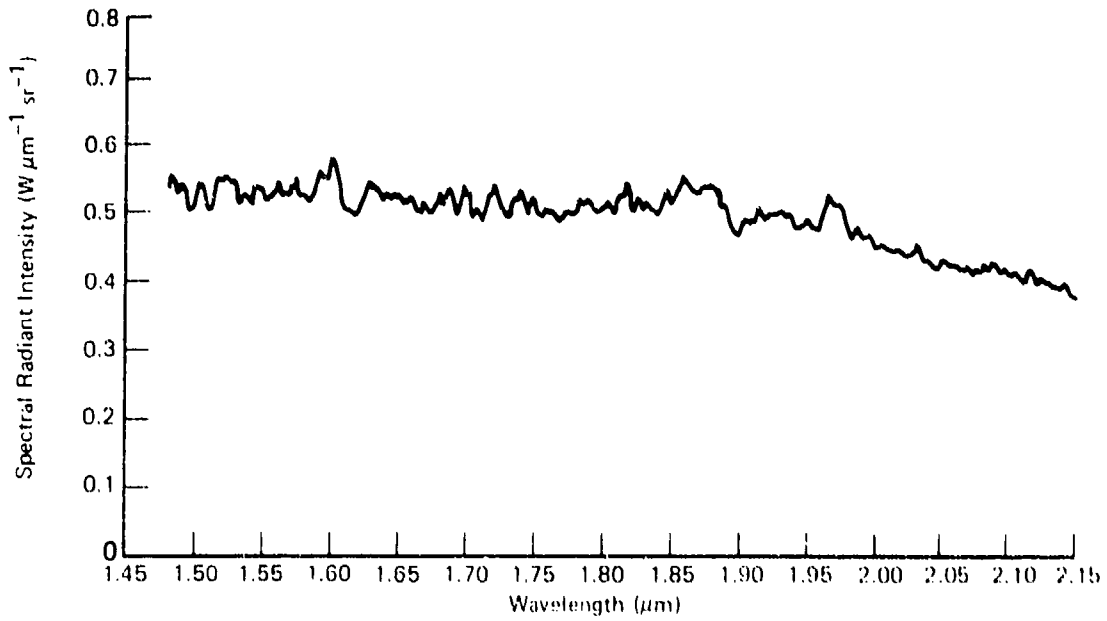
(c) 640-810 nm



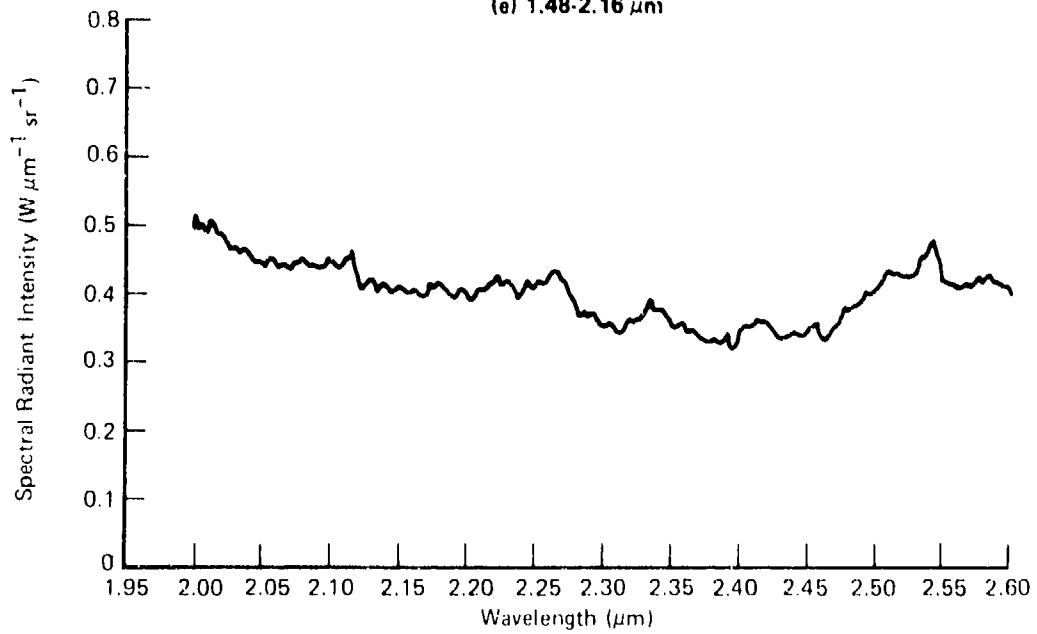
(d) 0.8-1.48 μm

FIGURE 31 SPECTRAL RADIANT INTENSITY OF JP-4 BURNING  
AT 35,000 FT (190 TORR)

CONTINUED



(e) 1.48-2.16  $\mu m$



(f) 2.00-2.65  $\mu m$

FIGURE 31 SPECTRAL RADIANT INTENSITY OF JP-4 BURNING AT 35,000 FT (190 TORR)

(f). Five of the six scans show a featureless continuum with a broad maximum at approximately  $1.4 \mu\text{m}$ , but some structure is evident at the low wavelength end of the spectral range, Figure 31 (a). This spectral structure was most pronounced for the high altitude burns such as the 35,000 ft experiment represented in Figure 31. Identifiable peaks include the 306 - 309 nm bands of the OH radical, the 390 and 430 nm OH band system and the first of the Swan Bands associated with the  $\text{C}_2$  radical, in the 436 - 474 nm range.

As before, the radiant intensity curves were summarized using the H-P 9810A and the resulting composite curve for JP-4 is shown in Figure 32. The lower curve in this figure was traced from the six curves in Figure 31 and the continuity between the six scans, taken several hours apart, is excellent.

The composite curves in Figure 32 emphasize the featureless nature of the spectra, apart from a suggestion of an emission band near  $2.7 \mu\text{m}$ . It is apparent that the radiation emitted by the flames at these wavelengths originated from hot particles of unburnt carbon in the diffusion flame. This is the source of the familiar yellow color of a candle flame and other diffusion flames, although these measurements indicate that the bulk of the radiation is emitted in the near infrared, rather than at visible wavelengths. As the maxima in the emission curves occurred between  $1.5 \mu\text{m}$  and  $2.0 \mu\text{m}$ , the

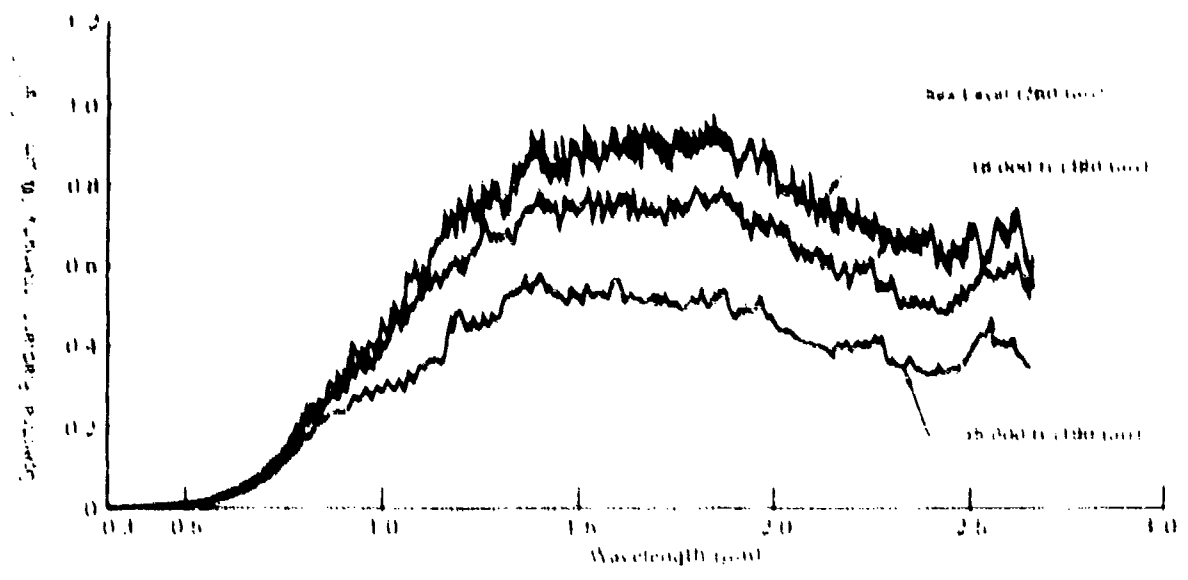


FIGURE 32 VISIBLE AND NEAR INFRARED EMISSIONS FROM JP 4 BURNING AT VARIOUS ALTITUDES



characteristic temperature of the carbon particles was in the 1500 K - 2000 K range.

Similar conclusions can be drawn from the results of JP-5 (Figure 33), JP-8 (Figure 34) and Aviation Gasoline (Figure 35). The 35,000 ft data for JP-5 and JP-8 exhibit weak emission bands around 1.5  $\mu\text{m}$ , 1.8  $\mu\text{m}$  and 2.7  $\mu\text{m}$  which are associated with the  $\text{H}_2\text{O}$  molecule, otherwise the results are similar to those for JP-4. Aviation Gasoline was difficult to burn at high altitudes and thus the data at 35,000 feet was erratic (lower curve in Figure 35).

One feature common to all the visible and near-infrared spectra recorded was that the intensity of the emitted radiation decreased with increasing altitude. This point is discussed in Section IV.

### 3. FAR INFRARED EMISSION SPECTRA (2.5 $\mu\text{m}$ - 15 $\mu\text{m}$ )

Fire detectors sensitive to wavelengths longer than 2  $\mu\text{m}$  are not yet in common use in aircraft but the lack of significant solar radiation in this range makes such devices potentially useful. Hot surfaces in an aircraft engine nacelle will emit strongly at these wavelengths but such noise might be discriminated against.

Far infrared spectra were recorded on the burning fluids using the interferometric spectrometer and optical system described in paragraph II 3 c, page 27. The interferometric spectrometer is a fast-scan

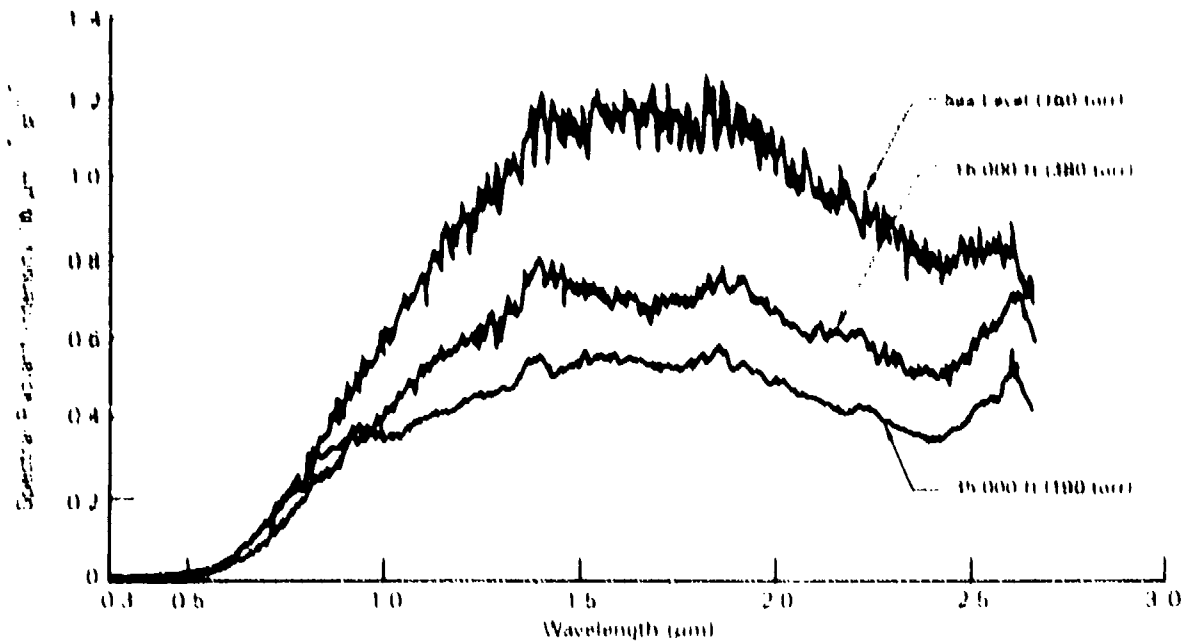


FIGURE 33 VISIBLE AND NEAR INFRARED EMISSIONS FROM JP-5 BURNING AT VARIOUS ALTITUDES

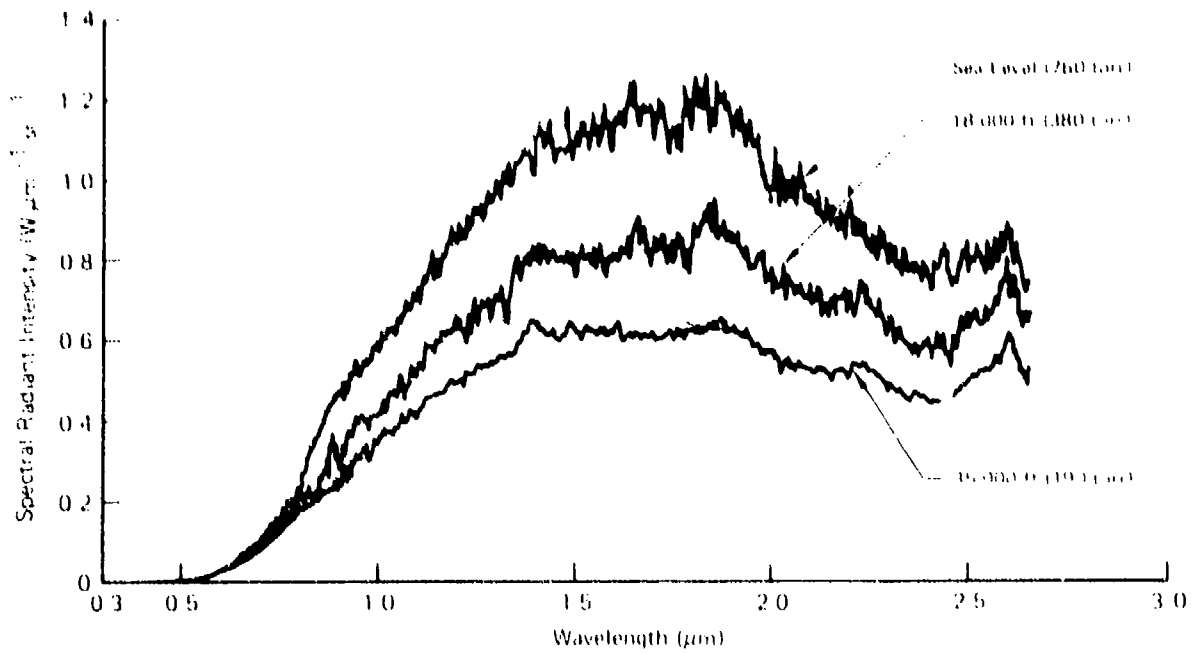


FIGURE 34 VISIBLE AND NEAR INFRARED EMISSIONS FROM JP-8 BURNING AT VARIOUS ALTITUDES

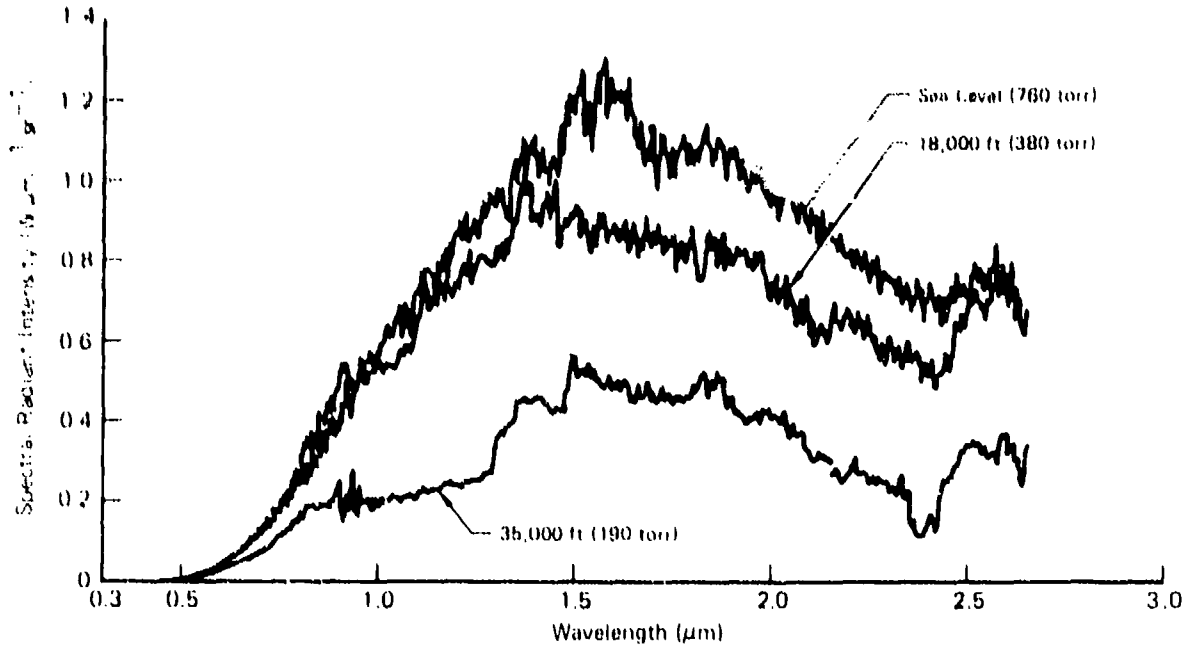


FIGURE 35 VISIBLE AND NEAR INFRARED EMISSIONS FROM AVIATION GAS BURNING AT VARIOUS ALTITUDES

instrument which completes a single scan in approximately one second; therefore, only short combustion times were necessary to obtain good data. The repetitive voltage output from the detector was signal-averaged on the instrument computer and as few as 64 scans, requiring as little as one minute of combustion, were necessary to establish an adequate signal-to-noise ratio. As a result all the fuels were burned at five selected altitudes; however, both MIL-5606B and MLO-68-5 hydraulic fluids still resisted attempts to maintain stable flames for more than a few seconds.

The data accumulated from a total of twenty different combustion experiments was remarkable for its lack of variation. Regardless of the fuel or the combustion atmosphere pressure, the spectra resembled that illustrated in Figure 36. The dominant feature of this curve is the strong emission band centered at  $4.4 \mu\text{m}$ , which is characteristic of an excitation state of the  $\text{CO}_2$  molecule. A lesser peak at  $2.7 \mu\text{m}$  can be attributed to a combination of  $\text{CO}_2$  and  $\text{H}_2\text{O}$  emissions.

The continuum between  $2.5 \mu\text{m}$  and  $4.0 \mu\text{m}$  is the long wavelength end of the blackbody type spectrum observed in the earlier experiments below  $2.6 \mu\text{m}$ . The data represented in Figure 36 was taken for the same fuel and burning conditions that were used to produce the upper curve in Figure 32. There is good agreement between the two sets of

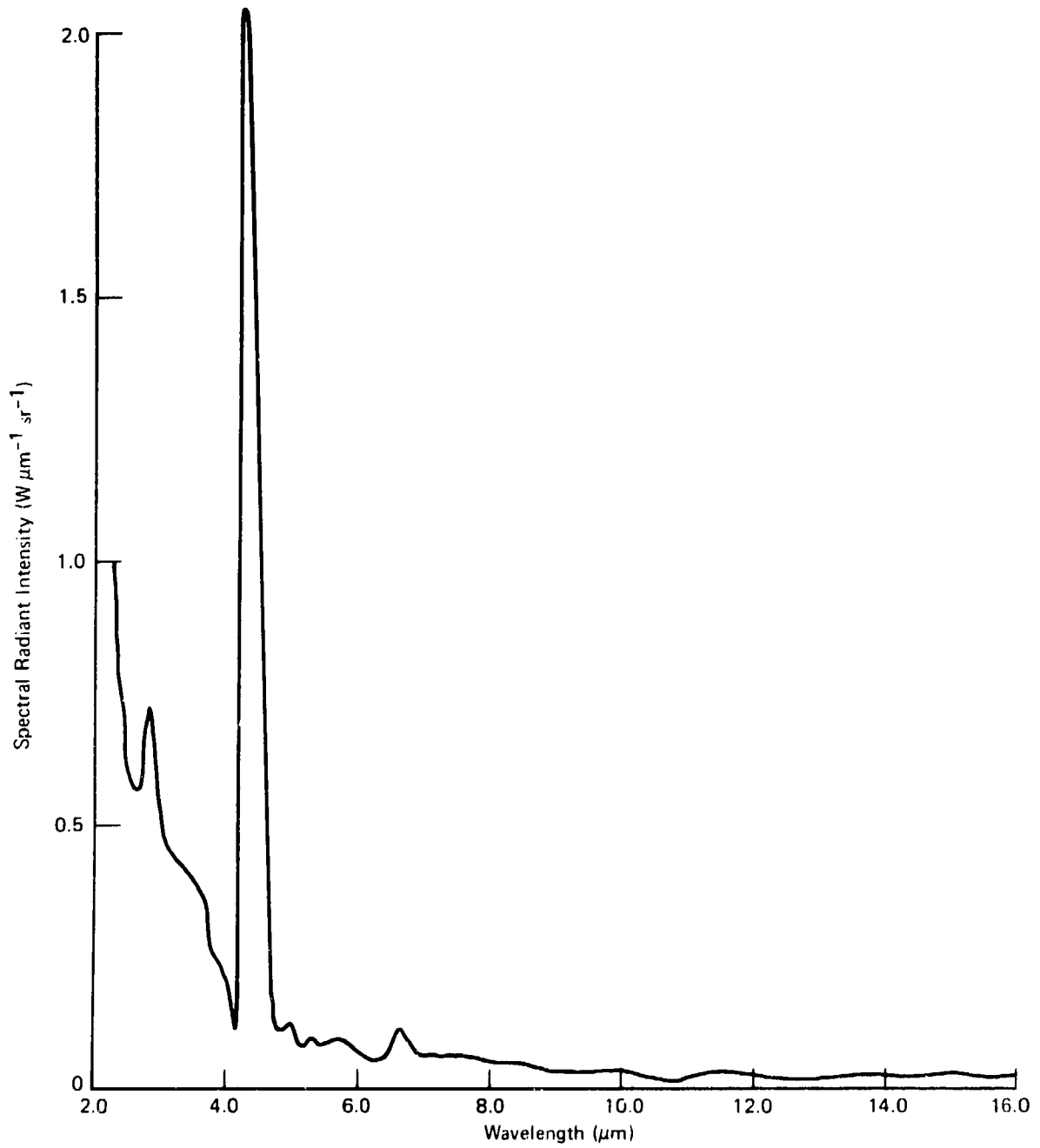


FIGURE 36 FAR INFRARED EMISSIONS FROM JP4 BURNING AT SEA LEVEL

results in the region of overlap at 2.6  $\mu\text{m}$ , despite the fact that entirely different optical systems were used to record the data, and the two sets of data were taken several weeks apart.

The lack of variation in the spectra of the different fuels burnt at the various altitudes made it superfluous to present more than one curve in this report; instead, the single amplitude of the single dominant peak at 4.4  $\mu\text{m}$  has been summarized in Table 4. This tabulation of the peak radiant intensity at 4.4  $\mu\text{m}$  further emphasizes the small changes observed between fuels and altitudes. In this form the intensity appears to have been at its maximum value at 18,000 feet but, as discussed in Section IV, this is attributed to variations in the absorption of the radiation by the atmosphere in the combustion chamber as the pressure was varied.

**TABLE 4 SPECTRAL RADIANT INTENSITY OF THE 4.4  $\mu\text{m}$  CO<sub>2</sub> EMISSION BAND  
MEASURED AT SEVERAL ALTITUDES**

Fuel	Sea Level	18,000 Ft (380 torr)	25,000 Ft (300 torr)	28,000 Ft (250 torr)	35,000 Ft (190 torr)
JP-4	2.10 ( $\text{W}\mu\text{m}^{-1} \text{sr}^{-1}$ )	2.60 ( $\text{W}\mu\text{m}^{-1} \text{sr}^{-1}$ )	2.50 ( $\text{W}\mu\text{m}^{-1} \text{sr}^{-1}$ )	2.40 ( $\text{W}\mu\text{m}^{-1} \text{sr}^{-1}$ )	2.25 ( $\text{W}\mu\text{m}^{-1} \text{sr}^{-1}$ )
JP-5	1.56	2.13	2.13	2.00	1.94
JP-8	1.47	2.38	2.22	2.13	1.85
Aviation Gas	1.65	2.31	2.14	2.14	1.96

SECTION IV  
DISCUSSION

Optical emissions from burning aircraft fluids were successfully measured over a wide range of both wavelength and intensity. These experiments required the use of several different optical systems, detectors and calibration sources; and the data were recorded in ten different spectral ranges over a period of several months. Despite the fragmentation of the experiment, excellent continuity and repeatability were obtained for all the data.

To demonstrate the scope and quality of the experiments, Figure 37 was prepared. This is a composite curve of the data for JP-4 burning at 35,000 feet; this set of data was selected because of the relatively strong spectral features. Each of the spectral ranges defined in Table 2 is identified on the upper edge of Figure 37; the far infrared range 10 was curtailed at 5.0  $\mu\text{m}$  for ease of presentation. The curve in the figure was prepared on the Hewlett-Packard 9810A Calculator using ten computer-generated radiant intensity curves of the type illustrated in Figure 16. Excellent matching was achieved, although the scale of the final figure is too small to demonstrate the fact that better than five percent agreement was obtained between ranges.

The bulk of the energy emitted by the diffusion flames studied in this program was at visible and infrared wavelengths; peak intensities



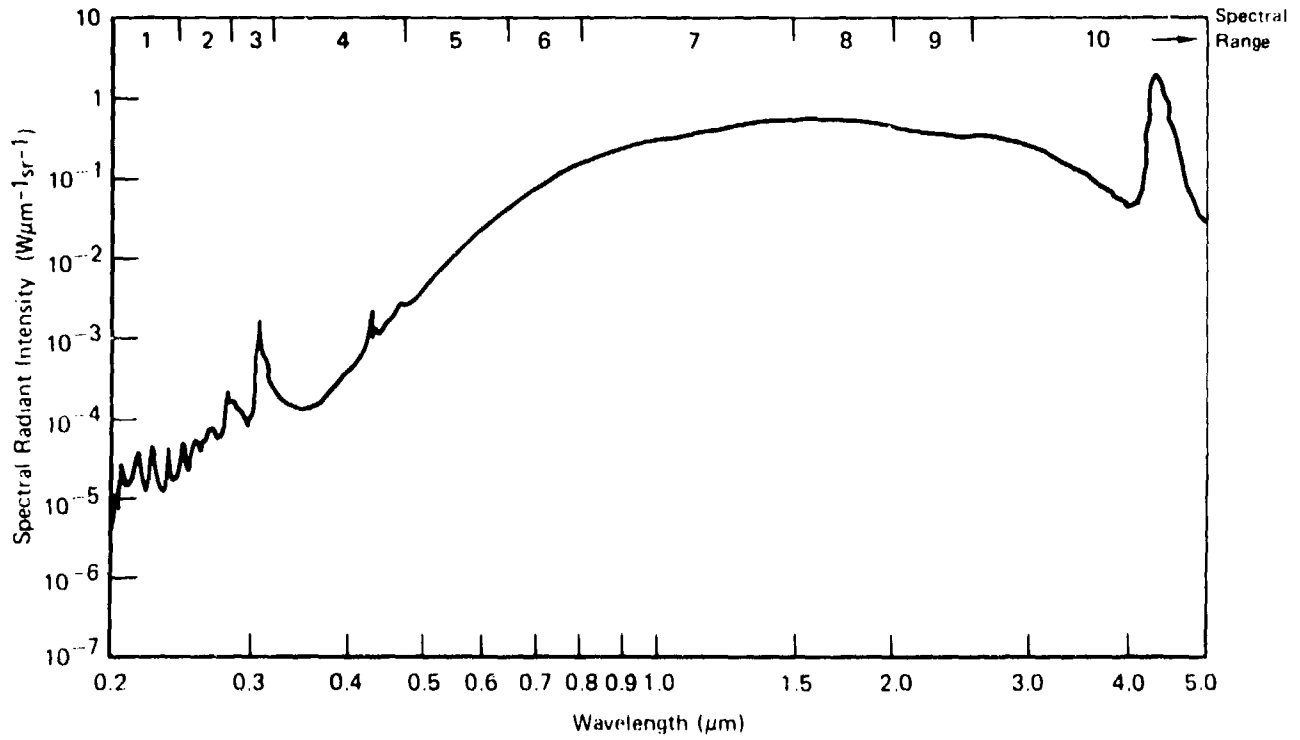


FIGURE 37 OPTICAL EMISSIONS FROM JP-4 BURNING AT 35,000 FT (190 TORR)

in excess of  $1 \text{ W cm}^{-1} \text{ sr}^{-1}$  were recorded at  $4.4 \text{ }\mu\text{m}$ . A detector with an area of  $1 \text{ cm}^2$ , and a bandwidth of  $0.5 \text{ }\mu\text{m}$  centered at  $4.4 \text{ }\mu\text{m}$ , would receive approximately  $3 \text{ }\mu\text{W}$  at a distance of  $3\text{m}$ . In applications where the background radiation incident on the detector is substantially less than  $1 \text{ }\mu\text{W}$  in this waveband, a pyroelectric detector or similar sensor could be incorporated into a sensitive fire detection system.

#### 1. ALTITUDE EFFECTS

In Figure 28 the ultraviolet emissions from JP-4 flames are shown to have increased with increasing altitude and this trend is emphasized by the data illustrated in Figure 38. The ultraviolet power emitted by the burning fuels was determined by integrating the total area under curves, such as those drawn in Figure 31. In mathematical terms the emitted power  $P_F$  in the 200 to 320 nm waveband is given by:

$$P_F = \int_{200}^{320} J_F(\lambda) d\lambda \quad (\text{W sr}^{-1}) \quad (4-1)$$

For all three fuels for which data is included in Figure 38 the ultraviolet power emitted at 35,000 feet is nearly double that emitted at sea level by the same size of flame.

In contrast, the power emitted at visible and near infrared wavelengths decreased at higher altitudes, as illustrated in Figure 39. One possible explanation of these differing mechanisms for the two spectral regions is that the visible/near-infrared emission spectra

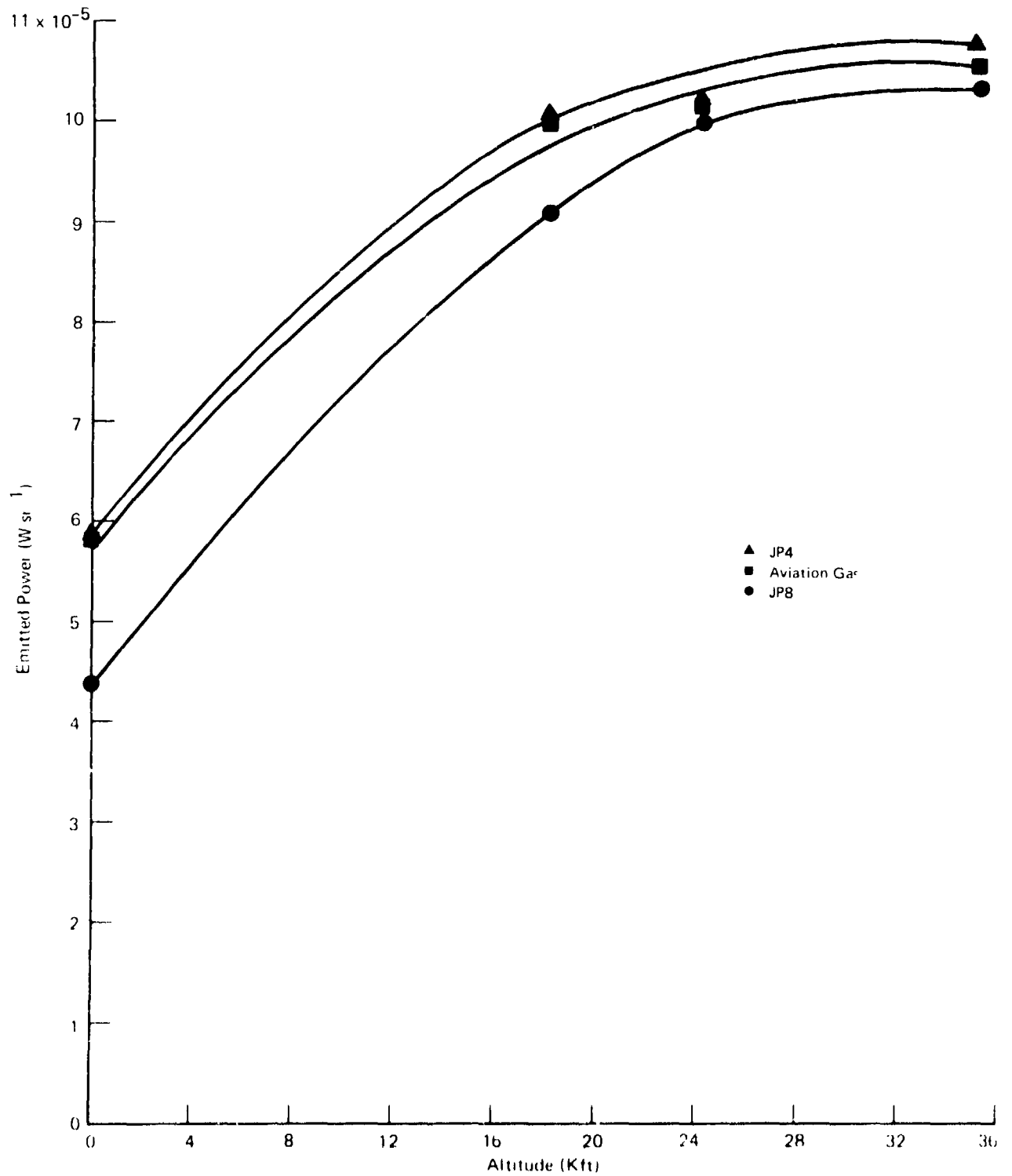


FIGURE 38 ULTRAVIOLET POWER EMITTED BY BURNING AIRCRAFT FUELS AT VARIOUS ALTITUDES

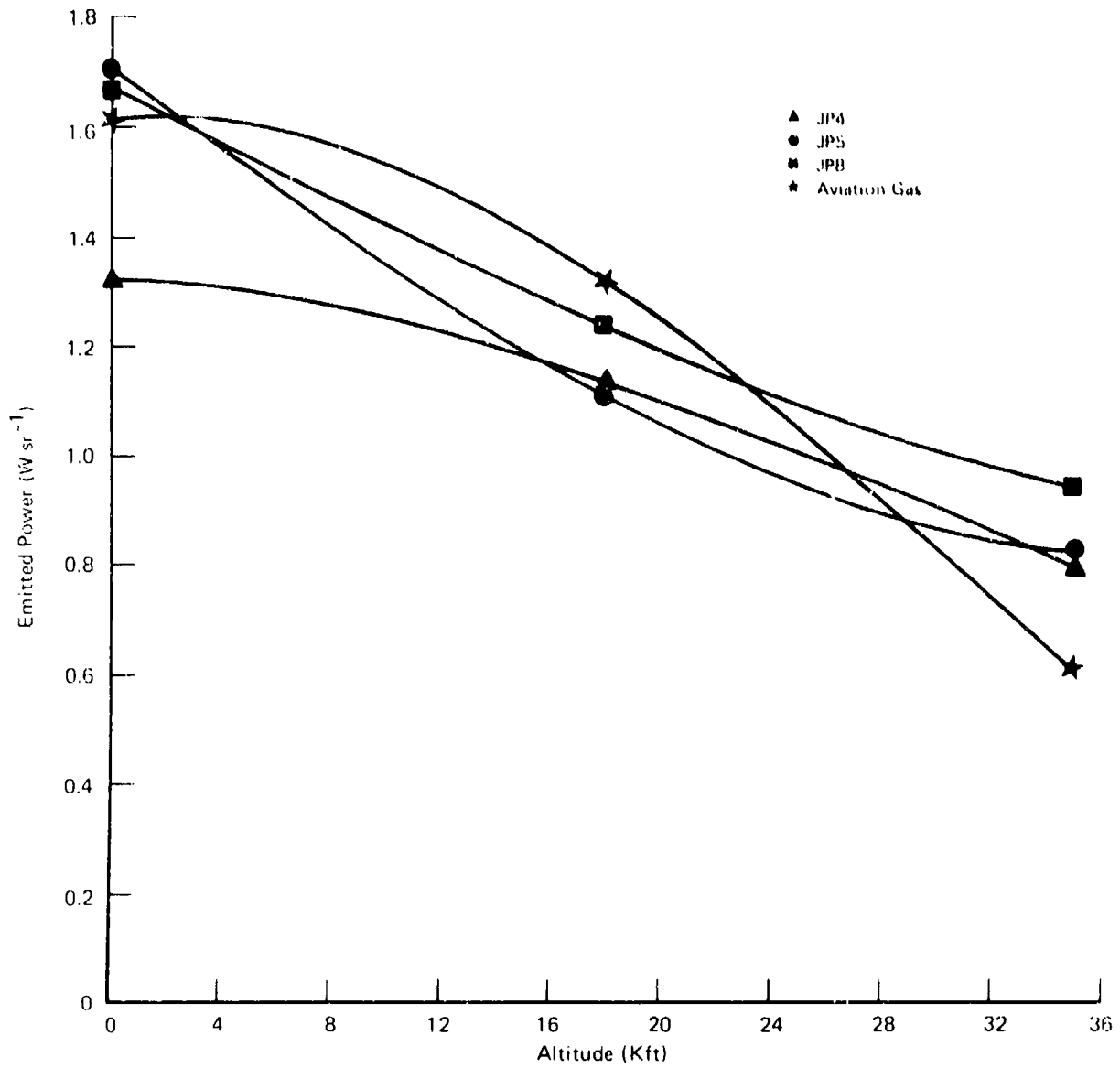


FIGURE 39 VISIBLE AND NEAR INFRARED POWER EMITTED BY BURNING AIRCRAFT FUELS AT VARIOUS ALTITUDES

are mainly attributable to the hot carbon particles in the diffusion flame, while the energy emitted at ultraviolet wavelengths is associated with the electronic transitions of free radicals in the flame. These radicals are generated at intermediate steps in the combustion process, the principal end products of which are carbon, carbon monoxide, carbon dioxide and water vapor. As the altitude was increased, i.e., the pressure in the combustion chamber was decreased, the reduction in the available oxygen to complete the combustion process may have resulted in an increase in the density of these radicals, and the subsequent stronger emissions of the ultraviolet radiation. In contrast the reduction in oxygen pressure may have reduced the flame temperature and thus the intensity of the visible/near infrared radiation emitted by the carbon particles.

The 4.4  $\mu\text{m}$  emission band dominated the far infrared spectra of all the burning fuels; therefore, the peak radiant intensity of this band was summarized, rather than the total power emitted across the complete 2 to 15  $\mu\text{m}$  range. Data for all the fuels is listed in Table 4 and the JP-4 data is plotted in Figure 40. The upper, broken curve was drawn through the uncorrected data points calculated by the computer data-reduction programs.

Correction of the data was necessary due to the presence of atmospheric carbon dioxide in both arms of the optical system, resulting in significant absorption of the emitted radiation in a band centered

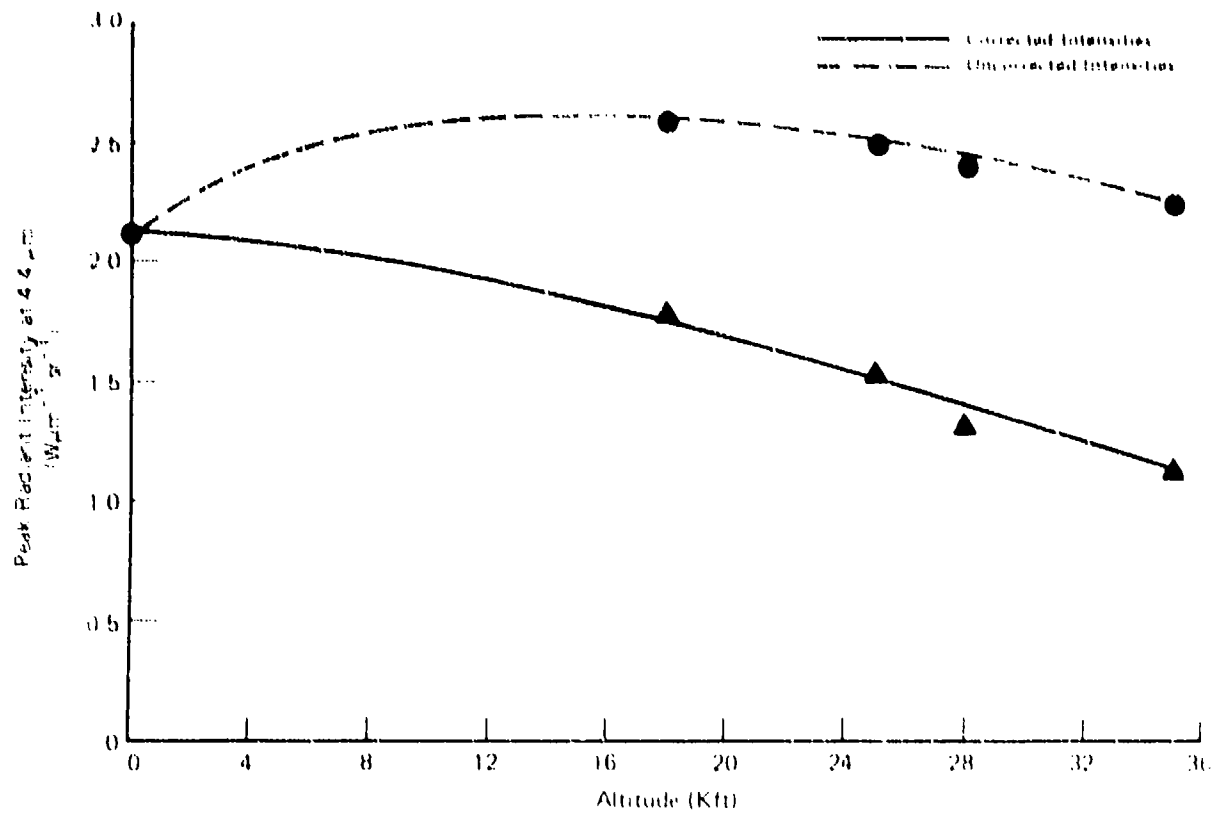


FIGURE 40 SPECTRAL RADIANT INTENSITY OF THE 4.4 μm CO<sub>2</sub> EMISSION PEAK FOR JP-4 BURNING AT SEVERAL ALTITUDES

at  $4.3 \mu\text{m}$ . (Note that the peaks of the absorption and emission bands are centered at wavelengths approximately  $0.1 \mu\text{m}$  apart.) During the design of the optical system considerable care was taken to ensure that the path length from the spectrometer to the flame was equal to the separation between the spectrometer and the calibration standard. Under ideal conditions the absorption in the two paths would be the same and the calculated value of the intensity at  $4.4 \mu\text{m}$  would be correct. Such conditions were achieved during the sea level experiments, but, as the combustion chamber pressure was reduced, the absorption of the radiation emitted from the flame decreased relative to the absorption during the calibration experiments, resulting in artificially high values of the computed intensity. Thus the uncorrected intensity data plotted in Figure 40 exhibits a broad maximum at about 16,000 feet. To correct for the unbalance in the two arms of the optical system the absorption at  $4.4 \mu\text{m}$  was calculated from the raw data recorded during calibration runs. Assuming an exponential absorption law, an allowance was made for the effective path length inside the combustion chamber at reduced pressure, and the intensity data was corrected accordingly. The results of this adjustment are plotted as a solid curve in Figure 40.

The intensity of the  $4.4 \mu\text{m}$  emissions is shown to decrease with increasing altitude; the variation is similar to that observed in the visible/near-infrared data. Like the radiation emitted from the hot

carbon particles the radiation generated by the  $\text{CO}_2$  molecule is proportional to the completeness of combustion and the temperature of the flame.

## 2. EMITTING SPECIES

At ultraviolet wavelengths all the emission spectra exhibited pronounced band structure characteristic of the electronic structure of various chemical species generated during the combustion process. To assist in the identification of the emitting species two additional spectral scans were made of JP-4 flames. For these scans the bandwidth of the spectrometer was decreased to 0.64 nm (from 1.6 nm), the scanning speed was slowed to 5 nm/min (from 12.5 nm/min) and electrical time constants of up to 3 seconds were used (cf 300 ms). Reproductions of the raw data curves in Figures 41 and 42 have been marked with the characteristic wavelengths of several spectral systems. It is apparent that the strong bands emitted in the 200 - 280 nm region are due to a combination of the Cameron Bands of the CO radical ( $a^3\pi - X^1\Sigma$ ) and the ( $A^2\Sigma^+ - X^2\pi$ ) system of the OH radical. Below 200 nm (Figure 42) the finely divided structure is attributed to the 4th positive system of CO ( $A^1\pi - X^1\Sigma$ ).

The other spectral features that can be discerned in Figure 37 are discussed elsewhere in the text of the report; to summarize these, strong emission band systems were observed and identified at 310 nm



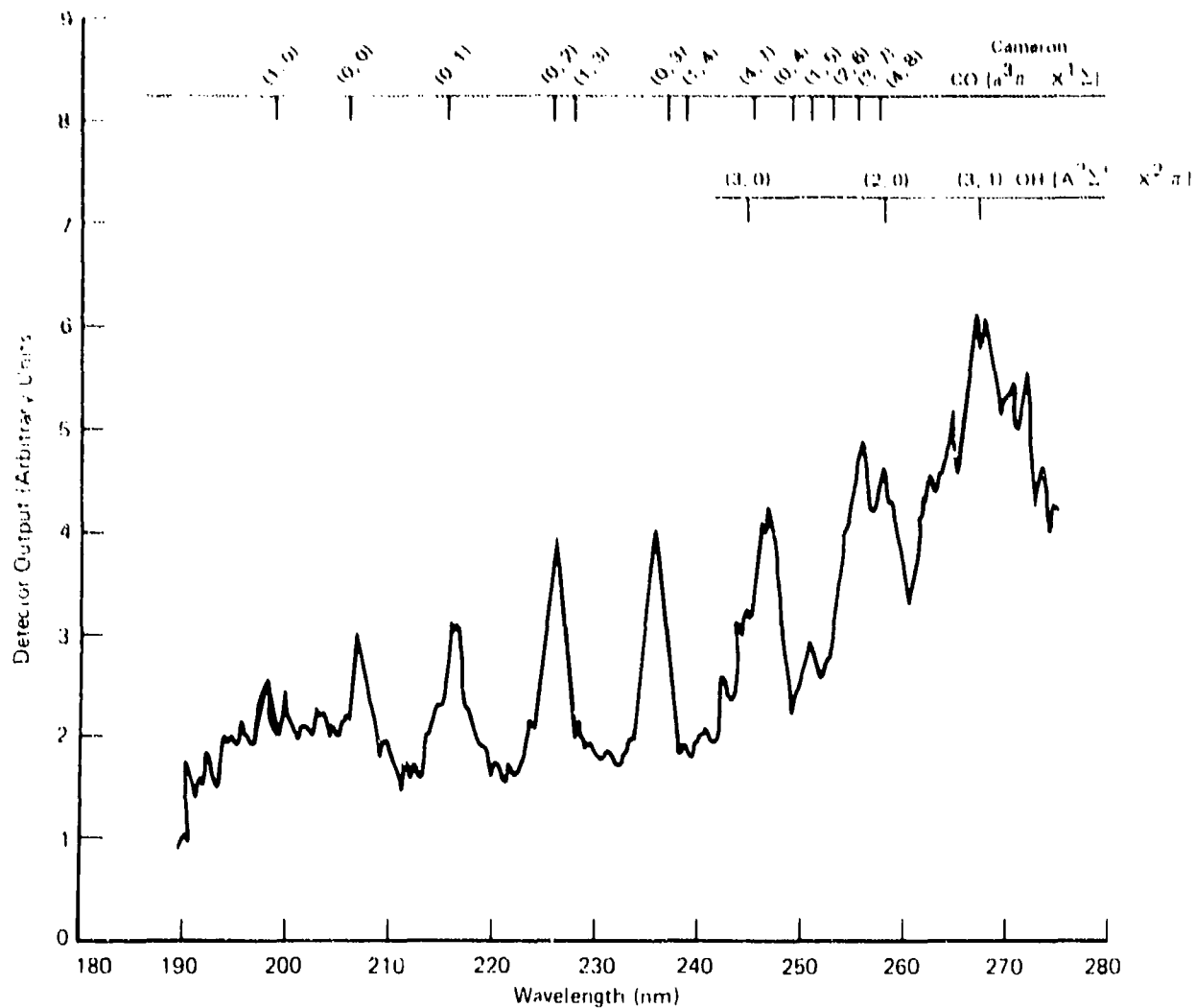


FIGURE 41 EMISSION SPECTRA OF JP-4 BURNING AT 35,000 FT (190 TO 275 NM)

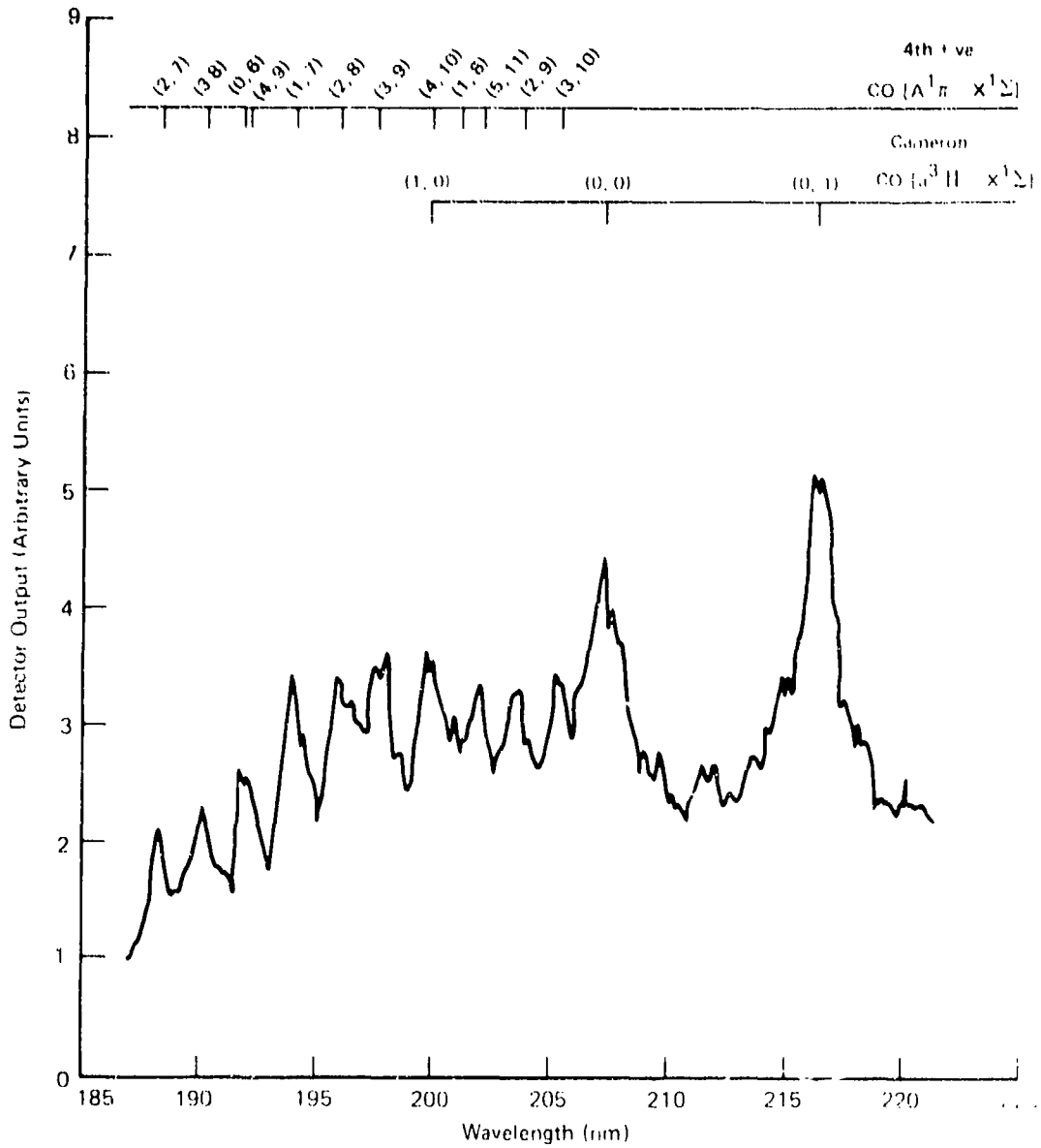


FIGURE 42 EMISSION SPECTRA OF JP-4 BURNING AT 35,000 FT (185 TO 220 NM)

(OH), 390 nm (CH), 430 nm (CH) and 436 - 474 nm (C<sub>2</sub>).

### 3. SIGNIFICANCE OF RESULTS

Apart from generating a wealth of data that should be valuable to designers of fire detection systems the results of the program are significant in other areas.

Diffusion flames were studied as the most realistic simulation of an aircraft fire and the measured spectra were found to be a combination of emission bands superimposed on a blackbody type continuum. Such a spectral distribution differs significantly from the spectra of pre-mixed JP-4/air and hydrogen/air flames that are frequently used as "standard flames" to characterize the sensitivity of a fire detector. Use of such standard flames will result in quite erroneous conclusions as to the potential ability of a sensor to detect fuel fires in an aircraft engine nacelle; or, indeed, in any aerospace system. Consideration should be given to the development of a new standard based on a diffusion flame.

The dominance of the CO<sub>2</sub> emission band at 4.4 μm over all other features of the emission spectra for the combustible fluids recommends this spectral region for fire detection. It is an awkward spectral region for photoconductive detectors operating at room temperature (lead selenide is still responsive at these wavelengths, but its sensitivity is greatly enhanced if cryogenically cooled), however,

AFAPL-TR-73-83

thermal detectors, such as sensitive thermopiles, pyroelectric detectors, and thermistors, could be used with appropriate filtering. The problem of high background radiation could be readily solved by the use of a two color system operating, for instance, at 4.4  $\mu\text{m}$  and 5.5  $\mu\text{m}$ .

SECTION V  
CONCLUSIONS

The following conclusions can be drawn from the results of the program:

Optical emission data, from the middle ultraviolet to the far infrared, were successfully recorded on a variety of aircraft combustible fluids as a function of altitude.

Data recorded in ten separate spectral ranges exhibited good continuity at each overlap point, indicating the excellence of the experimental technique.

Emissions from each of the six fluids studied differed only in minor detail; the total power emitted by each of the flames varied by less than 20% between fluids, for similar combustion conditions.

The total energy emitted by the flames decreased at high altitudes, although the intensity of the ultraviolet emissions increased.

At visible and near infrared wavelengths the bulk of the radiation was emitted by hot carbon particles in the diffusion flames.

Several species emitted radiation at ultraviolet wavelengths, including CO, OH, CH and C<sub>2</sub>; and at infrared wavelengths, including H<sub>2</sub>O and CO<sub>2</sub>.

Several areas of future activity are recommended:

New standard flames should be developed for the evaluation of fire-detection systems.

Consideration should be given to the development of fire-detection systems sensitive to 4.4  $\mu\text{m}$  radiation.

Experimental and analytical studies should be directed toward determining the spectral distribution of the background radiation encountered by fire sensors in aerospace applications.

## LIST OF EQUIPMENT AND INSTRUMENTS

ITEM	MODEL NUMBER	MDC CONTROL NUMBER
COMBUSTION SYSTEM		
Wallace and Tiernan Absolute Pressure Gage	FA 129	A056092
Wallace and Tiernan Differential Pressure Gage	FA 145	B143691
Fisher and Porter Rotameter	FP-1/16-10-G-5/81	B141780
Fisher and Porter Rotameter	FP-1/16-10-G-5/81	B141692
Welch Scientific Vacuum Pump	8730-97	A46485
Powerstat Variable Transformer	3PF 136	B167036
G.E. 15 kV Transformer	9T61Y21	-
ELECTRO OPTICAL SYSTEM		
Jarrell Ash 1/2m Scanning Spectrometer	82000	A54458
Varian Photomultiplier Tube	G-26H215	-
EMI Photomultiplier Tube	9558QC	-
Fluke High Voltage Power Supply	408B	A56026
Princeton Applied Research:		
Lock-In Amplifier	HR-8	A60152
Research Modulator	125	A59883-3
Plug-In Amplifier	Type A	A60152-1
Radiant Intensity Standard	-	-
NJE Power Supply	CR-36-50	A45721
Device Technology Digital Panel Meter	DT 540	-
Leeds and Northrup Standard Resistor	4361	-
Electro Optical Industries Radiant Intensity Source	143	-
Electro Optical Industries Temperature Controller	2158	-
Barnes Engineering Infrared Emission Spectrometer	195T	-
DATA ACQUISITION SYSTEM		
Fabritek:		
Instrument Computer	1072	A61283
A-D Converter	SD-74A	-
Sweep Controller	SW-71	A61285
Header Record	282	A61286
Tektronix Oscilloscope	RM 504	A61283-1
Peripheral Equipment Corporation Tape Deck	2207-7	A61287

REFERENCES

1. Proceedings of the International Symposia on Combustion, published by the Combustion Institute, Pittsburgh, Pa.
2. G. M. Custard and J. D. Donahue, U. S. Army Aviation Material Laboratories, Report 67-39, July 1967
3. Military Specification MIL-T-5624H, 30 October 1970
4. J. M. Kuchta and R. J. Cato, "Ignition and Flammability Properties of Lubricants," SAE Air Transportation Meeting, New York, April 1968
5. J. L. Herr and N. J. Pierce, "Evaluation of MLO-68-5 Less Flammable Hydraulic Fluid," ASD-TR-70-36, September 1970
6. C. A. Seil, L. T. Bouchez, and J. P. Skyrns, "Evaluation of Candidate Fire-Resistant Hydraulic Fluids," AFML-TR-67-4, April 1967



AFAPL-TR-73-83

APPENDIX A

CALIBRATION CERTIFICATES FOR EQUIPMENT

USED IN THE EXPERIMENTS

N C A I R  
BUREAU OF STANDARDS

DEPT. 257K EXT. 25004

DATE 16 June 72

TEST REPORT

INSTRUMENT NAME Spectral Radiance Source MFR. G.E.

MODEL 30A/T24/3 SERIAL NO. 7423-78 PROPERTY NO. None

REQUESTED BY R. M. Linford DEPT. NO. 256

CALIBRATION INSTRUMENTATION GE 30A/T24/3 Q15 Spectral Radiance Standard Lamp; MBS 14  
1505 Spectroradiometer

DATA:

<u>Wavelength (Angstroms)</u>	<u>Spectral Radiance (W-CM<sup>-2</sup> - SR<sup>-1</sup>)</u>	<u>Blackbody Temperature Kelvins (IPTS-68)</u>
2250	6.801 X 10 <sup>-1</sup>	2418.6
2300	1.298	2435.7
2400	4.120	2465.5
2500	1.113 X 10 <sup>1</sup>	2489.6
2600	2.537 X 10 <sup>1</sup>	2504.3
2700	5.199 X 10 <sup>1</sup>	2514.7
2800	9.728 X 10 <sup>1</sup>	2521.0
3000	2.948 X 10 <sup>2</sup>	2533.7
3250	8.754 X 10 <sup>2</sup>	2538.4

The estimated maximum uncertainty in the above tabular values of spectral radiance varies from 8% at 2250A to 5% at 3250A. The maximum uncertainty of the blackbody temperatures is about 3 Kelvins.

2000

ACCURACY OF INSTRUMENT See above

CALIBRATION EXPIRES N/A CALIBRATED BY J. Chodden/C. Dillow

APPROVED BY [Signature]

FIGURE 1A - CALIBRATION CERTIFICATE FOR THE  
FIRST RADIANCE STANDARD

AFAPL-TR-73-83

N O A I R  
BUREAU OF STANDARDS

DEPT. 337K EXT. 24034  
DATE 12 Feb. 1971

TEST REPORT

INSTRUMENT NAME Spectral Radiance Lamp & Imaging System MFR. O.E.  
MODEL 30A/1.1V (Lamp) SERIAL NO. none PROPERTY NO. none  
REQUESTED BY R.N.F. Linford DEPT. NO. 256  
CALIBRATION INSTRUMENTATION OE 30A/TR4/3 Q15 Spectral Radiance Standard Lamp; NBS 14  
1909 Spectroradiometer; OE 30A/TR4/5 191076A Pyrometer Strip Lamp; Electro Optical 146  
107 Radiation Source.

DATA:

<u>Wavelength</u> <u>(microns)</u>	<u>Spectral Radiance</u> <u>(W-cm<sup>-2</sup> - SR<sup>-1</sup>)</u>	<u>Blackbody Temperature</u> <u>Kelvins (ITS-68)</u>
0.300	1.292 x 10 <sup>2</sup>	2428
0.325	3.679 x 10 <sup>2</sup>	2418
0.360	1.182 x 10 <sup>3</sup>	2403
0.400	3.282 x 10 <sup>3</sup>	2389
0.450	8.221 x 10 <sup>3</sup>	2356
0.500	1.634 x 10 <sup>4</sup>	2328
0.550	2.671 x 10 <sup>4</sup>	2296
0.600	3.853 x 10 <sup>4</sup>	2264
0.650	5.096 x 10 <sup>4</sup>	2234
0.700	6.234 x 10 <sup>4</sup>	2201
0.750	6.968 x 10 <sup>4</sup>	2160
0.800	7.608 x 10 <sup>4</sup>	2123
1.00	1.059 x 10 <sup>5</sup>	2048
1.20	1.036 x 10 <sup>5</sup>	1994
1.50	7.690 x 10 <sup>4</sup>	1808
1.75	5.617 x 10 <sup>4</sup>	1687
2.00	3.941 x 10 <sup>4</sup>	1578
2.35	2.481 x 10 <sup>4</sup>	1451
2.50	2.040 x 10 <sup>4</sup>	1401

The estimated maximum uncertainty in the above tabular values of spectral radiance varies from 6% at .30 microns to 4% at 2.5 microns.

ACCURACY OF INSTRUMENT See above  
CALIBRATION EXPIRES N/A CALIBRATED BY L. Shadden/C. Eilow  
APPROVED BY [Signature]

FIGURE 2A - CALIBRATION CERTIFICATE FOR THE  
SECOND RADIANCE STANDARD

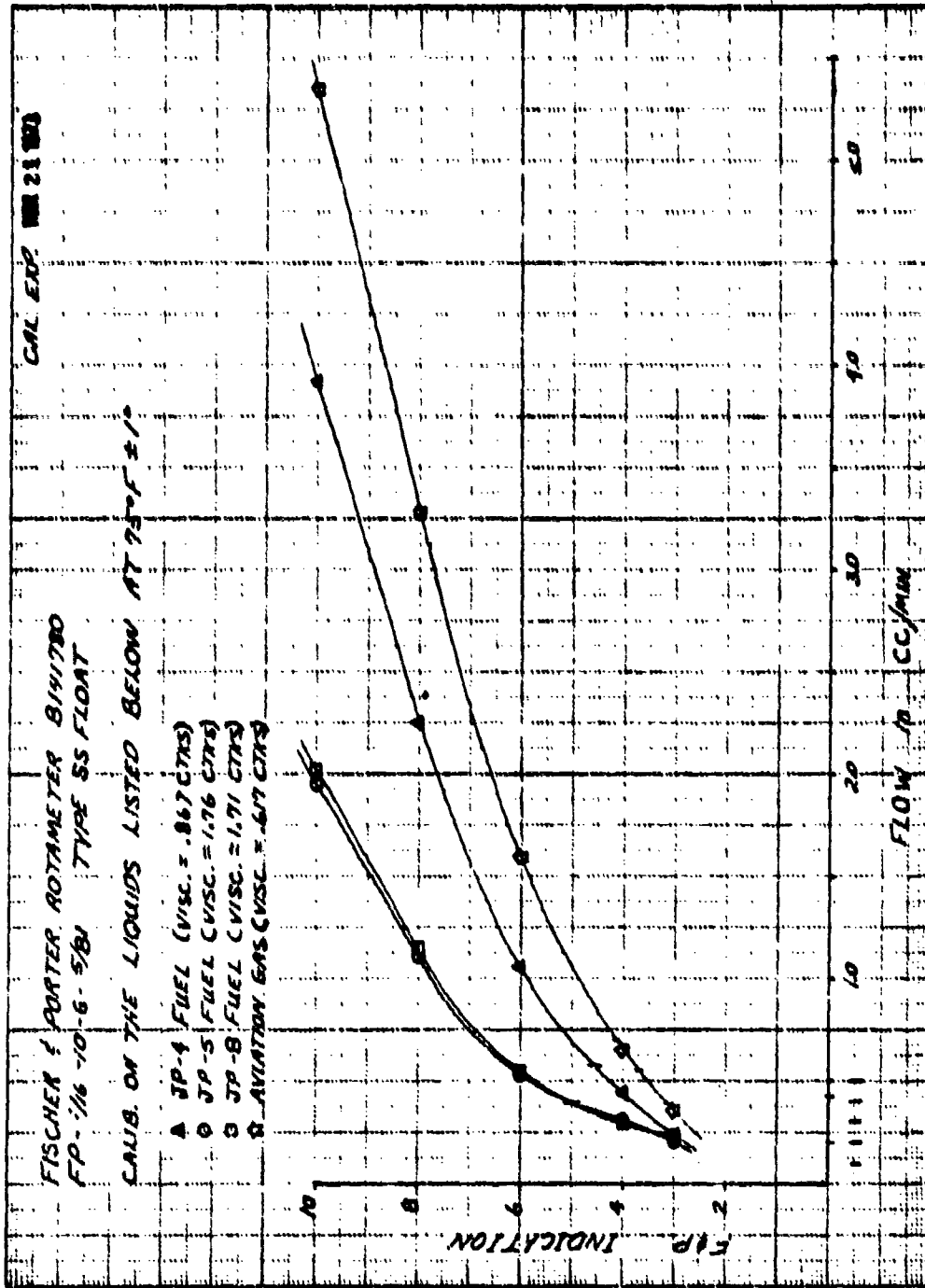


**FIGURE 3A - CALIBRATION CURVES FOR THE FUEL FLOWMETER**

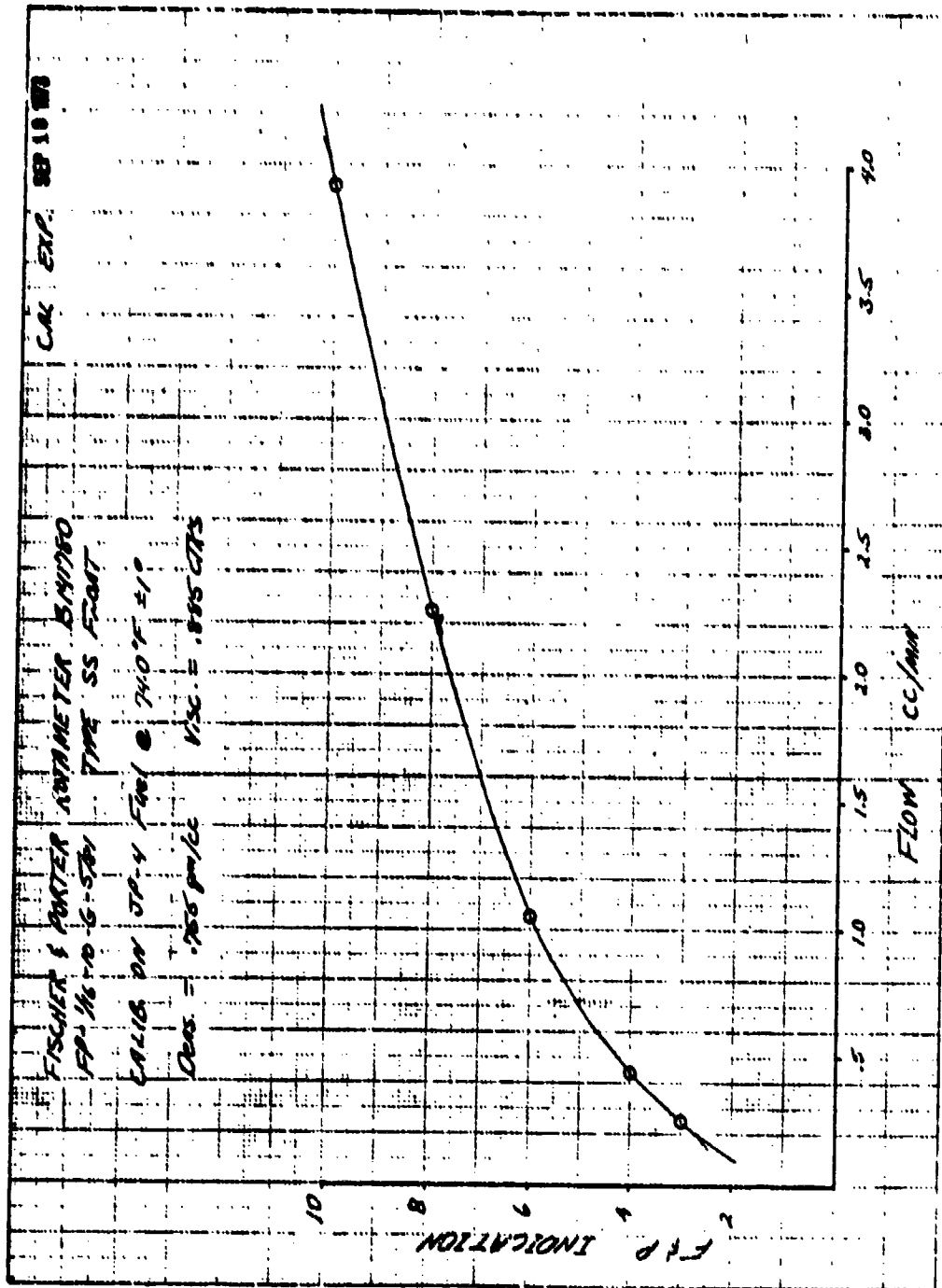


FIGURE 4A - RECALIBRATION CURVE FOR THE FUEL FLOWMETER

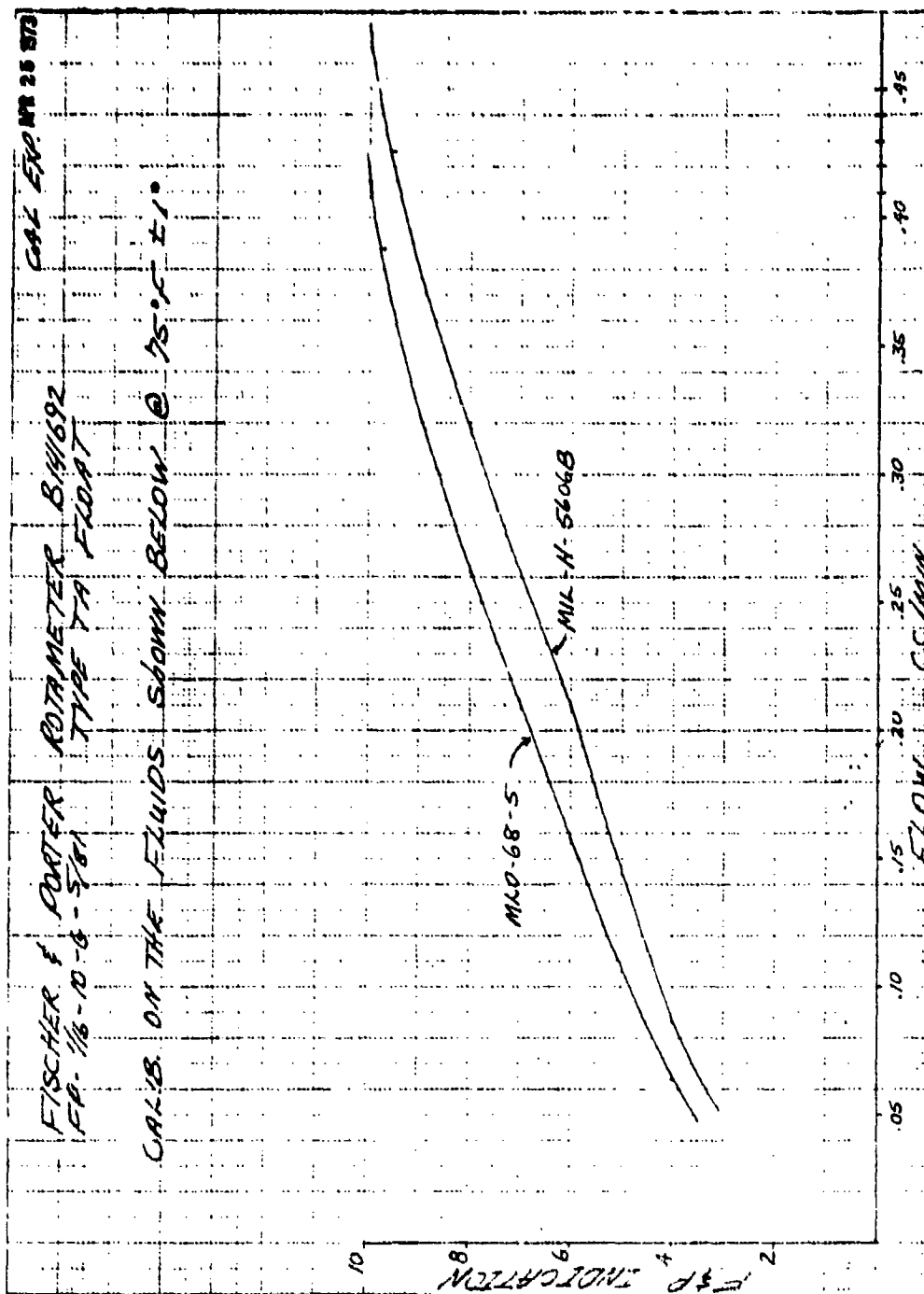


FIGURE 5A - CALIBRATION CURVES FOR THE  
HYDRAULIC FLUID FLOWMETER

AFAPL-TR-73-83

APPENDIX B

DATA REDUCTION COMPUTER PROGRAMS

```

PROGRAM UVPIPE (INPUT,OUTPUT,TAFF5=INPUT,TAFF6=OUTPUT,TAP,TAPE9)
COMMON/ROO/A(300)
DEFINITION WL(1030,1),VSTC(1030,6),VF(1030,1),RADST(1030,1),
1RADFL(1030,1),NCOFF(5),ARRAY(10),T(1030),SOG(1040),GSTC(6)
2,AUX(1030)
CNFILE=NC. OF FILES ON INPUT TAPE
000003 READ(5,7)CNFILE
000004 IFILE=1
000011 77 READ(5,8)NCOCK,NTYPE,NFTS,GAIN,CASE,M
000012 READ(5,333)(ARRAY(I),I=1,8)
000032 PRINT 334,(ARRAY(I),I=1,8)
000044 IF(NTYPE)100,100,200
000056 100 GFLAMP=GAIN
000060 CALL READ2(SOG)
000062 DO 70 K=1,1023
000063 LL=K+5
000065 IF(VF(K).LT.3.)VF(K)=3.
000073 70 VF(K)=SOG(L)
000100 GO TO 150
000100 200 GSTC(M)=GAIN
000102 CALL READ2(SOG)
000104 DO 71 K=1,1023
000106 LL=K+5
000110 71 VSTC(K,M)=SOG(LL)
000116 DO 72 K=1,1023
000117 IF(VSTC(K,M).LT.F.)VSTC(K,M)=F.
000127 72 CONTINUE
000131 150 IF(NCOCK)500,500,300
000133 300 READ(5,10)NPROF,WL(1),WL(1023)
000146 DO 310 K=1,1023
000147 PN=K-1
000151 310 WL(K)=(WL(1023)-WL(1))*(PN/1022.)+WL(1)
000160 IF(NTYPE)500,500,400
000162 400 IF(NPROF)500,500,410
000164 410 DO 410 K=1,NFTS
000166 11) AUX(K)=VSTC(K,M)
000174 CALL CALCOM(WL,AUX,9,CASE,1,NFTS,SHFLAMP,1H3,
1ARRAY,14H,WAVELENGTH(NM),SHVCLTS,0,1,1,1,0.)
PRINT 2230
GO TO 500
500 DO 400 K=1,NFTS
000222 400 AUX(K)=VF(K)
CALL CALCOM(WL,AUX,9,CASE,1,NFTS,SHFLAMP,1H3,ARRAY,
114H,WAVELENGTH(NM),SHVCLTS,0,1,1,1,0.)
DO 510 K=1,1023
000251 T(K)=1.27F3
000253 APG=(1.43PF7)/(WL(K)*T(K))
000255 RADST(K)=((1.176E20)/(WL(K)**5))*(1./(EXP(APG)-1.))
000260 A=1.99E-5
000270 IF(VSTC(K,M))505,505,505
000272 505 PRINT 220F,K
000275 GO TO 510
000303 505 RADFL(K)=A*(GFLAMP/GSTC(M))*(VF(K)/VSTC(K,M))
1RADST(K)
000317 510 CONTINUE
000321 PRINT 2220
000325 PRINT 2225,(WL(I),RADFL(I),I=1,1023)

```

FIGURE 1B - DATA REDUCTION COMPUTER PROGRAM FOR  
GRATING SPECTROMETER MEASUREMENTS



FIGURE 1B (cont'd)

```

000341      CALL CALCCMF(ML,PAOFL,9,CASE,1,NPTS,5*FLAME,1H3,ARRAY,
000342      114*WAVELENGTH(M),15*INTENSITY(W/SR),0,1,1,1,1,0.)
000342      PRINT 2240
000346      600 IFILE=JFILE+1
000370      IF(IFILE=NFIL5)77,77,610
000372      610 CONTINUE
000372      7  FORMAT(I2)
000372      8  FORMAT(3I5,F10.2,A20,I5)
000372      10 FORMAT(I2,2X,2F10.3)
000372      33  FORMAT(4F15.7)
000372      333 FORMAT(2A10)
000372      334 FORMAT(1H1,9A10)
000372      2001 FORMAT(1H ,I5,F8.3,F(3X,I5,F8.3))
000372      2200 FORMAT(1H1,30H SPECTRAL RADIANCE OF STD. LAMP)
000372      2205 FORMAT(1H0,20H ZERO VALUE FOR VSTD(I5,1H))
000372      2220 FORMAT(1H1,35H SPECTRAL RADIANT INTENSITY OF FLAME)
000372      2225 FORMAT(1H ,F8.3,2X,F14.5,4(F8.3,2X,F14.5))
000372      2230 FORMAT(1H1,37H FLOT CF STD. LAMP INPUT DATA OBTAINED)
000372      2240 FORMAT(1H1,40H FLOT CF FLAME SPECTRAL RADIANT INTENSITY OBTAINED)
000375      CALL FLCT(0,0,999)
000375      STOP
000377      ENC

```

AFAPL-TR-73-83

```

PROGRAM ANALY (INPUT, OUTPUT, TAPE=INPUT, TAPE=OUTPUT, TAP, TAPE)
COMMON/SAP/A(300)
DIMENSION TRT(1000), TIT(1000), FX(1000), PY(1000), AUX(1000),
1 ARRAY(10), FXT(500), QX(10,1), QY(10,1),
2 PAST(1000), RAFL(1000), ARG(1000)
INTEGER CASE
KLCF=0
C NFILE=NO. OF FILES ON INPUT TAPE
C JCURF=0 IMPLIES 4-40 MICRON Y-CURVE
C JCURF=1 IMPLIES 2.5-15 MICRON Y-CURVE
000004 READ(F,7)NFILE,JCURF
000014 DO 500 I=1,NFILE
C NGCON=0 IMPLIES SKIP THE FILE
C =1 IMPLIES USE THE FILE
000016 READ(F,7)NGCON
000023 REAL(5,100)(ARRAY(I),I=1,9)
000035 PRINT 134,(ARRAY(I),I=1,9)
000047 CALL READ2(TRI)
C NMIN=LOCATION OF FIRST USABLE POINT
C NMAX=LOCATION OF SAMPLE WITH LARGEST MAGNITUDE
C NMP=LOCATION OF LAST USABLE POINT
C NPT=NUMBER OF SAMPLES
C NAF=0 IMPLIES APODIZATION
C =1 NO APODIZATION
C JSTOR=0 SAVE AMPLITUDE SPECTRUM
C =1 DO NOT SAVE
C JPAT=0 COMPLETE REFLECTANCE SPECTRUM
C =1 NO RATIO COMPUTED
C JAMP=0 PLOT AMPLITUDE SPECTRUM
C =1 DO NOT PLOT
C JOB=0 COMPUTE RATIO
C =1 DO NOT COMPUTE
C KOP=0 STORE TOTAL REFLECTANCE
C =1 DO NOT STORE
000051 IF(NGCON)999,999,47
000052 47 READ(F,1)NMIN,NCENT,NMAX,NPT,NAF,JSTOR,JPAT,JAMP,JCF,KOP
000103 PRINT 4,NMIN,NCENT,NMAX,NPT,NAF,JSTOR,JPAT,JAMP,JOB,KOP
000133 174 FORMAT(1H1,PA10)
000133 NMTN=30
000134 NMTN=NMTN+5
000136 DO 11 I=1,NMTN
000137 11 TRI(I)=0.0
000142 K=1
000143 DO 12 J=5,1029
000145 TRI(K)=TRI(J)
000150 12 K=K+1
000152 DO 13 J=1024,1029
000154 13 TRI(J)=0.0
C REMOVE DC LEVEL
000157 SUM=0.0
000160 DO 15 I=1,1024
000161 15 SUM=SUM+TRI(I)
000165 AVF=SUM/1024.0
000167 PRINT1047,AVF
000174 NMTN=NMTN-5
000176 DO 20 I=NMIN,1023
000177 20 TRI(I)=TRI(I)-AVF

```

FIGURE 2B - DATA REDUCTION COMPUTER PROGRAM FOR INTERFEROMETRIC SPECTROMETER MEASUREMENTS

## FIGURE 2B (cont'd)

```

000200      TRI(1024)=0.0
          C      APOOIZE
000204      IF(NAP)30,30,35
000206      30 DO 33 IJ=1,511
000210      AB=IJ
000211      CR=(1.0-(AB/512.0)**2)**2
000215      II=512-IJ
000217      JJ=512-IJ
000220      TR1(II)=TRI(II)*CR
000222      33 TR1(JJ)=TR1(JJ)*CR
000226      35 CONTINUE
          C      COMPUTE FOURIER TRANSFORM
000228      CALL FOUR1(TRI,TII,NMAX)
          C      COMPUTE AMPLITUDE SPECTRUM
000231      DO 40 J=1,1024
000233      TEMPA=TRI(J)
000235      TEMPB=TII(J)
000236      TR1(J)=SQRT(TEMPA**2+TEMPB**2)
          C      PRINTER, CALCOMP PLOTS OF AMPLITUDE SPECTRUM
000247      IF(JAMP).0,40,54
000251      40 DO 41 J=1,1024
000253      41 PY(J)=TR1(J)
000257      55 LTOP=995
000260      IF(JCUBE.EQ.0.0)LTOP=975
000262      DO 721 K=LTOP,1030
000264      721 PY(K)=0.0
000267      LIM=759
000270      IF(JCUBE.EQ.0.0)LIM=730
000272      DO 722 K=1,LIM
000274      722 PY(K)=0.0
000277      N=LIM+1
000301      NPIS=LTOP-LIM
000302      DO 723 L=1,NPIS
000304      PY(L)=PY(N)
000307      723 N=N+1
000312      N=LIM+1
000314      NN=LTOP-1
000316      DO 724 K=NN,NN
000320      724 PY(K)=0.0
000323      DO 725 L=1,NPIS
000325      XL=L
000326      IF(JCUBE)799,799,798
000330      799 WAVELE=.283726-(3.556E-4)*XL
000333      GO TO 727
000334      798 WAVELE=.305-(0.002100*XL)
000337      727 PX(L)=1./WAVELE
000342      725 PX(L)=.1319+1.0221*PX(L)+4.0E-3*PX(L)**2
000344      IF(KLOP)726,726,83
000346      726 PRINT2011
000350      PRINT 2001,(PX(I),PY(I),I=1,NPIS)
000353      DO 97 I=1,NPIS
000377      QX(I,1)=PX(I)
000401      97 QY(I,1)=PY(I)
000405      CASE=IKUN
000407      CALL CALCOMP(PX,PY,9,CASE,1,NPIS,9,AMPLITUDE,
1143,ARKAY,19,HWAVELENGTH (MICRON),11,REFLECTANCE,0,1,1,1,1)
000426      99 IF(JSTOR)5,55,50
000430      55 DO 57 K=1,NPIS

```

## FIGURE 2B (cont'd)

```

000432      AUX(K)=PY(K)
000434      T=1.273F3
000436      A=.76
000437      ARG(K)=(1.4385E4/(T*PX(K)))
000438      57 RADST(K)=1*1.176E-7*((PX(K)**5)*(EXP(ARG(K))-1))
000439      PRINT2001,(PX(K),RADST(K),K=1,NPTS)
000440      60 IF(JRAT)5,55,999
000441      65 DO *11 K=1,NPTS
000442      IF(AUX(K)-0.)577,711
000443      677 PRINT31,K,AUX(K)
000444      AUX(K)=1.
000445      711 RADFL(K)=RADST(K)*PY(K)/AUX(K)
000446      83 KLOP=0
000447      PRINT 2220
000448      PRINT 2220,(PX(I),RADFL(I),I=1,NPTS)
000449      CALL CALCOMPI(PX,RADFL,9,CASE,1,NPTS,5,NFLAME,1M3,ARRAY,
000450      11,MMWAVELENGTH(NM),15,INTENSITY(W/SR),0,1,1,1,0.)
000451      PRINT 2240
000452      1 FORMAT(10,3(1X,15),5(1X,12))
000453      7 FORMAT(12,8X,12)
000454      8 FORMAT(14,15,3(1X,15),6(1X,12))
000455      333 FORMAT(A410)
000456      491 FORMAT(14,*,DENOMINATOR AUX(*,15,*)=*,E12.5)
000457      1040 FORMAT(141,*INTERFERUGRAM DC LEVEL=*F12.5)
000458      2000 FORMAT(14,*,(15,E20.5))
000459      2001 FORMAT(14,*,F8.3,E14.5,5(2X,F8.3,E14.5))
000460      2003 FORMAT(141,*APD 1750 INTERFERUGRAM*)
000461      2005 FORMAT(141,*COSINE FOURIER TRANSFORM*)
000462      2007 FORMAT(141,*SINE FOURIER TRANSFORM*)
000463      2009 FORMAT(141,*AMPLITUDE (INFRARED) SPECTRUM*)
000464      2011 FORMAT(141,*PLOTED AMPLITUDE SPECTRUM*)
000465      2017 FORMAT(140,*PLOTED REFLECTANCE SPECTRUM*)
000466      2019 FORMAT(140,*PLOTED DIFFUSE/TOTAL RATIO*)
000467      2020 FORMAT(14,10,E14.5,5(10,E14.5))
000468      2220 FORMAT(141,354,SPECTRAL RADIANT INTENSITY OF FLAME)
000469      2225 FORMAT(14,*,F8.3,2X,E14.5,*(F8.3,2X,E14.5))
000470      2240 FORMAT(141,*,PLOT OF FLAME SPECTRAL RADIANT INTENSITY OBTAINED)
000471      999 CONTINUE
000472      70 DO 73 I=1,1030
000473      T=I(I)=0.0
000474      T1(I)=0.0
000475      PY(I)=0.0
000476      73 PY(I)=0.0
000477      998 CONTINUE
000478      CALL PLOT(0,0,9,9)
000479      STOP
000480      END

```